



University of Mohamed Kheider of Biskra
Exact Sciences and Sciences of Nature and Life Matter Sciences
Department of Material Sciences

Final Dissertation in Master

Field of Material Sciences

Physics

Specialty: Energy Physics and Renewable Energies

Ref. : Entrez la référence du document

Presented by:

Semmari Maroua & Ataoua Mounira

Monday 28/06/ 2021

Study of a Metal- Insulator- Semiconductor (MIS) solar cell

Jury:

SengougaNouredine	Professor	Med KhiderUniversity- Biskra	President
MeftahAmjad	Professor	Med KhiderUniversity- Biskra	Supervisor
BoudibOuahiba	MAA	Med KhiderUniversity- Biskra	Examiner

Academic Year:2020/2021

Acknowledgement

First of all, we thank "Allah" Almighty who has given us the strength to do this work that we wish it will achieve our aspirations, God willing.

*I would like to thank my advisor **Pr. Meftah Amjad** for his valuable guidance and support during my dissertation and I am benefited a lot from her profound knowledge.*

It was a very nice experience to work with her.

*To the one who gave me the strength and the determination to continue the journey my dear sister **Souhir Semmari**.*

And we cannot fail to express our heartfelt thanks to every teacher who taught us a letter and endeavored to illuminate our path with knowledge from the very first letter we learned to this day.

I thank all those who, from near or far, have helped me to carry out this work,

Dedication

*If this work is part of the fulfillment, I dedicate this work;
To whom her supplication was the secret of my success, and
with her presence I knew the meaning of life.*

*To the symbol of love and the sea of tenderness my mother, my
beloved Bouslimani Mariam.*

*To the one who paved the path of knowledge for me, so give me
the best of all. To whom I carry his name
with pride My dear father Ahmed.*

*To my sanctuary, my strength, and my support after God
Almighty, and my soul mates with whom I lived
the most beautiful memories My siblings Djalloul, Ammar,
Mahdi, Noufel, Jahida, Souhir, Bouchra,
Hadjer.*

*To whom we walked together, paving the way to success and
creativity my friends Manal, Radia, Fati,
Maria, chafika, Amira.*

To those who taught me letters of gold my dear teachers

Maroua

Dedication

Praise be to God, who enabled us to complete this work and provided us with health, wellness and determination, Praise be to God, thank you very much.

I give thanks:

- ✓ *To the fountain that never tires of giving, to the one who woven my happiness with threads woven from her heart, to my dear mother " . . . **Fozia** . . . " may God prolong her life.*
- ✓ *To those who strive and miserable to enjoy comfort and contentment and push me to the path of success to my dear father. . . " **Mohamed** . . . " May God prolong his life and grant him health and wellness.*
- ✓ *To my partner in life, to the one who supported me and took my most important steps with me, and eased the difficulties to my husband, my beloved" . . . **Naili Mohamed** . . . " who endured a lot for my standing in this place, it would not have happened without his encouragement Continuing me, I don't say thank you, but I live life for you thank you.*
- ✓ *To all my dear brothers. . . " **Tawfiq-Haidar-Ayman-AmalFathya** . . . " I especially mention my brother, the goodness" . . . **Yassen** . . . " Without interdependence and cooperation, it means nothing, may God protect you and your care.*
- ✓ *To my little girl and sister" . . . **Sundus** . . . " who changed the world in our eyes when she was born. I grew up in God's care and protection.*
- ✓ *To whom we walked together as we paved the road to success and creativity, to whom we joined hands hand in hand as we pick a flower, we learned to" . . . **AshourNaima-Ben RayalaRadhiya** . . . " without forgetting my colleague in the memo" . . . **SamariMarwa** . . . "*
- ✓ *To those who taught me letters of gold and clear phrases in science. To those who crafted letters from their knowledge and thought a beacon illuminating us the path of knowledge and success. To my honorable professors, and especially the remembrance" . . . **my teacher MeftahAmjad** . . . " may God saDve her.*
- ✓ *To all of them I dedicate this humble deed, asking God Almighty to benefit us with it and grant us success.*

Mounira

Abstract

We have investigated two MISsilicon-based solar cells. The first one consists of Au / SiO₂ / n-type c-Si, and in the second one, the anode metal (Au) is replaced by heavily doped ZnO (n⁺-type) to give (n⁺-type ZnO / SiO₂ / n-type c-Si) structure. The investigation of the thickness variation effect, of the silicon layer in the range [10- 500 μm], shows an optimal thickness of 175 μm for the first cell with a conversion efficiency η of ~11.87 %. For the second one, the optimal thickness is 150 μm with a conversion efficiency η of ~12.50%. An enhancement is notified, particularly in J_{sc} and the conversion efficiency η , as the anode metal (Au) is replaced by heavily doped ZnO (n⁺-type). The thickness variation effect of the oxide (SiO₂) layer in the range [2-20 Å], shows better output parameters for FF and η , as the oxide layer becomes thinner. The J_{sc} and V_{oc} , however, display insignificant sensitivity to the oxide layer thickness variation. The optimal value of doping is $N_d = 7 \times 10^{15} \text{ cm}^{-3}$ for the first cell with a conversion efficiency η of ~11.87%, and is $N_d = 7 \times 10^{16} \text{ cm}^{-3}$ for the second solar cell with a conversion efficiency η of ~12.558%. The V_{oc} is significantly enhanced as the doping concentration increases for both solar cells. Varying the ZnO layer thickness in the range [0.05-10 μm] brings further improvement to the second cell; a significant enhancement of the J_{sc} is notified leading to a conversion efficiency improvement from ~ 11.97% to 13.94%.

Keywords

MIS solar cell; Silicon, Silvaco-Atlas; Tunnelling

List of Figures

Figure number	Titles	Page number
I.1	Generation of charge carrier by photon absorption	5
I.2	Simple solar cell model.	6
I.3	Solar irradiance spectrums versus wavelength.	7
I.4	Ideal solar cell.	8
I.5	Photovoltaic cell equivalent circuit.	9
I.6	<i>IV</i> characteristic of photovoltaic cell under illuminated and dark.	10
I.7	I_{sc} and V_{oc} representation in <i>VI</i> curve.	11
I.8	Attaining fill factor from <i>VI</i> characteristics curve.	12
I.9	Typical n-type Si and p-type Si MIS structures.	15
I.10	Energy-band diagram of n-type Si and p-type Si MIS structures, at thermal equilibrium of the depletion regime; where Schottky barrier is established at the oxide/semiconductor interface.	16
I.11	Dark-current components in forward biased MIS (n-type) diode.	16
I.12	Energy-band diagrams for n-type MIS-Schottky barriers in the dark (a) $V = 0$ (b) applied voltage $V > 0$.	17
I.13	Band diagrams for n-type MIS-SB solar cell under solar illumination (a) $V = 0$ (short circuit conditions, external load $R = 0$), and (b) $V > 0$ (voltage induced by illumination for external load $R > 0$).	18
I.14	Schematic illustration of ZnO-based MIS type solar cell.	21
I.15	Band diagram of ZnO/SiO ₂ /n-type Si solar cell.	21
II.1	Screenshot from Deckbuild.	24
II.2	Atlas statement hierarchy.	25
II.3	Mesh example for MIS solar cell based on Silicon (n-type).	26
II.4	Tonyplot screenshot showing the layout of the x and y-coordinate system in Atlas for MIS solar cell based on Silicon (n-type).	29
II.5	Electrode positions of the Si (n-type)-based MIS solar cell.	30
II.6	Simulated characteristics of the Si -based MIS solar cell, in the dark and illumination conditions with	35

	AM	
III.1	Structure of the studied MIS silicon solar cell with: (a) Gold (Au) anode, (b) ZnO anode	37
III.2	Two dimensional (2D) mesh of the studied MIS silicon solar cell with : (a) Gold (Au) anode, (b) ZnO anode.	38
III.3	Spectre of absorption coefficient (α) in the different layers of the studied MIS silicon solar cell: (a) structure with gold (Au) anode, (b) structure with ZnO anode.	42
III.4	Spectre of optical index of refraction (n) in the different layers of the studied MIS silicon solar cell: (a) structure with gold (Au) anode, (b) structure with ZnO anode.	43
III.5	Band diagram of the MIS silicon solar cell with gold (Au) anode: (a) at thermal equilibrium, (b) at short circuit condition.	46
III.6	Band diagram of the MIS silicon solar cell with ZnO anode: (a) at thermal equilibrium, (b) at short circuit condition.	48
III.7	Carrier density distributions in the MIS silicon solar cell at thermal equilibrium and short circuit condition: (a) with gold (Au) anode, (b) with ZnO anode.	49
III.8	Simulated $J - V$ and $P - V$ characteristics of the MIS silicon solar cell with gold (Au) anode, under the AM1.5 standard spectrum and $T = 300^{\circ}K$.	49
III.9	Silicon layer thickness effect on the photovoltaic output parameters of the simulated MIS silicon solar cell with gold (Au) anode.	50
III.10	Thickness effect of the oxide (SiO_2) layer on the photovoltaic output parameters of the simulated MIS silicon solar cell with gold (Au) anode.	51
III.11	Doping concentration effect of the silicon layer on the photovoltaic output parameters of the simulated MIS solar cell with gold (Au) anode.	52
III.12	Simulated $J - V$ and $P - V$ characteristics of the MIS silicon	54

	solar cell with ZnO anode, under the AM1.5 standard spectrum and $T = 300^{\circ}K$.	
III.13	Silicon layer thickness effect on the photovoltaic output parameters, and comparison between the two simulated MIS solar cells: with gold (Au) anode (without ZnO) and with ZnO anode.	55
III.14	Oxide thickness effect on the photovoltaic output parameters, and comparison between the two simulated MIS solar cells: with gold (Au) anode (without ZnO) and with ZnO anode.	57
III.15	Doping concentration effect on the photovoltaic output parameters, and comparison between the two simulated MIS solar cells: with gold (Au) anode (without ZnO) and with ZnO anode.	58
III.16	Thickness effect of the ZnO anode layer on the photovoltaic output parameters of the simulated silicon solar cell with ZnO anode.	59

List of Tables

Table number	Titles	Page Number
III.1	Brief description of the employed models in simulation.	40
III.2	Input parameters of the MIS silicon solar cell simulated by Silvaco-Atlas.	43
III.3	Silicon layer thickness effect on the photovoltaic output parameters of the simulated MIS silicon solar cell with gold (Au) anode.	50
III.4	Thickness effect of the oxide (SiO ₂) layer on the photovoltaic output parameters of the simulated MIS silicon solar cell with gold (Au) anode.	51
III.5	Doping concentration effect of the silicon layer on the photovoltaic output parameters of the simulated MIS solar cell with gold (Au) anode.	53
III.6	Comparison between the photovoltaic output parameters of the simulated MIS solar cell with gold (Au) anode and with ZnO anode.	55
III.7	Silicon layer thickness effect on the photovoltaic output parameters of the simulated MIS silicon solar cell with ZnO anode.	56
III.8	Thickness effect of the oxide (SiO ₂) layer on the photovoltaic output parameters of the simulated MIS silicon solar cell with ZnO anode.	57
III.9	Doping concentration effect of the silicon layer on the photovoltaic output parameters of the simulated MIS solar cell with ZnO anode.	58
III.10	Thickness effect of the ZnO anode layer on the photovoltaic output parameters of the simulated silicon solar cell with ZnO anode.	59

List of symbols

Symbol	Definition	Unit
E	Photon energy	eV
I_s	the diode saturation current	A
V	the voltage of the cell	V
K	Boltzmann constant	J/K
T	Absolutetemperature	K
I_L	the photo generationcurrent	A
I_{oc}	the open circuit current	A
q	ElectronCharge	C
E_g	band-gap energy of the semiconductor	eV
η	Conversion efficiency	%
p_{out}	the maximum output power	mW.cm ⁻²
p_{in}	the input power	mW.cm ⁻²
V_{max}	the maximum power point voltage	V
I_{max}	the maximum power current	A
FF	Fill factor	%
E_C	Conduction band energyedge	eV
E_V	Valence band energyedge	eV
h	ThePlanck constant	J.S
I_{ph}	The densityof the currentphoto	
V_{co}	Open circuit voltige.	Ω cm
ρ	Materialresistivity	
E_{ph}	Photoenergy	eV
E_g	Band-gap energy of the semiconductor	eV
ν	Wave frequency	
I	Current supplied by the photovoltaic cell	A
p_{max}	Maximum power	W
V_m	Current which circles in the shunt resistance	A
I_s	Reverse saturation or leakage current of the diode	A
R_s	Resistanceseris	Ω
R_{sh}	Shuntresistance(parallel)	Ω
C	The speed of light	m/s
E_i	The intrinsic fermi level	eV
E_f	The energy of fermi	eV
I_o	Primarecurrent	A
V_{out}	External voltage	V
I_{out}	Externalcurrent	A
Q_m	Multi-extraction action	eV
Q_s	the work function of the semiconductor ‘electronic affinity’	eV
J_{sc}	Short circuit current.	eV
N_d	the density of donors in the n-type semiconductor	cm ⁻³

AM	Air mass	–
E_{ph}	La quantité d'énergie transportée par le photon	C
e^-	Charge de l'électron ($-1,602 \times 10^{-19}$)	C
(J-V)	Characteristic (voltage –current)	

TABLE OF CONTENTS

<u>Acknowledgement</u>	i
<u>Dedication</u>	ii
<u>Abstract</u>	iv
<u>List of Figures</u>	v
<u>List of Tables</u>	viii
<u>List of symbols</u>	ix
<u>Table of contents</u>	xi
<u>General introduction</u>	1
<i>Chapter I: MIS silicon-based solar cell</i>	
I.1. Introduction	3
I.2. Photovoltaic and solar cells	3
I.2.1. Working principle of photovoltaic cell	4
I.2.1.1.Generation of charge carriers due to photon absorption	5
I.2.1.2.Separation of photo generated charge carriers	6
I.2.1.3.Extraction of photogenerated charge carriers	6
I.2.2.Solar radiation	7
I.2.3. Equivalent circuit of solar cell	8
I.2.4.Characteristic of a photovoltaic device	10
I.2.4.Basic photovoltaic parameters of the solar cell	11
I.2.4.1 Short circuit current	11
I.2.4.2.Open circuit voltage	11
I.2.4.3.Fill factor	12
I.2.4.4.Maximum power	13
I.2.4.5.Power conversion efficiency	13
I.2.4.6. Quantum efficiency	14

I.3. Metal-Insulator-Semiconductor (M-I-S) structure.....	14
I.4. TCO-based MIS type solar cell.....	20
I.5. Conclusion.....	22

Chapter II: Solar cell simulation using SILVACO-ATLAS software

II.1. Introduction.....	23
II.2. SILVACO- ATLAS as numerical modelling software.....	23
II.3. Application of Silvaco-Atlas in the numerical simulation of the MIS solar cell based on Silicon (general steps).....	25
II.3.1. Building the device.....	25
II.3.2 Defining the Structure.....	26
II.3.3. Regions.....	27
II.3.4. Electrodes.....	29
II.3.5 .Doping.....	30
II.3.6. Modifying Parameters.....	30
II.3.7. Numerical Solutions.....	31
II.3.8 .Obtaining Solutions.....	31
II.3.9. Results.....	32
II.3.10. Luminous.....	33
II.3.11. Solarcell simulation.....	33

Chapter III: Investigation of the MIS silicon solar cell

III.1. Introduction.....	36
III.2. Description of the studied MIS silicon solar cell.....	36
III.3. Results and discussion.....	44

III.4.Conclusion.....	60
General conclusion.....	63
References.....	66
Abstract.....	71
المخلص.....	71



General introduction



General introduction

A solar cell is a photovoltaic device designed to directly convert sunlight into electric power and to deliver this power into a suitable load in an efficient manner. The most important commercial solar cells are silicon p-n junction devices. They are generally fabricated by diffusing a thin layer of phosphorous n-type dopants into a p-type boron-doped silicon substrate [1]. Not only does this diffusion process account for about a quarter of the total cost of the cell but it also causes minority carrier lifetimes throughout the entire cell to degrade to about a third of their starting values [2]. Various alternatives have been sought in order to reduce this cost. Schottky barrier (or rectifying metal-semiconductor contact) solar cells have been examined for their suitability in large scale terrestrial applications since they are simpler to fabricate with lower cost technology [3-4,6,7,5]. They are formed at low temperatures without any degradation in the bulk properties of the semiconductor. However, it can be shown that these cells will always have a smaller open circuit voltage than a p-n junction cell [8]. Typically it is about half the value, and the overall cell efficiency is reduced by this factor. Many works [8-9,10,11] have shown that inserting a very thin insulating layer between the metal and semiconductor can increase the open circuit voltage of the cell and hence increase the photovoltaic conversion efficiency without increasing the associated cost. Current flow mechanisms in Schottky barrier and metal-insulator semiconductor (M-I-S) diodes are similar. However with this structure it is possible to produce minority carrier dominated diodes if the proper type of semiconductor and metal contact are chosen [12]:

The use of (M-I-S)heterojunctions is among the several possibilities to increase the photovoltaic systems efficiency with low cost. In these structures, the use of transparent conducting oxidesthin films offers more advantages for the structures. Furthermore, they can be used with poly-crystalline and amorphous materials. Transparent conducting oxides (TCOs) are n-type degenerated semiconductors (metallic oxides). They are formed from binary compounds such as SnO_2 , In_2O_3 , ZnO ...etc, and from ternary compounds like Cd_2SnO_4 , ZnSnO_3 , $\text{Zn}_2\text{In}_2\text{O}_5$... [13, 14, 15]. The most useful TCO are tin oxide SnO_2 and zinc oxide ZnO .

In this work, we will study two silicon-based solar cells. The first one consisting of $\text{Au} / \text{SiO}_2 / \text{n-type c-Si}$ (MIS structure). In the second cell, the anode metal (Au) is replaced by heavily doped ZnO (n+-type) to give (n+-type $\text{ZnO} / \text{SiO}_2 / \text{n-type c-Si}$) structure. For the two considered solar cells, we will investigate the thickness variation effect of the silicon layer in the range [10- 500 μm], the thickness effect of the oxide (SiO_2) layer in the range

General introduction

[2-20°A], and the n-type doping concentration effect of the silicon layer (N_d) in the range [$7 \times 10^{12} - 7 \times 10^{18} \text{cm}^{-3}$]. For the second solar cell, further investigation will be achieved under ZnO thickness effect in the range [0.05-10 μm] to bring more improvement to the solar cell performance. The two studied solar cells are exposed to the AM1.5 standard spectrum at ambient temperature (300°K°). The investigation will be realised using the numerical simulation software SILVACO-ATLAS, which allows the calculation of all the internal parameters of the solar cell such as the distribution of the band diagram, the electron and holes concentrations...etc. The external parameters are also be calculated such as the current density-voltage ($J - V$) and the provided power - voltage ($P - V$) characteristics under illumination, which allow the extraction of the output photovoltaic parameters of the solar cell namely the short circuit current density J_{sc} , the open circuit voltage V_{oc} , the fill factor FF , the maximum power P_{max} provided by the cell and the photovoltaic conversion efficiency η of the cell.

In addition to the general introduction and conclusion, our thesis will be organized as follow:

In the first chapter, we give an overview on photovoltaic and working principle of photovoltaic cell. Then, we present a physical description of the Metal/Insulator/Semiconductor (M-I-S) and TCO-based MIS structures for solar cells.

In the second chapter, we present a description of Silvaco-Atlas simulation software; which we will use to simulate the electrical characteristics of the two considered solar cells.

In the third chapter, we will present a detailed description of the studied MIS silicon solar cell; in the first case with gold (Au) anode and in the second case with ZnO-based anode. Then, we will discuss the results obtained by our simulation.



Chapter I



MIS silicon-based solar cell



I.1. Introduction:

Among different possibilities to improve the solar cell efficiency with low cost, the tunnel metal–insulator–semiconductor (MIS) junction was reported as an attractive alternative of the ordinary diffused p-n junction [16,17,18]. Under optimum conditions, it has been affirmed that the open-circuit voltages of both MIS and p-n junction solar cells are approximately equivalent [18]. Indeed, the presence of an ultrathin insulating layer ($< 40 \text{ \AA}$) in a MIS structure improves appreciably their photovoltaic properties by increasing the open-circuit voltage relatively to the Schottky-barrier solar cells [19,20, 21]. Many advantages can be displayed by the MIS configuration that can include [17, 13]: (i) the possibility of low temperature processing which preserve the long minority-carrier lifetime, (ii) the absence of a diffused layer, and the corresponding dead layer [22,23], which can improve the short-circuit current densities, (iii) the compatibility of the structure with any semiconductor type such as polycrystalline and amorphous materials. The low cost and the simplicity of fabrication, as well as the compatibility with arbitrary semiconductors, make the MIS structure as a good candidate for terrestrial photovoltaic applications.

In the first sections of this chapter, we give an overview on photovoltaic and working principle of photovoltaic cell. The last sections are devoted to the description of the Metal/Insulator/Semiconductor (M-I-S) and TCO-based MIS structures for solar cells.

I.2. Photovoltaic and solar cells:

Renewable energy resources contribute a significant role in the production of energy. The solid-state semiconductor photovoltaic devices have emerged as a newer and a relatively sustainable energy source. Which is eco-friendly and cost-effective if the production is on large scale. Following are the advantages that make the photovoltaic cells an efficient renewable energy source [24]

- ✚ Conversion of electricity from sunlight or the sun's radiation is direct. So, there is no need to install a bulky generator.
- ✚ Solar electrical energy generation is environment-friendly. A photovoltaic panel provides clean and green energy. There is no emission of gases during ii. Electricity generation.
- ✚ Free from the use of fuels and water.

- ✚ Solar energy is generated by nature, it is free and simple.
- ✚ Where sunlight is available solar energy can be generated easily.
- ✚ Photovoltaic energy is suitable for smart energy networks with distributed power generation.
- ✚ Photovoltaic cells have no mechanically moving parts as in wind turbines, so they have less breakage and also require little maintenance than other renewable energy sources.
- ✚ Photovoltaic panels are completely soundless and not providing noises.
- ✚ They can be used in distant zones, where the installation of an electric power grid is too expensive.
- ✚ Photovoltaic panels are easily installable on grounds or on rooftops at residences without the interference of the residential lifestyle. [25]
- ✚ They have a long lifetime, up to 30 years.

I.2.1. Working principle of photovoltaic cell:

Photovoltaic cell working principle is based on the photovoltaic effect; which is the formation of a potential difference at the junction of two different materials. This effect is closely related to the photoelectric effect, where the emission of electrons from a material is due to light absorption with a frequency above a material-dependent threshold frequency. This effect was explained by the scientist Albert Einstein in 1905 by assuming that the light comprises of well-defined energy quanta, called photons. The energy of such a photon is:

$$E = h\nu \quad (I.1)$$

Where $\nu = c/\lambda$ and c is the speed of light in a vacuum ($c = 3 \times 10^8 \text{ m/s}$), h is the Planck's constant ($h = 6.626 \times 10^{-34} \text{ Js}$) and ν is the frequency of the light. For the explanation of this effect, Einstein received the Nobel Prize in Physics in 1921. The photovoltaic effect can be divided into the following three basic processes [26]

I.2.1.1. Generation of charge carriers due to photon absorption:

Photon absorption in photovoltaic material excites the electrons and they move from initial energy state E_i to higher energy state E_f as given in Figure I.1. Figure I.1(a) shows that photon energy $E_{ph} = h\nu$ excites electrons present in the valence band (E_i , initial energy state) shifted to the conduction band (E_f , final energy state) after absorption of photon energy. Figure I.1 (b): shows that if $E_{ph} > E_g$, a part of the energy is thermalized.

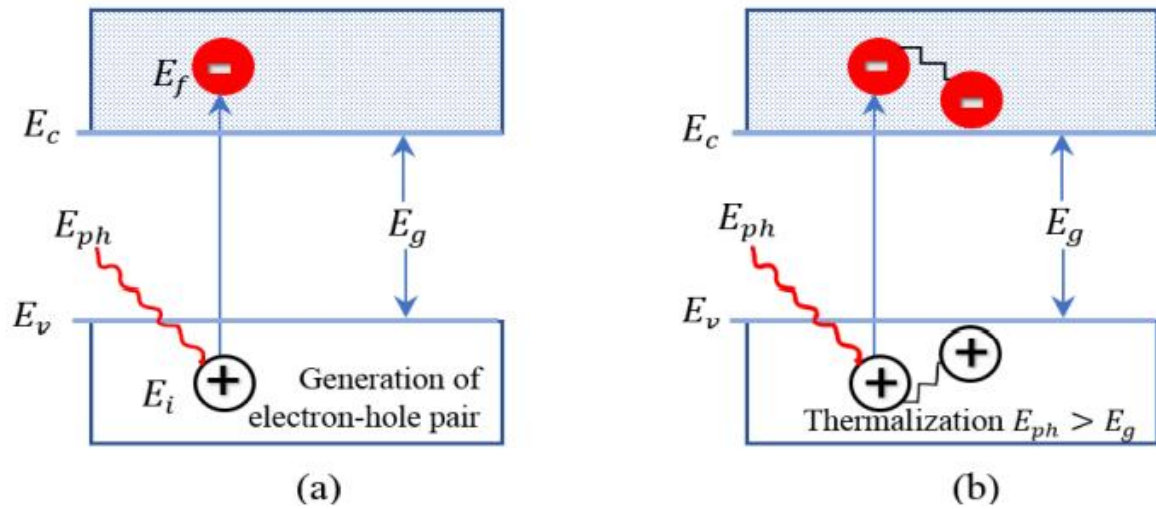


Figure I.1: Generation of charge carrier by photon absorption.

Photon energy can be absorbed in the presence of E_f and E_i electron energy levels. Photon energy is equal to the difference of E_f and E_i as given in Eq. (I. 2).

$$h\nu = E_f - E_i \quad (I.2)$$

In ideal case electron populates below than valence band edge E_v and above the edge of conduction band E_c in semiconductor. There is no other energy level for the electron population in amongst these two states. Hence the energy difference between E_c and E_v is called the band gap energy as given in Eq.(I.3). Therefore, the photon energy smaller than this band gap energy will not be absorbed.

$$E_g = E_c - E_v \quad (I.3)$$

I.2.1.2. Separation of photo generated charge carriers:

Recombination takes place in electron-hole pair. The electron will fall back to its initial energy state and energy releases in a form radiative recombination (photon emission) or non- radiative recombination (transfer of energy to other holes and electrons) Presence of semi membrane on both sides of the absorber allows the use of energy stored in these electron-hole pairs in an external circuit. Electron flows out from one membrane whereasholes from other as shown in Figure I.2 [27]. From the figure, it is illustrated that electrons and holes are separated due to semipermeable membranes. P-type and n-type materials are used for the formation of the membranes. The solar cell is designed in such a way that before recombination of electron-hole pair, they must be reached to the membrane. It means that the time required to reach these charge carriers to their respected membrane must be shorter than their lifetime, due to this absorber thickness is limited.

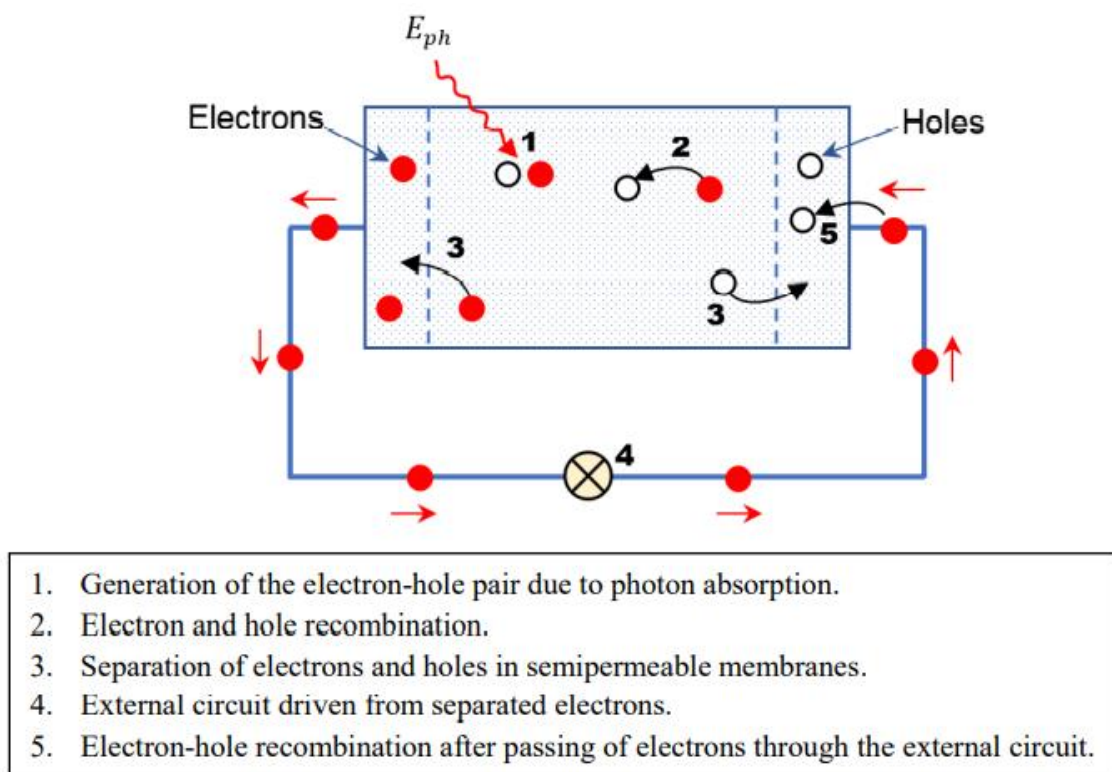


Figure I.2: Simple solar cell model.

I.2.1.3. Extraction of photogenerated charge carriers:

Photo-generated charge carrier due to light absorption is extracted by using externally connected electrical contacts and allows the energy use in the external circuit. This phenomenon is well illustrated in Figure I. 2. In this stage, light energy is converted into electrical energy. At the back contact and absorber layer, electrons recombine with holes after passing from the external circuit.

I.2.2.Solar radiation:

A solar cell having *apn* junction or Schottky barrier structure can convert sunlight directly into electricity. Precise incident solar irradiance power, under different conditions, is used for the calculation of power conversion efficiency of a solar cell [28].The radiant energy particularly electromagnetic energy emitted by the sun is solar radiation. Figure I. 3 illustrates the solar irradiance spectra for two air-mass (*AM*) conditions. The upper curve is the *AM0* solar irradiance spectrum and is measured above the earth's atmosphere. Under *AM0* conduction the irradiant power of the sun is $136.61\text{mW}/\text{cm}^2$.

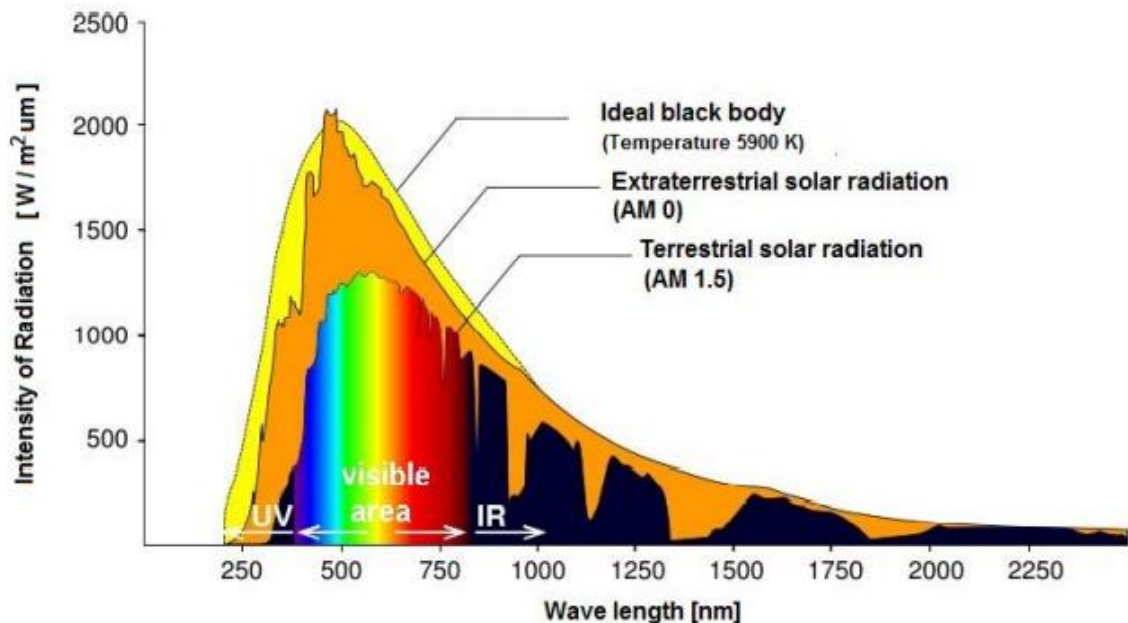


Figure I.3: Solar irradiance spectrums versus wavelength. [28].

The lower curve is the *AM1* solar irradiance spectrum characterizes the sunlight on the earth's surface when the sun is at its zenith angle. Under *AM1* condition, total incident power of sunlight is $92.5\text{mW}/\text{cm}^2$. *AM1.5G*(global) is the standard spectrum at the earth's surface. *AM1.5G* spectrum ($\theta = 48.2^\circ$) has been normalized to give $100\text{mW}/\text{cm}^2$.For the

calculation of solar cell power conversion efficiency in the terrestrial environment, $AM1.5G$ spectrum is the most suitable incident solar irradiance. To calculate the power conversion efficiency of the solar cell, specifying the exact AM condition is very important [28].

I.2.3. Equivalent circuit of solar cell:

To understand the working principle of a solar cell, it is appropriate to make a model which is electrically equivalent. The ideal solar cell simplest model is given in Figure I.4 and consists of a constant current source and parallel connected diode. Constant current source works like a generator to push the electrons to the external circuit. Photocurrent I_L is generated due to the photovoltaic effect. Photocurrent depends on the intensity of the available sunlight, I_L of a current source is directly proportional to solar radiation. It means that with an increase of intensity of available sunlight, I_L must be increased. I_D is the diode dark current of a solar cell [29].

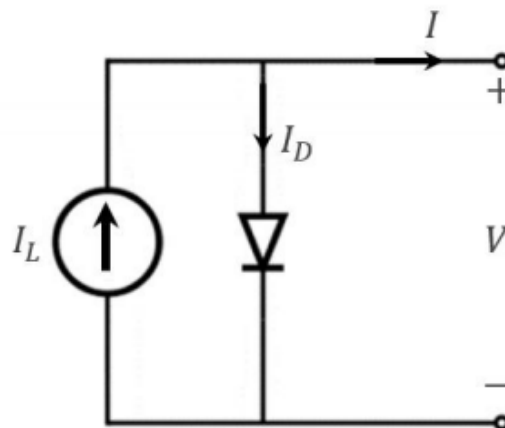


Figure I.4: Ideal solar cell.

Practically photovoltaic cells are not ideal. So, shunt and series resistance components are added to the equivalent circuit. The subsequent equivalent circuit is given in Figure I. 5.

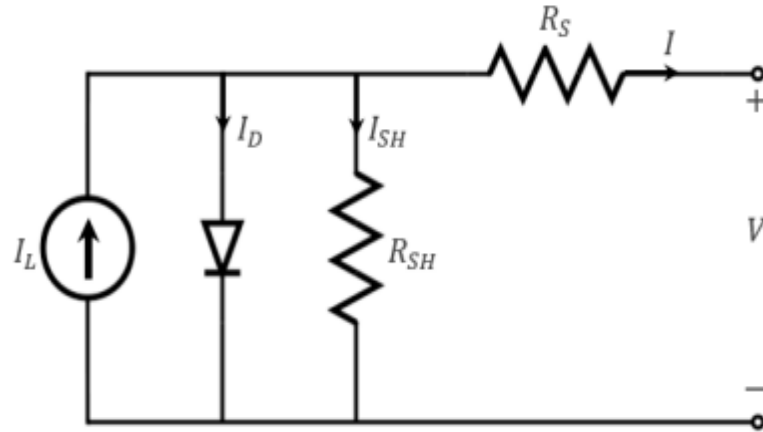


Figure I.5: Photovoltaic cell equivalent circuit.

From the schematic of a solar cell equivalent circuit, it is exemplified that the output current of a photovoltaic cell is the difference of photogenerated current, diode current, and shunt resistance current given in Eq.(I.4)[24].

$$I = I_L - I_D - I_{SH} \quad (I.4)$$

The voltage across these components governed the flow of currents.

$$V_D = V + IR_S \quad (I.5)$$

Where V_D is the voltage across shunt resistance and diode, V is the output terminal voltage and the voltage across the series resistance is IR_S :

Diode current from Shockley diode equation is:

$$I_D = I_S \left[\exp\left(\frac{qV_D}{nk_B T}\right) - 1 \right] \quad (I.6)$$

I_S is the reverse saturation current.

Current flows through shunt resistance can be calculated from ohms law

$$I_{SH} = \frac{V_D}{R_{SH}} \quad (I.7)$$

By substituting these values in Eq.(I.4), we get:

$$I = I_L - I_S \left[\exp\left(\frac{q(V+IR_S)}{nk_B T}\right) - 1 \right] - \left(\frac{V+IR_S}{R_{SH}}\right) \quad (I.8)$$

I.2.4.Characteristic of a photovoltaic device:

Current-voltage ($I - V$) characteristics curve is the graphical representation of the operation of a photovoltaic cell. It can be well understood by considering the equivalent circuit of a solar cell. ($I - V$) characteristic of a photovoltaic cell is the superposition of the ($I - V$) curve of a device in dark (absence of light) and illuminating (under light) conditions [30,31]. In dark conditions, photovoltaic cell has similar electrical characteristics as of large diode. When light falls on the photovoltaic cell, electrical power can be extracted and ($I - V$) curve down into the fourth quadrant. Amount of shift is directly proportional to the incident light intensity on a solar cell as shown in Figure I.6.

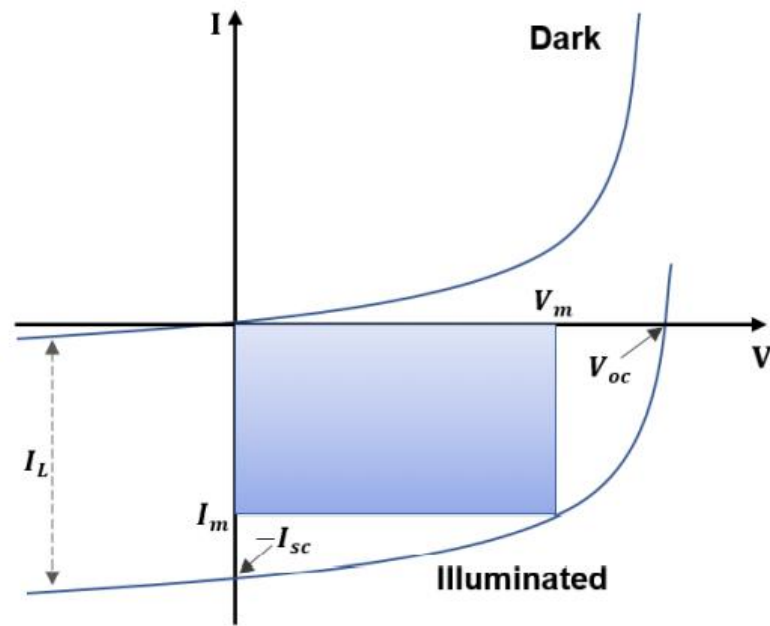


Figure I.6: $I - V$ characteristic of photovoltaic cell under illuminated and dark.

The maximum power is indicated by the shaded area. Illuminated cell added with diode dark currents, diode law becomes:

$$I = I_D - I_L = I_S \left[\exp\left(\frac{qV}{nk_B T}\right) - 1 \right] - I_L \quad (I.9)$$

where I_S is the diode leakage current under dark or dark saturation current, I_L is the light generated current, V is the applied terminal voltage across diode, q is the electronic

charge, k_B is the Boltzmann's constant, n is the ideality factor and T is the temperature.

I.2.4. Basic photovoltaic parameters of the solar cell:

I.2.4.1 Short circuit current:

The maximum current flow through the solar cell at zero load condition (at $R_L = 0$) or short-circuited is known as short-circuit current (I_{SC}). At the largest value of I_{SC} . The voltage of a solar cell will be zero [28]. The flow of I_{SC} is due to the generation and collection of light generated carriers. It mainly depends on the number of incident photons as well as the spectrum, area of solar cell, optical properties and the collection probability of light generated carriers. The graphical representation of I_{SC} is given in Figure I.7.

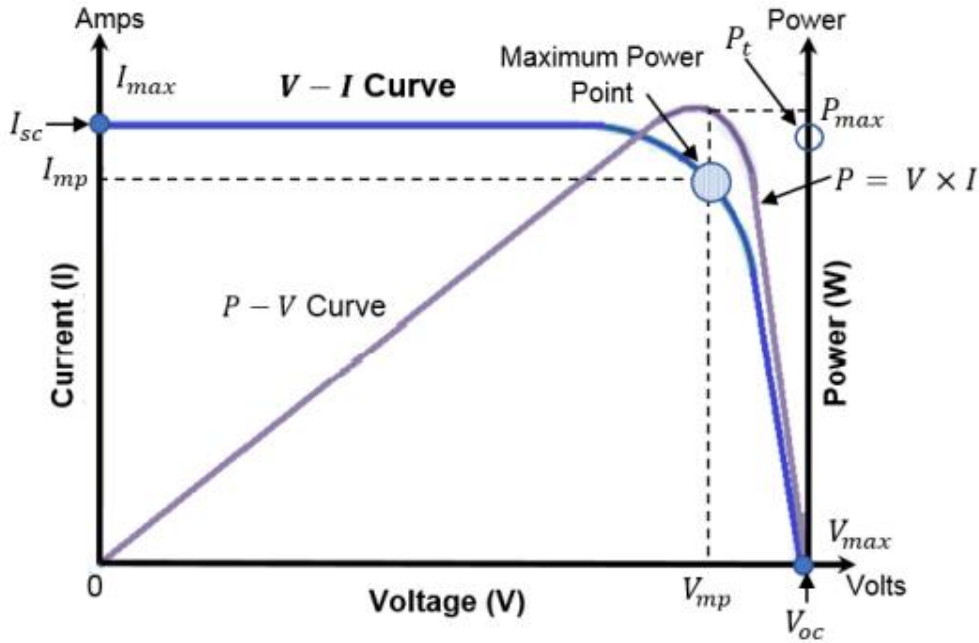


Figure I.7: I_{sc} and V_{oc} representation in $I - V$ cure.

I.2.4.2. Open circuit voltage:

The maximum voltage is taken from the solar cell (at $R_L = \infty$), and is known as open circuit voltage (V_{oc}). When a solar cell is an open circuited, and no load is connected across the solar cell, then current will be at its minimum (zero) value whereas the voltage will be at maximum value [32]. From solar cell equation, V_{oc} can be derived by setting the net current to zero and is given in Eq.(I.10):

$$V_{oc} = \frac{nk_B T}{q} \ln \left(\frac{I_L}{I_S} + 1 \right) \text{ at } I = 0 \quad (I.10)$$

From the above equation, it is clear that open circuit voltage depends on I_S (the saturation current) and I_L , (the light generated current). I_S in the solar cell may be limited by diffusion, recombination or thermionic emission [19]. So, V_{oc} is a measure of the amount of the dominant mechanism in the solar cell (diffusion, recombination or thermionic emission). The graphical representation of open circuit voltage is given in Figure I.7.

I.2.4.3. Fill factor:

The measure of a photovoltaic cell quality is fill factor (FF), which is derived by equating the maximum power (P_{max}) to the theoretical power (P_t). Where power (P_t) would be output at both the open circuit voltage (V_{oc}) and short-circuit current (I_{sc}) given in Eq. (I.11) and (I.12) [33]. Fill factor can be interpreted graphically as the ratio of the rectangular areas depicted in Figure I.8.

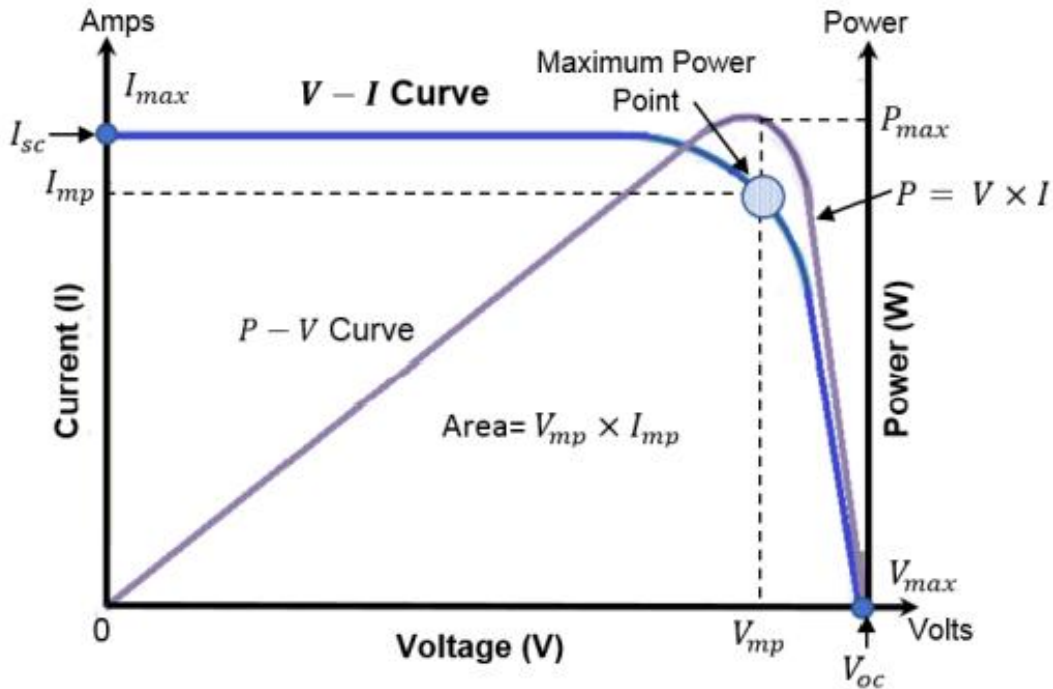


Figure I.8. Attaining fill factor from $I - V$ characteristics curve.

$$FF = \frac{P_{max}}{P_t} \quad (1.11)$$

$$FF = \frac{V_{max}I_{max}}{V_{oc}I_{sc}} \quad (1.12)$$

I.2.4.4. Maximum power:

The output power of a solar cell is given in watts and is equal to the product of voltage times the current and is defined as

$$P_{out} = V_{out}I_{out} \quad (I. 13)$$

Under short and open circuit conditions, no power is generated. The power output will be zero if both or anyone will be zero. The device will provide maximum power for maximum values of voltage and current.

$$P_{max} = V_{max}I_{max} \quad (I. 14)$$

In terms of fill factor, maximum power is by putting Eq.(I.12) in Eq.(1.14), we get:

$$P_{max} = V_{oc}I_{sc}FF \quad (I. 15)$$

I.2.4.5. Power conversion efficiency:

The power conversion efficiency (η) is the most frequently used parameter to relate the performance of two solar cells and is termed as η or *PCE*. It is defined as the ratio of output power from a solar cell to the input power from the sun [32].

$$\eta = PCE = \frac{P_{max}}{P_{in}} \quad (I. 16)$$

$$\text{Where } P_{max} = V_{oc}I_{sc}FF \quad (I. 17)$$

$$\text{and } P_t = V_{oc}I_{sc} \quad (I. 18)$$

Therefore, from Esq. (I.16) and (I. 17), the product of theoretical power (P_t) and fill factor (FF), divided by the power of the energy input from the sun is the power conversion efficiency (η)[34]. η is mathematically expressed in Eq.(I.19).

$$\eta = PCE = \frac{V_{oc}I_{sc}FF}{P_{in}} \quad (I. 19)$$

η or PCE depends on the parameters like incident sunlight intensity, solar cell working temperature and spectrum type. So, to compare two or more solar cells, it is important carefully control the conditions under which PCE is measured. Typical measurement setup for terrestrial solar cells is with an $AM1.5G$ spectrum at a temperature of $25^{\circ}C$.

I.2.4.6. Quantum efficiency:

The quantum efficiency (QE) is the ratio of the extracted free charge carriers by the solar cell to the number of incident photons. In other words, QE relates to the response of a solar cell to different wavelengths. It may be given either as a function of energy or wavelength. The QE will be unity at the precise wavelength if all certain wavelength photons are absorbed and the resulting minority carriers are collected.

I.3. Metal-Insulator-Semiconductor (M-I-S) structure:

The MIS structures with ultrathin insulating layers exhibit many interesting properties by virtue of the direct tunnelling currents which flow between the metal and semiconductor. The physics and applications of these structures have been the subject of many researches [35,17,36,10,37]. One of the most promising applications of MIS tunnelling devices is for solar cells, since it has been conclusively shown that their photovoltaic properties are superior to those of the ideal Schottky barrier. In comparing the MIS solar cell with the p-n junction solar cell it has become clear that the open-circuit voltages of the two under the optimum conditions are approximately equivalent. There are reasons which can improve the short-circuit current densities; in particular 1) the absence of a "dead layer" associated with the diffusion of a surface layer of high doping concentration, and 2) the avoidance of high-temperature diffusion processes is expected to preserve the long minority-carrier lifetime of pure materials such as single-crystal silicon. Perhaps the most important advantage of the MIS solar cell is that this structure is compatible with an arbitrary semiconductor, and in particular with polycrystalline semiconductors since it avoids the problem of diffusion of impurities along the grain boundaries during fabrication. The MIS solar cell has properties which are in general intermediate between those of a Schottky barrier and a p-n junction. The dark current in the MIS device may be dominated either by majority carriers (as in a Schottky barrier) or by minority carriers (as in a p-n junction). This creates two classes of MIS cells, the so called majority-carrier and minority-carrier cells. The photocurrent, of course, is in both cases due to minority

carriers[17]. The MIS structure can be based on n-type silicon, the common structure for that is Au / SiO₂ / n-type Si. The high work function of the frontal electrode (ϕ_m), relatively to the electronic affinity of the n-type Si (χ_s), ensures the establishment of a Schottky barrier at the semiconductor surface; the latter is further increased by the oxide layer inserted between the metal and the semiconductor. The common MIS structure with p-type silicon is Al / SiO₂ / p-type Si. A low metal work function will cause a very large barrier to be induced at the semiconductor surface. Figure I.9 shows typical n-type Si and p-type Si MIS structures. The corresponding energy-band diagram at thermal equilibrium is shown on Figure I.10.

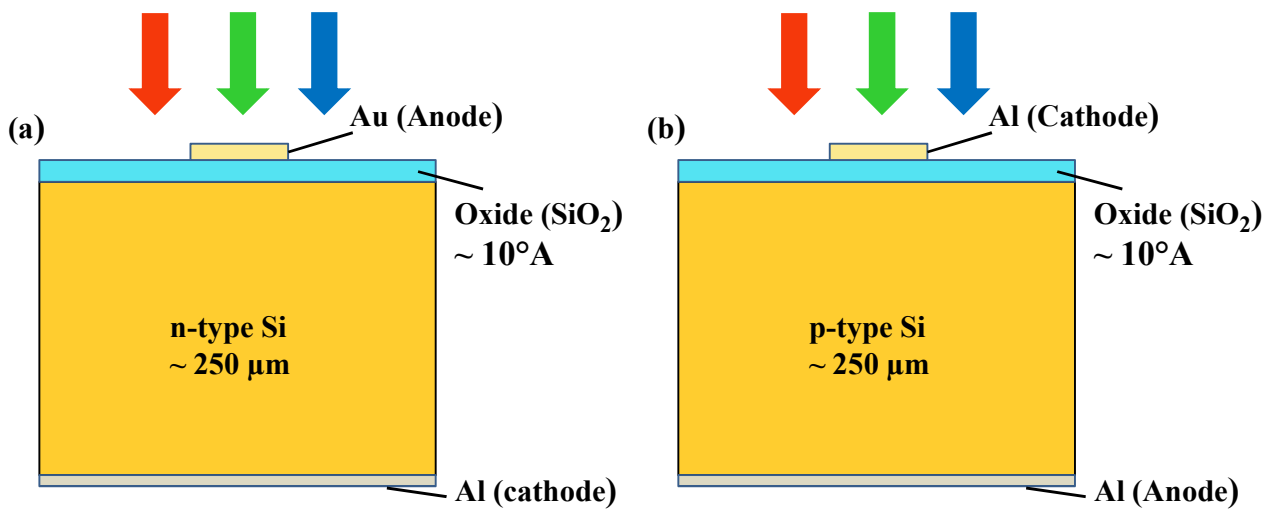


Figure I.9: Typical n-type Si and p-type Si MIS structures.

In MIS solar cells the insulator energy bandgap is considered to be too high to lead to any sunlight absorption and, providing the insulator is kept thin enough ($\leq 20 \text{ \AA}$ in silicon MIS solar cell [18]), tunnelling through the insulator does not cause a photocurrent bottleneck. Thus short-circuit currents in MIS cells should closely match that of p-n junction cells [1]. The saturation current density, J_S , is the major factor influencing the value of FF and V_{oc} [18]. Figure I.11 illustrates the possible dark-current mechanisms in an MIS (n-type semiconductor) diode, and the total dark current is given by [18]:

$$J_D = J_{th} + J_{rg} + J_a + J_{ST} \quad (I.20)$$

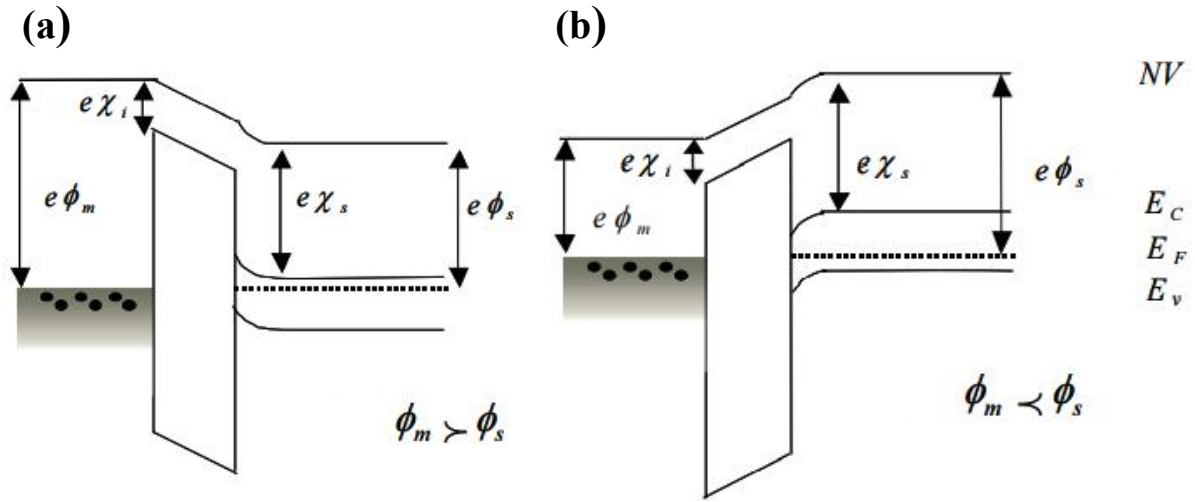


Figure I.10: Energy-band diagram of n-type Si and p-type Si MIS structures, at thermal equilibrium of the depletion regime; where Schottky barrier is established at the oxide/semiconductor interface.

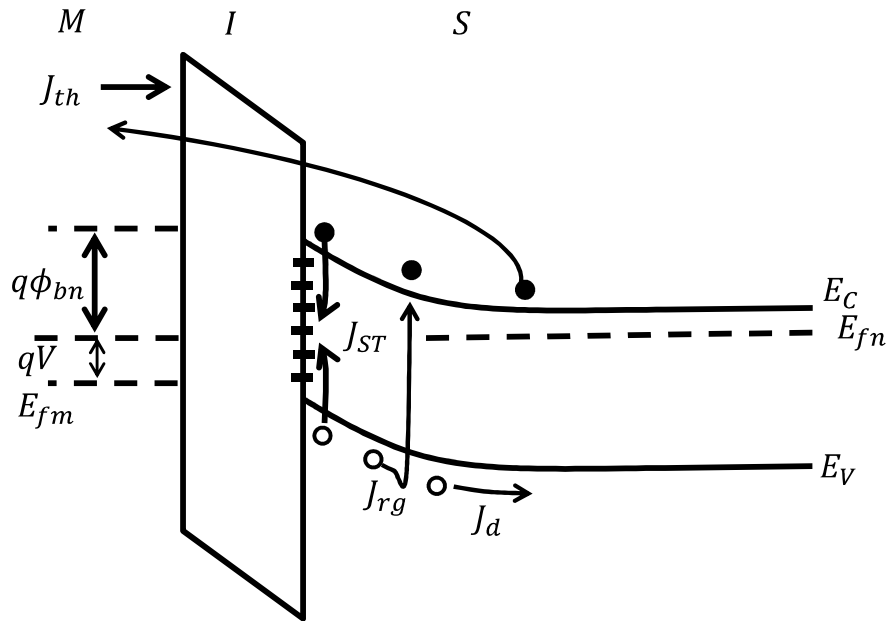


Figure I.11: Dark-current components in forward biased MIS (n-type) diode.

where J_{th} arises from the thermionic emission of electrons into the metal, J_{rg} is the depletion layer recombination-generation current density, J_d is the injection-diffusion current density, and J_{ST} , represents the surface state current density due to charge exchange between the metal and semiconductor band edges via surface states.

Figures I.12 and I.13 show the energy band diagrams for MIS-Schottky barrier solar cell made on n-type semiconductor for dark and illuminated conditions [34].

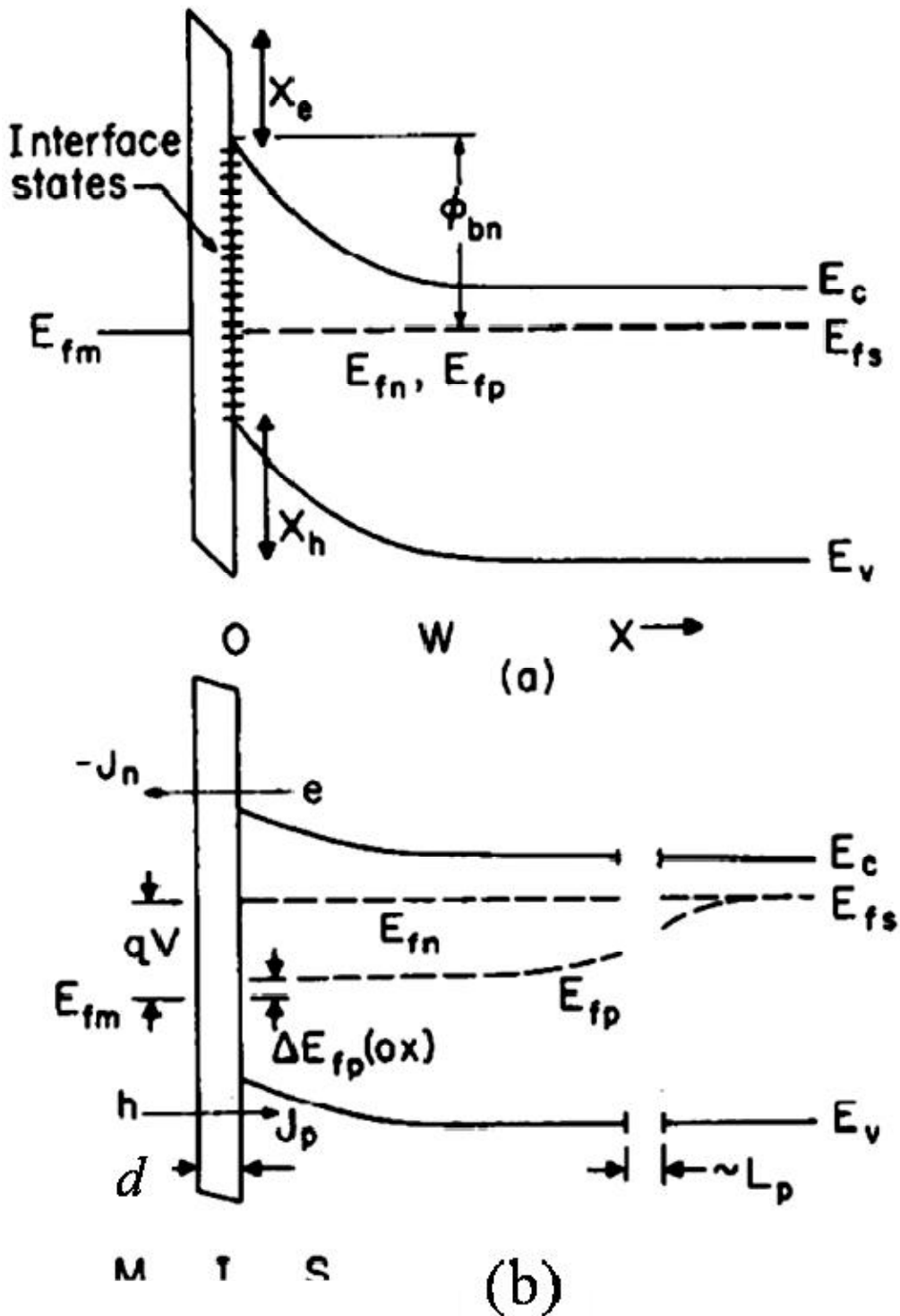


Figure I.12: Energy-band diagrams for n-type MIS-Schottky barriers in the dark (a) $V = 0$ (b) applied voltage $V > 0$.

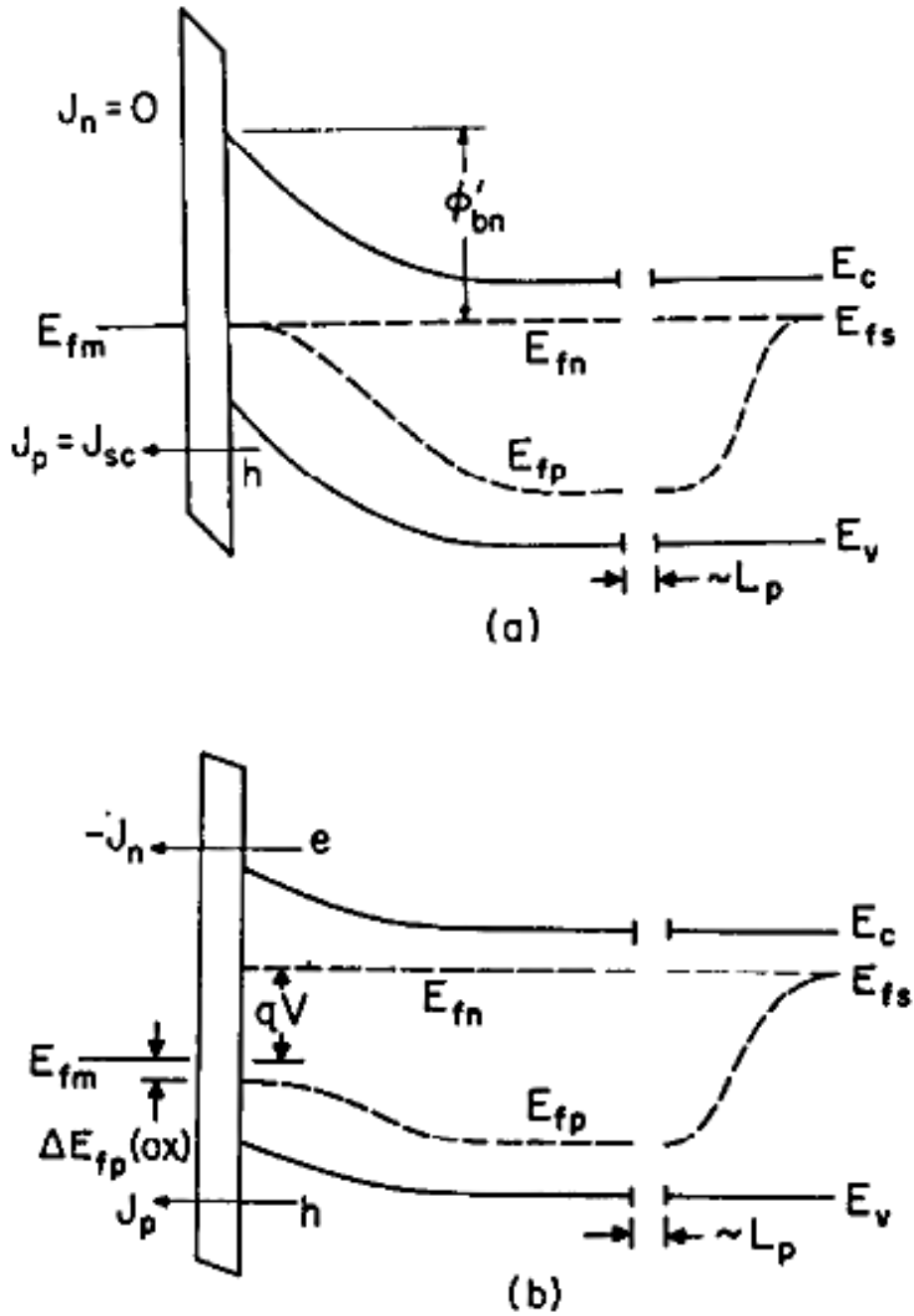


Figure I.13: Band diagrams for n-type MIS-SB solar cell under solar illumination (a) $V=0$ (short circuit conditions, external load $R=0$), and (b) $V > 0$ (voltage induced by illumination for external load $R > 0$).

In the semiconductor, both in the space-charge region ($x < W$) and in the quasi-neutral region ($x > W$), the electron and hole current densities may be written as [38]:

$$J_n = qn\mu_n E + qD_n \frac{dn}{dx} = n\mu_n \frac{dE_{fn}}{dx} \quad (I.21)$$

$$J_p = q p \mu_p E - q D_p \frac{dp}{dx} = p \mu_p \frac{dE_{fp}}{dx} \quad (I.22)$$

where the quasi Fermi levels for electrons (majority-carriers) and holes (minority-carriers), E_{fn} and E_{fp} respectively, are defined by:

$$n = N_C \exp\left(\frac{E_{fn} - E_C}{k_B T}\right) \quad (I.23)$$

$$p = N_V \exp\left(\frac{E_V - E_{fp}}{k_B T}\right) \quad (I.24)$$

In these expressions, $n(x)$ and $p(x)$ are the concentrations of electrons and holes for any position x , E_C and E_V are the energies of the conduction and valence band edges, N_C and N_V , are the effective densities of states in the conduction and valence bands; μ_n , μ_p , $D_n D_p$ are the mobilities and diffusion coefficients.

In the steady state, the currents given by Eqs.(I.21) and (I.22) are equal to the tunnel currents through the oxide layer. In the dark, the electron (majority-carrier) tunnel current through the oxide is given, for $V \geq (k_B T/q)$, by[39]

$$J_n = \frac{q^4 \pi m_{te}^* (k_B T)^2}{h^3} \exp\left(\frac{E_{fn}(0) - E_C(0)}{k_B T}\right) \exp(-(\chi_e)^{1/2} \cdot d) \quad (I.25)$$

$$J_n = A^* T^2 \exp\left(-\frac{q \phi_{bn}}{k_B T}\right) \exp(-(\chi_e)^{1/2} \cdot d) \exp\left(\frac{qV}{nk_B T}\right) \quad (I.26)$$

There are also small contributions from the injection of minority carriers into the quasi-neutral region of the semiconductor, and from recombination in the space-charge region.

The (short-circuit) minority carrier current for the MIS-SB solar cell is due to holes, which are photogenerated in the semiconductor and thereafter tunnel into the metal (equivalent to electrons from the metal tunnelling into the valence band). This current is given by an expression similar to Eq.(I.25), and may be written[39]

$$J_p = \frac{q^4 \pi m_{th}^* (k_B T)^2}{h^3 N_V} \times p(0) \left(\exp\left(-\frac{\Delta E_{fp}(Ox)}{k_B T}\right) - 1 \right) \exp(-(\chi_h)^{1/2} \cdot d) = J_{sc} \quad (I.27)$$

In Eqs.(I.25)-(I.27), χ_e and χ_h are the effective potential barrier of oxide to electrons, holes tunnelling into metal ($\chi_e = \chi_h = \chi$ in approximation), d is the oxide thickness, A^* is the modified Richardson constant $\left(\frac{q^4 \pi m_{te}^* (k_B T)^2}{h^3}\right)$, ϕ_{bn} and ϕ'_{bn} are Schottky barrier heights in

dark and under illumination, m_{te}^* and m_{th}^* effective mass for electrons, holes in the semiconductor with momentum transverse to the barrier.

The total current in the MIS-SB solar cell under illumination is therefore given by

$$J = J_{SC} - J_D \quad (I.28)$$

The diode structure shown on figure I.11 would produce a minority carrier solar cell with the dark current approaching the ideal value ($J_{ST} = 0, J_{rg} \rightarrow 0, J_{th} \rightarrow 0$) of [49]

$$J_{D,min} = J_d \quad (I.29)$$

and characteristics equivalent to that of p-n junction diodes would result.

I.4. TCO-based MIS type solar cell:

In the last decades, the development of MIS type solar cells has considerably much progressed, such as the use of transparent conductive oxides (TCO) to replace metals that have low transparencies [37,40,41,42,43]. TCO are basically semiconductors with wide band gap thus are mainly used as front contact allowing the incident light to penetrate into the substrate layer without losing much energy due to absorption [44]. TCO usually used in MIS structures are indium tin oxide (ITO), SnO₂, TiO₂, fluorine tin oxide (FTO) and ZnO [45,46,47,48]. Among these TCO, ZnO and ITO have the major advantage for their low-cost fabrication process and low-temperature needed for deposition [49]. However, ZnO has more superiority for its excellence property to enhance the light trapping effect owing to its textured surface [50, 51]. Typical structure of ZnO-based MIS solar cell is shown on Figure I.14. The corresponding energy-band diagram at thermal equilibrium is shown on Figure I.15. In our study, we will investigate first a MIS solar cell consisting of Au / SiO₂ / n-type Si. For the second cell, the anode metal (Au) is replaced by heavily doped ZnO (n+-type) to give (n+-type ZnO / SiO₂ / n-type c-Si) structure.

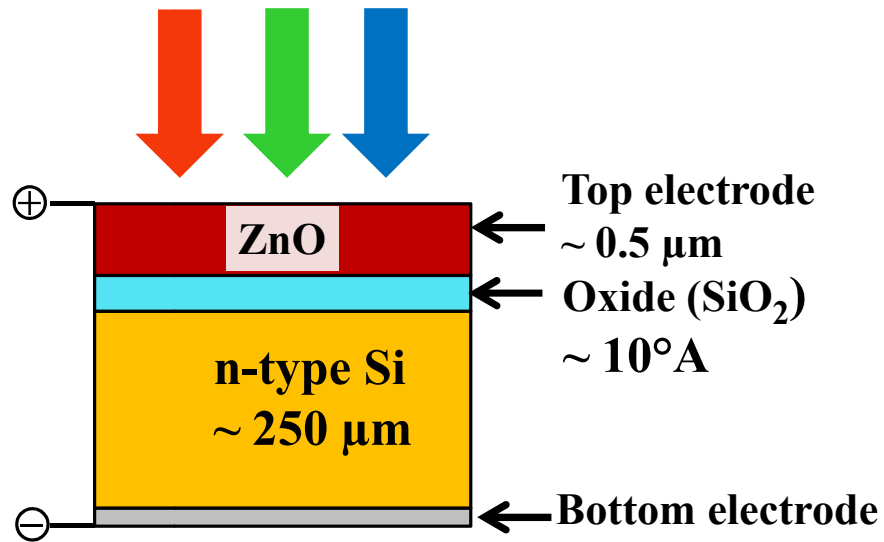


Figure I.14: Schematically illustration of ZnO-based MIS type solar cell.

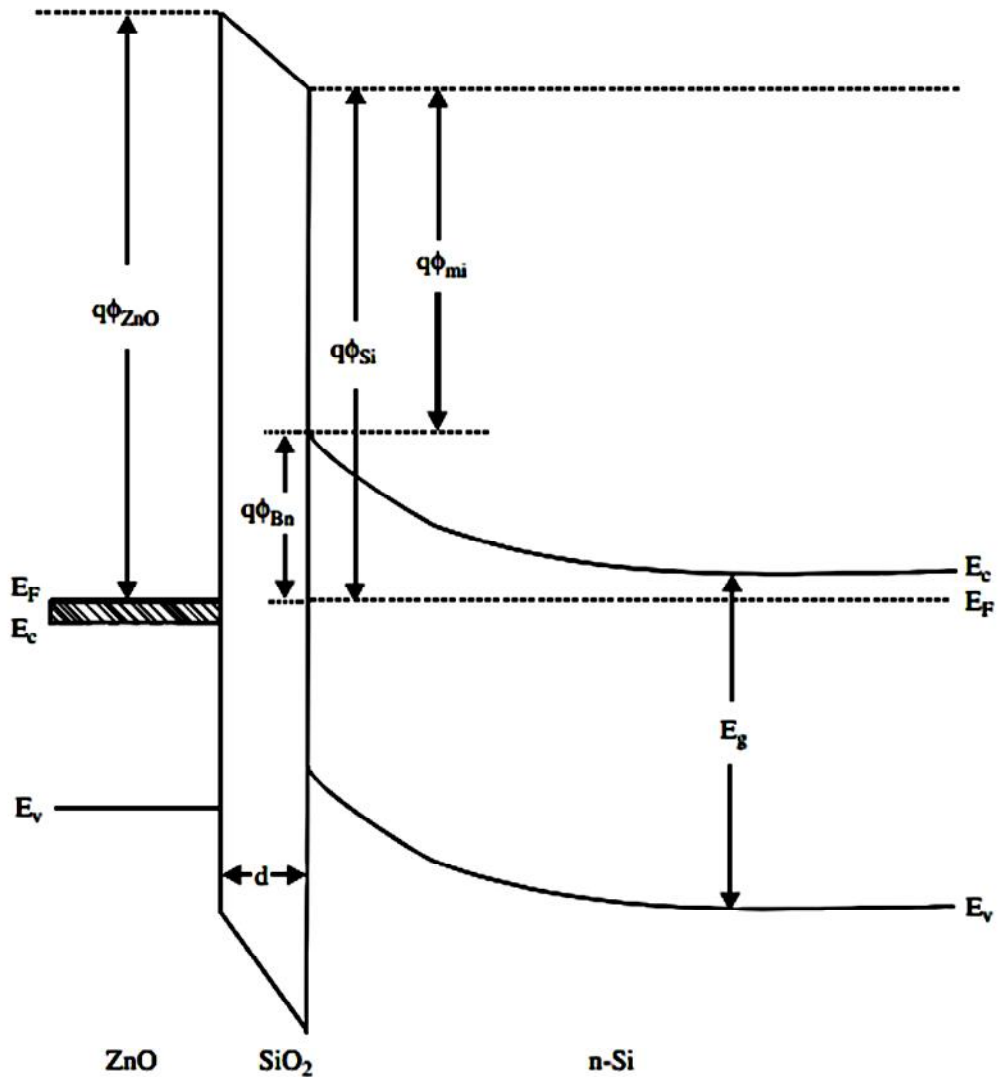


Figure I.15: Band diagram of ZnO/SiO₂/n-type Si solar cell.

I.5. Conclusion:

Metal-insulator-semiconductor (MIS) type solar cells have attracted a lot of interest in the search for low cost photovoltaic solar energy conversion. Compared to p-n junction solar cells, they are relatively easy to fabricate and much cheaper for large scale production. The introduction of insulating layer between the metal and semiconductor has been proven to be able to improve the performance characteristics of the solar cells. In the last decades, the development of MIS type solar cells has considerably much progressed, such as the use of transparent conductive oxides (TCO) to replace metals that have low transparencies.

In the first sections of this chapter, we presented an overview on photovoltaic and working principle of photovoltaic cell. The last sections were devoted to the physic description of the Metal/Insulator/ Semiconductor (M-I-S) and TCO-based MIS structures for solar cells.



Chapter II



***Solar cell simulation using SILVACO-ATLAS
software***



II.1. Introduction

Silvaco Atlas is a software package used to simulate semiconductor devices. It predicts the electrical behaviour of a device, which can be modelled in either two dimensions (2D) or three dimensions (3D). The software consists of several integrated programs that work together to achieve the desired results. The main programs are Deckbuild, Devedit, Tonyplot, and Athena, but there are several subprograms that are accessed during simulation that serve more specific functions. These programs give the user the ability to simulate the production process to manufacture a semiconductor device and test its characteristics. There are many models, numerical methods, and types of material built into the program, giving a wide range of functionality to the user. This allows the modelling of anything from simple devices to complex circuits [52].

Atlas is a physically-based device simulator that predicts the electrical characteristics based on physical structures and bias conditions. It does this by applying a set of differential equations based on Maxwell's laws and the semiconductor transport equations to the nodes of a grid overlaid on the device. The three equations derived from Maxwell's laws are Poisson's Equation, the continuity equations, and the transport equations. This allows the simulation of transport carriers through the structure.

II.2. SILVACO- ATLAS as numerical modelling software

Since its founding in 1984 by Dr. Ivan Pesic, SILVACO has grown to become the most important semiconductor device simulator[56]. SILVACO TCAD is the abbreviation of Silicon Valley Corporation Technology Computer Aided Design. It is a semiconductor process simulation package which consists of several physically based simulators (ATHENA, ATLAS, MERCURY, SSUPREM3 ... etc.) gathered under one environment called DECKBUILD. Each of them simulates different processes [53].

To simulate the device, Atlas may have to solve up to six equations depending on the models selected. For each model type there are three techniques, decoupled Gummel, fully-coupled Newton, and Block. The Gummel method solves each unknown while keeping the other variables constant. It continues to do this until a stable solution is found. The Newton method solves the total system of equations together to find a solution. The Block method solves the equations using a combination of the Newton and Gummel methods, in that some equations are solved fully coupled and the rest are de-coupled.

DECKBUILD :Deckbuild (see Figure II.1) is the main program that runs the simulation and calls the associated programs as needed. Deckbuild uses command line code to designate what and how to run. To run Atlas simply type:

Go atlas

This runs the Atlas program within Deckbuild and is usually the first command unless running one of the other programs, such as Athena, first. Once Atlas is initiated, the next step is to set the parameters of the device.

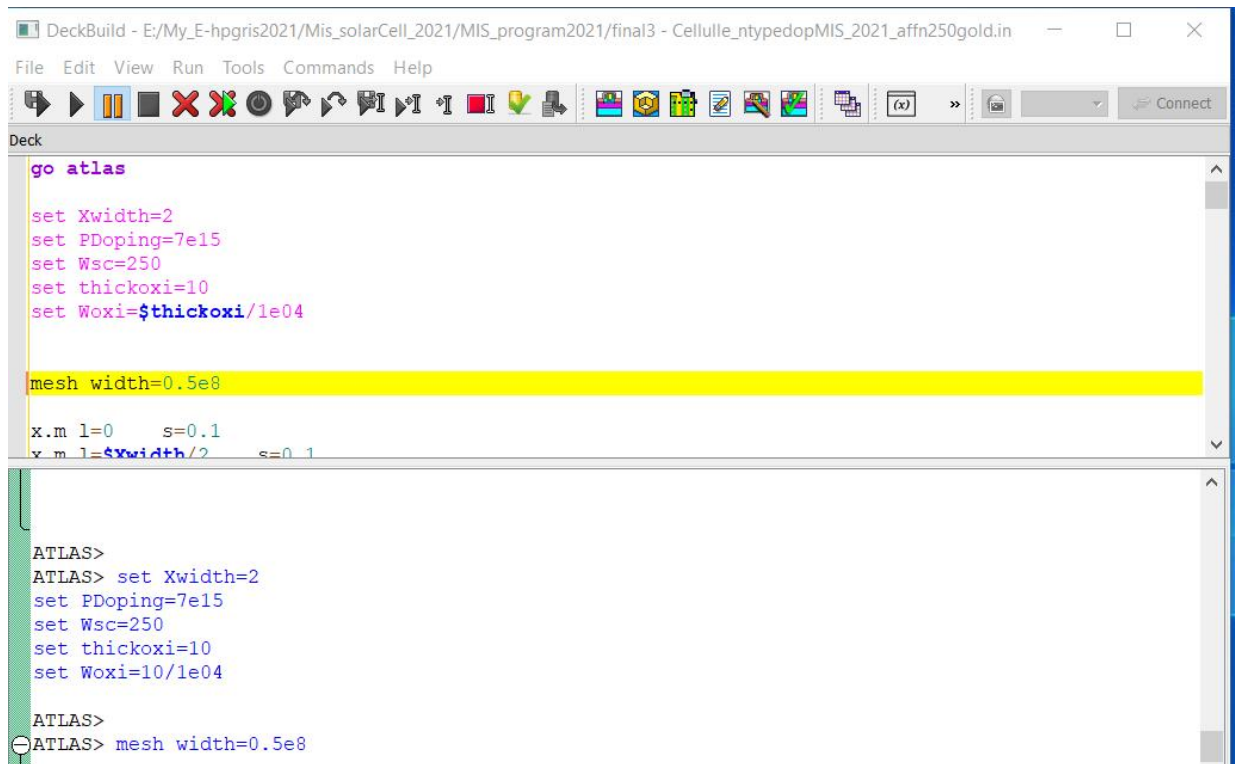


Figure II.1:Screenshot from Deckbuild.

Atlas has a specific order (see Figure II.2) in which the statements must be placed; otherwise the program may not function correctly. Even if it does run, it is possible that certain parameters may not be used, which causes inaccurate results. Generally the format is:

<STATEMENT><PARAMETER>=<VALUE>

Statements can have more than one parameter defined. Deckbuild provides many built-in examples of different devices that allow a user to run the simulation and view the results. The examples are helpful to see how the code is written when unsure how it is used.

<i>Group</i>		<i>Statements</i>
1. Structure Specification	————	MESH REGION ELECTRODE DOPING
2. Material Models Specification	————	MATERIAL MODELS CONTACT INTERFACE
3. Numerical Method Selection	————	METHOD
4. Solution Specification	————	LOG SOLVE LOAD SAVE
5. Results Analysis	————	EXTRACT TONYPLOT

Figure II.2:Atlas statement hierarchy, from [55, p. 34].

ATLAS is a physically based device simulator module which predicts the electrical characteristics that are associated with specified physical structures and bias conditions. This is achieved by approximating the operation of a device onto a grid (discretizing). The transport of carriers through this device can be simulated by applying a set of differential equations, derived from Maxwell’s laws onto this grid. This means that ATLAS provides a platform to analyse AC, DC and time domain responses for all semiconductor based technologies in two and three dimensions.

TONYPLOT: is a visualization tool which plots the results obtained from simulation. It provides scientific visualization capabilities including xy plots with linear and logarithmic axes, polar plots, surface and contour plots.

II.3. Application of Silvaco-Atlas in the numerical simulation of the MIS solar cell based on Silicon (general steps)

II.3.1 Building the device:

When building the device to be simulated, the first thing to do is to define the mesh that will be the framework for the model. A mesh is a collection of triangles that overlays the device (see Figure II.3). Each corner of the triangle is called a node. Nodes are where the equations used to solve for a solution are calculated. When running simulations for a 2D device, there is a limit of 100,000 nodes. A finer mesh results in more triangles, which give more nodes and increases the resolution of the solution to give more accurate results. The downside to this is that the larger number of calculations require an increase in the time it takes to run the simulation. A coarser mesh has the opposite effect. Fewer triangles, less nodes, and less accuracy, but the run time is shorter. The key to setting up a mesh is to recognize where in the device things are happening (such as at a junction). In these areas a finer mesh is desired so that information is not lost. If the triangles are too big, and the characteristics of the device changes too much, then the calculations will not reflect actual conditions.

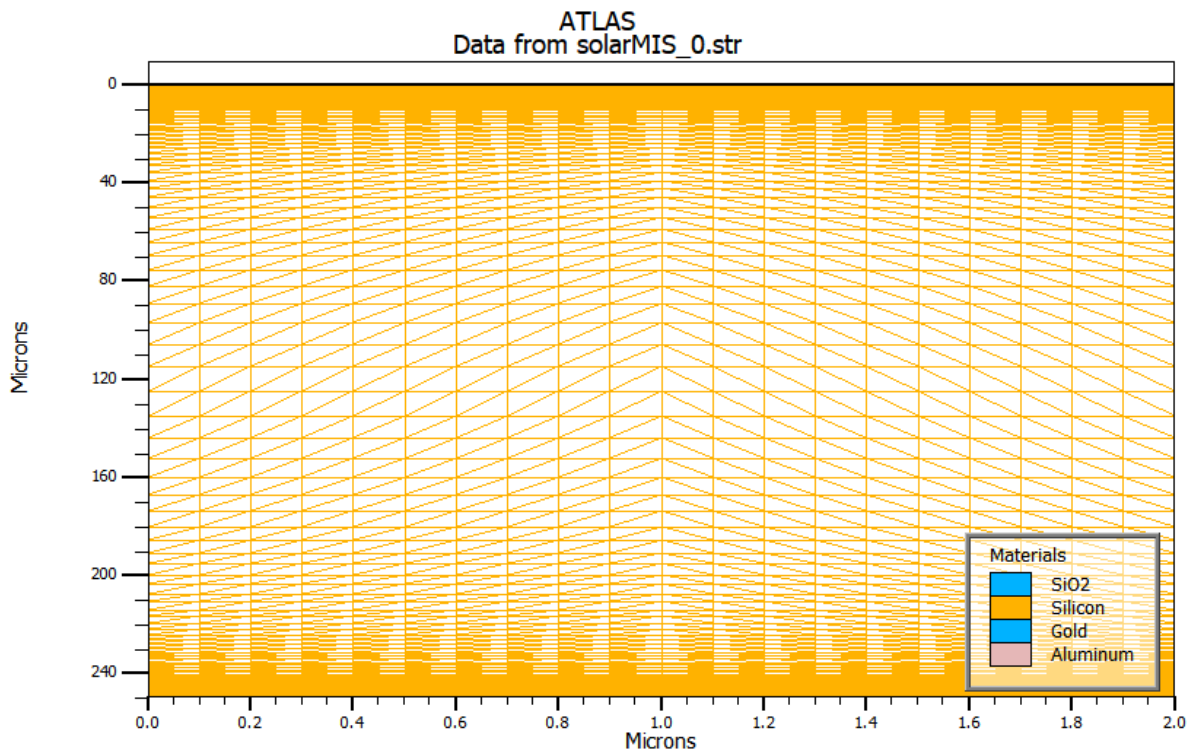


Figure II.3: Mesh example for MIS solar cell based on Silicon (n-type)

II.3.2 Defining the Structure

There are three ways a structure can be made. The first, is it can be read in by a previously created structure that has been saved in a separate file. This is done by typing the command line:

```
MESH INFILE=<filename>
```

The second way to define a structure is to use the automatic interface feature of Deckbuild. The automatic interface feature allows a user to run Athena or Devedit from within Deckbuild using the “Go Athena” (or “Go Devedit”) command input. Once the structure is built, run Atlas to run the simulation. This is all done within the same window. The automatic part is due to the handoff of structure information between Athena/Devedit and Atlas. The third way to define a structure is to simply use the command language in Deckbuild to define the structure. The command language for this is:

```
MESH SPACE.MULT=<value>
```

Space.mult is a scaling factor that controls the granularity of the mesh. The default value is one. Any value greater than one gives a coarser mesh, and a value less than one results in a finer mesh. The next statements define where mesh lines in the x and y direction will be:

```
X.MESH LOCATION=<value> SPACING=<value>
```

```
Y.MESH LOCATION=<value> SPACING=<value>
```

These two statements specify the location of the line and the spacing in microns. At least two x and two y statements are needed to define the mesh. If a different spacing is used, Deckbuild automatically inserts extra lines to allow for a gradual transition. An alternate method to the space.mult command is to use the automatic mesh function:

```
MESH AUTO
```

This statement is followed by x.mesh statements. When using the automatic mesh there is no need to use the y.mesh command inputs because the y-axis mesh is automatically determined based on the region statements.

II.3.3. Regions:

Once the mesh has been defined, the next step is to define the regions. If a region has been imported from Athena or Devedit, this may not be necessary unless more regions are needed. A typical region statement is:

```
REGION NUMBER=<integer><material_type><position_parameters>
```

When using the command line, these regions are numbered, starting with one, up to a maximum of 1000 for a device. Should a user misnumber the regions, Deckbuild automatically numbers them with consecutive numbers. Awkward numbering can be confusing when observing results because the region numbers in the code will not match those in the plots. The material type parameter defines the type of material for the region. The properties for many materials are already stored in the program. They can be changed in a material statement further down in the code once the entire mesh is complete and doping concentrations are defined. The position parameter defines the location in microns of the region. One way to define the location is with x.min, x.max, y.min and y.max statements that look like:

X.MIN=<location> X.MAX=<location> Y.MIN=<location> Y.MAX=<location>

The x.min lists the minimum position in the x-direction, and x.max lists the maximum position in the x-direction. The same holds true for the y-axis. It should be noted that the x-axis starts at zero on the left and is maximum on the right, just like a standard x-y Cartesian coordinate system. The y-axis, however, is opposite what one might expect. The y.min starts at zero on the top, and downward is maximum (see Figure II.4). It is important to remember the axis convention since many aspects of the program are position dependent and need to be accurate to ensure proper results. It would not be wise to define a light source underneath a solar cell when trying to simulate its output. Likewise, it would prove confusing for others trying to understand the code and simulation if the standard convention is not followed. It is not always necessary to define both a maximum and minimum for a particular direction. Defining only one suffices, and the program extends the region to the dimensions of the mesh. If x.min=10 was defined but no x.max, then the region starts at 10.0 microns and extend all the way to the maximum x-value defined in the mesh. The same thing occurs for the y-direction as long as y.max was defined for the mesh, which is not the case when using the auto mesh feature.

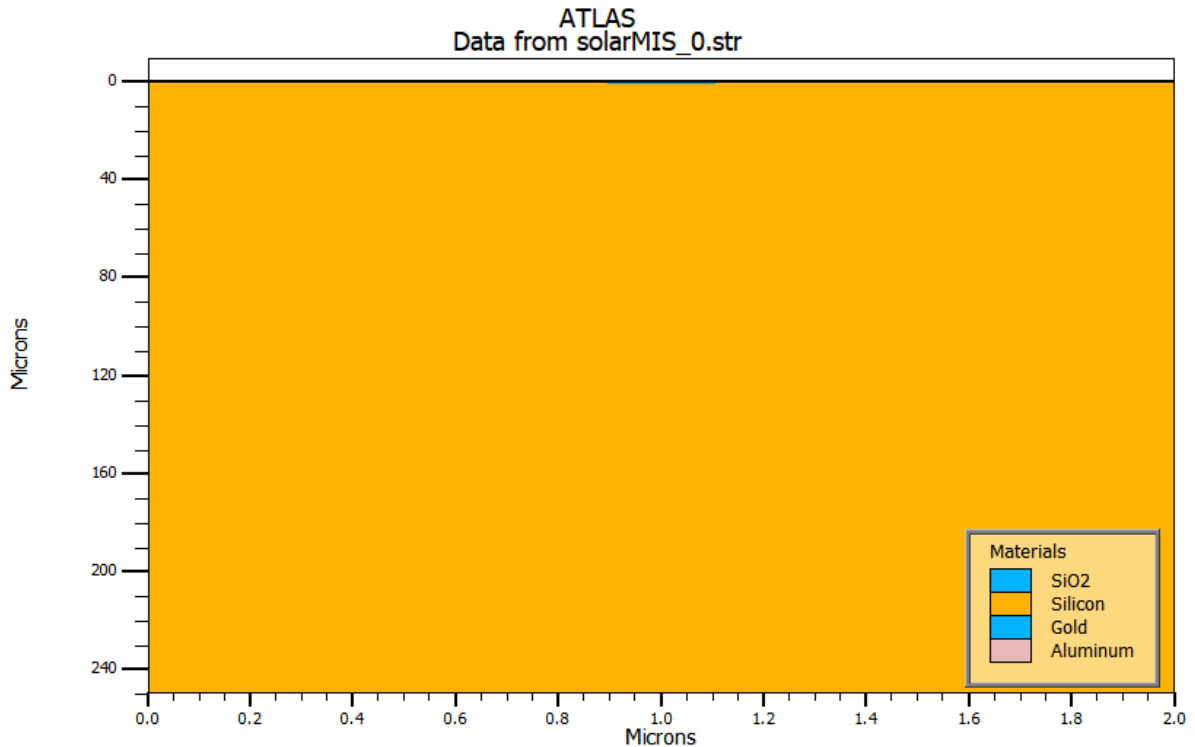


Figure II.4: Tonyplot screenshot showing the layout of the x and y-coordinate system in Atlas for MIS solar cell based on Silicon (n-type).

II.3.4 Electrodes:

Once the regions and materials are specified, the electrodes can be defined. There must be a minimum of one electrode (that touches the semiconductor material) defined for the program to work. Up to 100 electrodes can be specified, and if any of the defined electrodes are given the same name, then the electrodes are considered electrically connected. A typical electrode statement is:

```
ELECTRODE NAME=<electrode name><postion_parameter>
```

If no y-coordinate is given, then the electrode is placed at the top of the device. The top, bottom, right and left parameters can be used to define the location as well. Figure II.5 shows the electrode positions of the Si(n-type)-based MIS solar cell. The anode (gold) is placed on the top of the cell and is treated as a Schottky contact. The CONTACT statement is used to specify the metal workfunction of the anode as follows:

```
contact name=anode workfun=5.47
```

The cathode (aluminium) is placed on the bottom of the cell and is assumed to be ohmic. So, we don't specify a workfunction for the cathode.

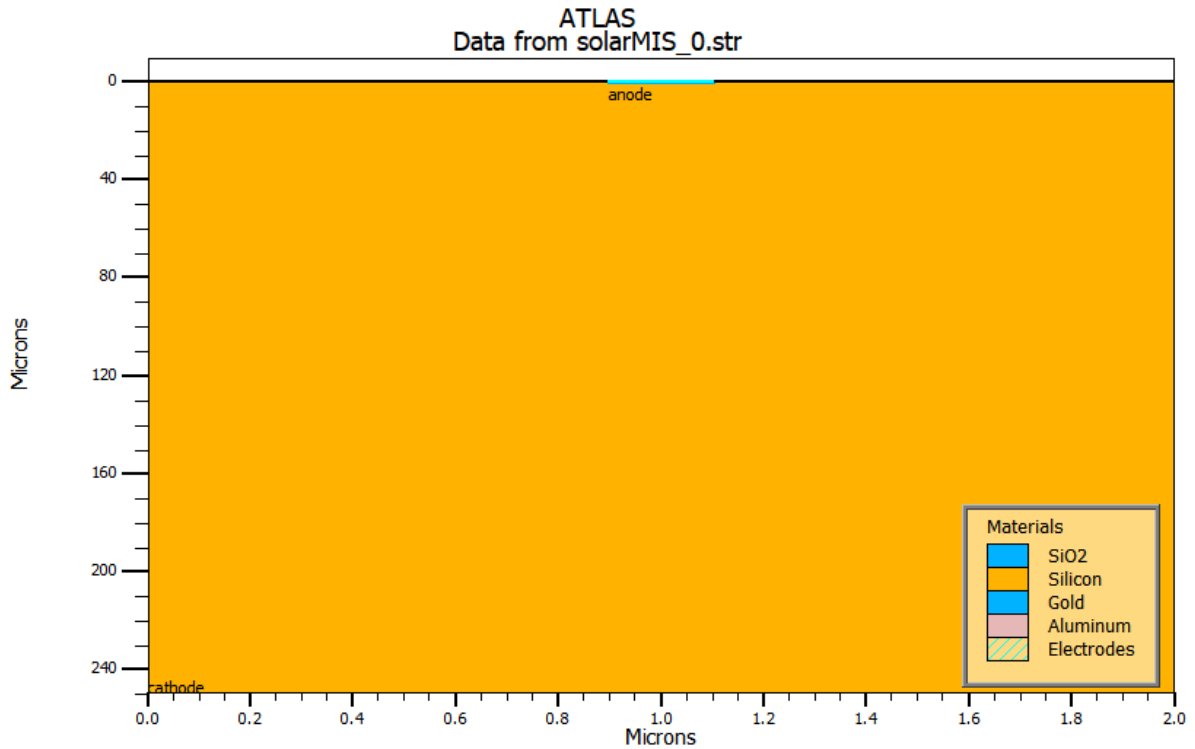


Figure II.5: Electrode positions of the Si (n-type)-based MIS solar cell.

II.3.5 Doping

Doping parameters are specified next and are generally in the form:

DOPING <distribution_type><dopant_type><postion_parameter>

The distribution type can be uniform, Gaussian, or complementary error function. The dopant type can be specified as n.type or p.type, and the concentration amount can be defined. The position parameter can be specified by region number or the minimum/maximum parameters.

II.3.6 Modifying Parameters

After the mesh, geometry, and doping parameters have been defined, the characteristics of the electrodes can be changed, the material parameters modified, and the physical models chosen. The electrodes in contact with a semiconductor material are ohmic by default. As we indicated in the electrode section (section II.3.4), defining a work

function with the contact statement causes it to be treated as a Schottky contact. Using the materials statement allows the user to change properties of the specified material such as electron mobility, bandgap, or carrier lifetime. Specifying region after the material statement changes the material properties for the material in only the specified region and is useful when multiple regions are made of the same material but not all of them need to be changed. To specify the physical models, use the models statement followed by the name of the models. Adding print in the model statement displays the models and parameters used during the simulation into the runtime output, and allows the user to ensure the correct parameters were used.

II.3.7 Numerical Solutions

The next thing to define is the numerical solution which tell the program which numerical methods to use when calculating solutions for the device. There are three methods that Deckbuild uses. They are Gummel, Block, and Newton which are specified after the method statement. Each numerical method uses a different approach to solving the equations. The Gummel method solves for each unknown while keeping the variables constant. It continues doing this until a stable solution is found. The Newton method solves the total system of unknowns together, and the Block method solves some of the equations the Gummel way and the rest the Newton way. Generally, the Newton method is preferred and is the default if the method statement is not used.

II.3.8 Obtaining Solutions

To obtain solutions for the created device, the user has the options of using DC, AC, small signal, and transient voltages for the calculations. Once the voltages for the electrodes are defined, Atlas calculates the currents and the internal quantities. To set the voltage of an electrode named anode:

```
SOLVE VANODE=1.0
```

This sets the anode voltage to one volt. Multiple solve statements can be used in succession to ramp up the voltage or a sweep can be used:

```
SOLVE VANODE=0 VSTEP=0.5 VFINAL=5 NAME=anode
```

```
SOLVE VSTEP=0.5 VFINAL=10 NAME=anode
```

This sweeps the voltage from zero volts to five volts in one-half volt increments. The second solve statement sweeps from five volts to ten volts in one-half volt increments. Atlas remembers the last voltage of the electrode, five volts after the first solve statement and ten volts after the second solve statement. If an anode voltage was stated in the second solve statement, then the starting voltage for the sweep is instead set to this value. When Atlas attempts to find a solution, the program uses an initial guess for the variables to be evaluated at each bias point. The initial guess usually comes from the two previous solutions, and if none are available convergence problems can arise. When previous solutions are not available, Atlas uses the doping profile to make the initial guess for potential and carrier concentration. To do this the initial solution must be made at zero bias which is done by:

```
SOLVE INIT
```

If this statement is not included, Atlas automatically evaluates an initial solution prior to the first solve statement.

II.3.9 Results

When running the simulation it is useful to open a log file to save the terminal characteristics calculated by Atlas. To save the terminal characteristics, open a log file prior to any solve statements:

```
LOG OUTFILE=<filename>
```

This opens a log file and saves it under the chosen filename. All outputs from solve statements are saved in this log file until either another log statement is opened under a different filename or the log is closed by using the log statement with the off parameter. Once the simulation is complete, this log file can be used in Tonyplot to view the results. The electrical current values stored in the log file are generally in Amperes per micron, because Atlas is a 2D simulator and sets the z-axis to be one micron. If a width dimension is specified, the cylindrical coordinate system is used, or when simulating a 3D device, then the units are in Amperes. The log file is also useful for extracting parameters by using the extract command:

```
EXTRACT INIT INF=<filename>
```

This uses the specified file to perform the extraction. If a log file is currently open, then there is no need to specify a file, as the extract statement defaults to the currently open log file. Calculation can be performed on the extracted data and the results saved in a file for later use such as viewing in Tonyplot. The results from the extraction display in the run-time output and are stored in a file called results.final. The user can also specify a different file in which to store the results by adding a different file at the end of the extract statement:

```
EXTRACT.....DATAFILE=<filename>
```

Another type of file that provides utility is a solution or structure file, which contains an image of the device at a particular bias point and gives the user the ability to view several parameters of the device. Having the ability to view the device parameters allows a user to see what is going on at that particular point in the simulation. These parameters can greatly assist in troubleshooting the simulation by giving the user an idea of what part of the code to examine for problems.

II.3.10 Luminous:

Luminous is a general purpose program integrated into Atlas that is used for light propagation and absorption. Luminous calculates the optical intensity within a device and uses this to find the photo-generation rates used in the solution equations. There are four physical models for light propagation. Ray tracing is a general method for resolving nonplanar geometries and is generally the preferred starting point but ignores the effects of diffraction and coherence. The transfer matrix method is a 1D method and is recommended for large area devices that includes interference effects. The beam propagation method is a general 2D method that is computationally intensive because it includes diffraction effects. Finally, the finite-difference, time-domain method is a general 2D and 3D method that is the most computationally intensive because it includes both diffraction and coherence effects.

II.3.11 Solar cell simulation

The light propagation and absorption properties of Luminous make it ideal for simulation of solar cells. The user has the ability to define the spectra used in the simulation or to use the built-in spectra for AM0 and AM1.5. To define a beam statement:

```
BEAM NUM=1 AM1.5 X.O=1 Y.O=-1.5 ANGLE=90 \
```

```
WAVEL.START=0.200 WAVEL.END=2.5 WAVEL.NUM=200
```

Here the AM1.5 spectrum is specified and is sampled between 0.2 microns and 2.5 microns with 200 samples. The propagation model for the light can also be stated in the beam statement. To get the simulation data, solve statements are used. The first statement is usually:

```
SOLVE B1=1.0
```

This turns on the light beam. In this example, the value one corresponds to full intensity. Values less than one reduce the intensity and larger values increase the intensity, such as with a solar concentrator. Once the beam is turned on, it is necessary to open a log file to save the current and voltage characteristics and set the voltage of one of the electrodes. Extract statements can also be used to pull pertinent data and solve for common characteristics of solar cells like the fill factor, efficiency, maximum output power, open circuit voltage, and short circuit current, which are shown in the following example:

```
extract name="ISC_[mA/cm^2]" y.val from curve(v."anode",i."cathode"*1e3) where  
x.val=0.0
```

```
extract name="VOC_[V]" x.val from curve(v."anode",i."cathode"*1e3) where  
y.val=0.0
```

```
extract name="Vmax_[V]" x.val from curve(v."anode",v."anode"*i."cathode") where  
y.val=max(v."anode"*i."cathode")
```

```
extract name="Imax_[mA/cm^2]" x.val from curve
```

```
(i."cathode"*1e3,v."anode"*i."cathode") where y.val=max(v."anode"*i."cathode")
```

```
extract name="power" curve(v."anode",(v."anode"*i."cathode"))
```

```
outfile="powerlight_MIS.dat"
```

```
extract name="Pmax" max(curve(v."anode", (v."anode" * i."cathode" )))
```

```
extractname="FF"
```

```
($"Vmax_[V]"*$"Imax_[mA/cm^2]"/($"VOC_[V]"*$"ISC_[mA/cm^2]"))
```

```
extractname="EFF_[%]" "$Vmax_[V]"*"$Imax_[mA/cm^2]"
```

With the graphical tool Tonyplot, we can plot data obtained from device simulations. It can be called directly in Deckbuild by typing:

```
TONYPLOT <filename> -overlay
```

If the file is a log file, Tonyplot displays the data in an x-y plot. If the file is a structure file, the information is displayed as a 2D mesh plot.

As an example, Figure II.6 shows the current density- voltage ($J - V$) characteristics obtained from the simulation of Si -based MIS solar cell, in the dark and illumination conditions.

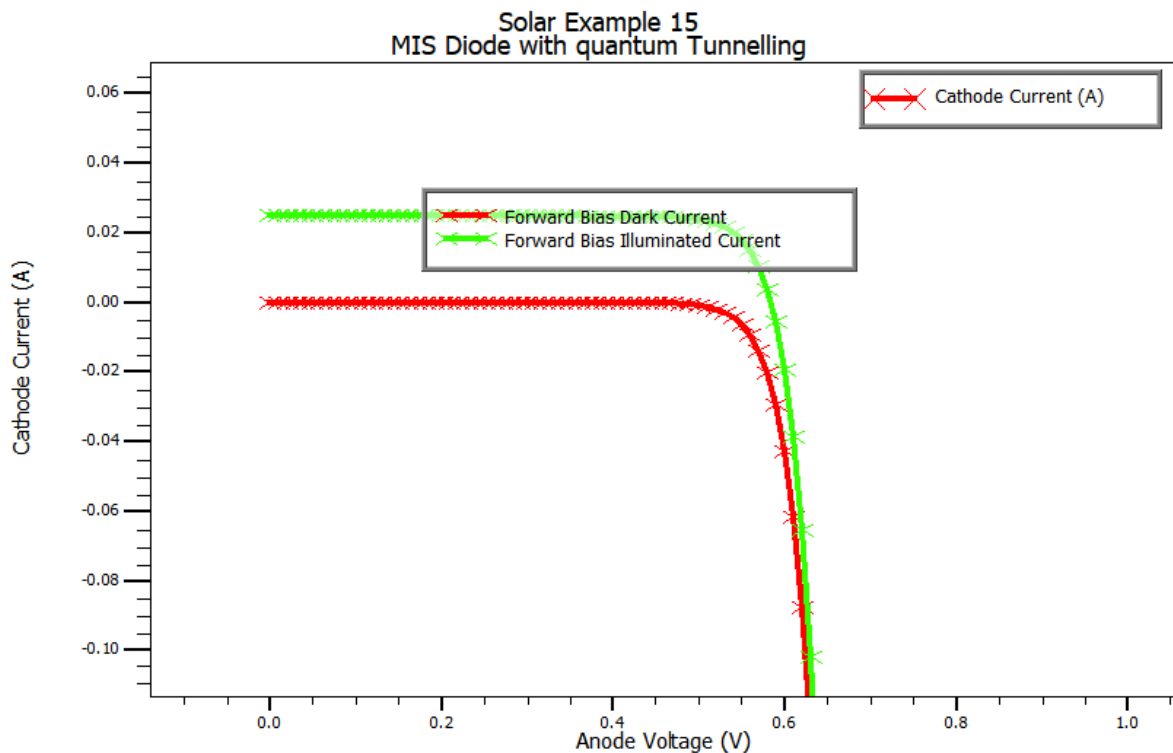


Figure II.6: Simulated $J - V$ characteristics of the Si -based MIS solar cell, in the dark and illumination conditions with AM1.5 spectrum.



Chapter III



Investigation of the MIS silicon solar cell



III.1. Introduction:

In this chapter, we present the performance study of a solar cell based on Metal-Insulator-Semiconductor (MIS) structure, in which the anode metal is gold (Au), the insulator is silicon dioxide (SiO_2) and the semiconductor is n-type crystalline silicon (c-Si) (Au / SiO_2 / n-type c-Si). The investigation is carried out using the numerical simulation software SILVACO-ATLAS, which allows the calculation of all the internal parameters of the solar cell such as the distribution of the band diagram, the electron and holes concentrations...etc. The external parameters are also calculated such as the current density-voltage ($J - V$) and the provided power - voltage ($P - V$) characteristics under illumination, which allow the extraction of the output photovoltaic parameters of the solar cell namely the short circuit current density J_{sc} , the open circuit voltage V_{oc} , the fill factor FF , the maximum power P_{max} provided by the cell and the photovoltaic conversion efficiency η of the cell.

In this study, we consider two solar cells, the first cell, as said above, consisting of Au / SiO_2 / n-type c-Si. In the second cell, the anode metal (Au) is replaced by heavily doped ZnO (n+-type) to give (n+-type ZnO / SiO_2 / n-type c-Si) structure. For the two considered solar cells, we investigate the thickness variation effect of the silicon layer in the range [10-500 μm], the thickness effect of the oxide (SiO_2) layer in the range [2-20 \AA], and the n-type doping concentration effect of the silicon layer (N_d) in the range [$7 \times 10^{12} - 7 \times 10^{18} \text{cm}^{-3}$]. For the second solar cell, further investigation is achieved under the variation effect of the ZnO layer thickness in the range [0.05-10 μm] to bring more improvement to the solar cell performance. The two studied solar cells are exposed to the AM1.5 standard spectrum at ambient temperature (300 $^\circ\text{K}$).

III.2. Description of the studied MIS silicon solar cell:

The two considered solar cells are presented respectively in cases (a) and (b) of figure III.1. The corresponding spatial mesh is shown on figure III.2.

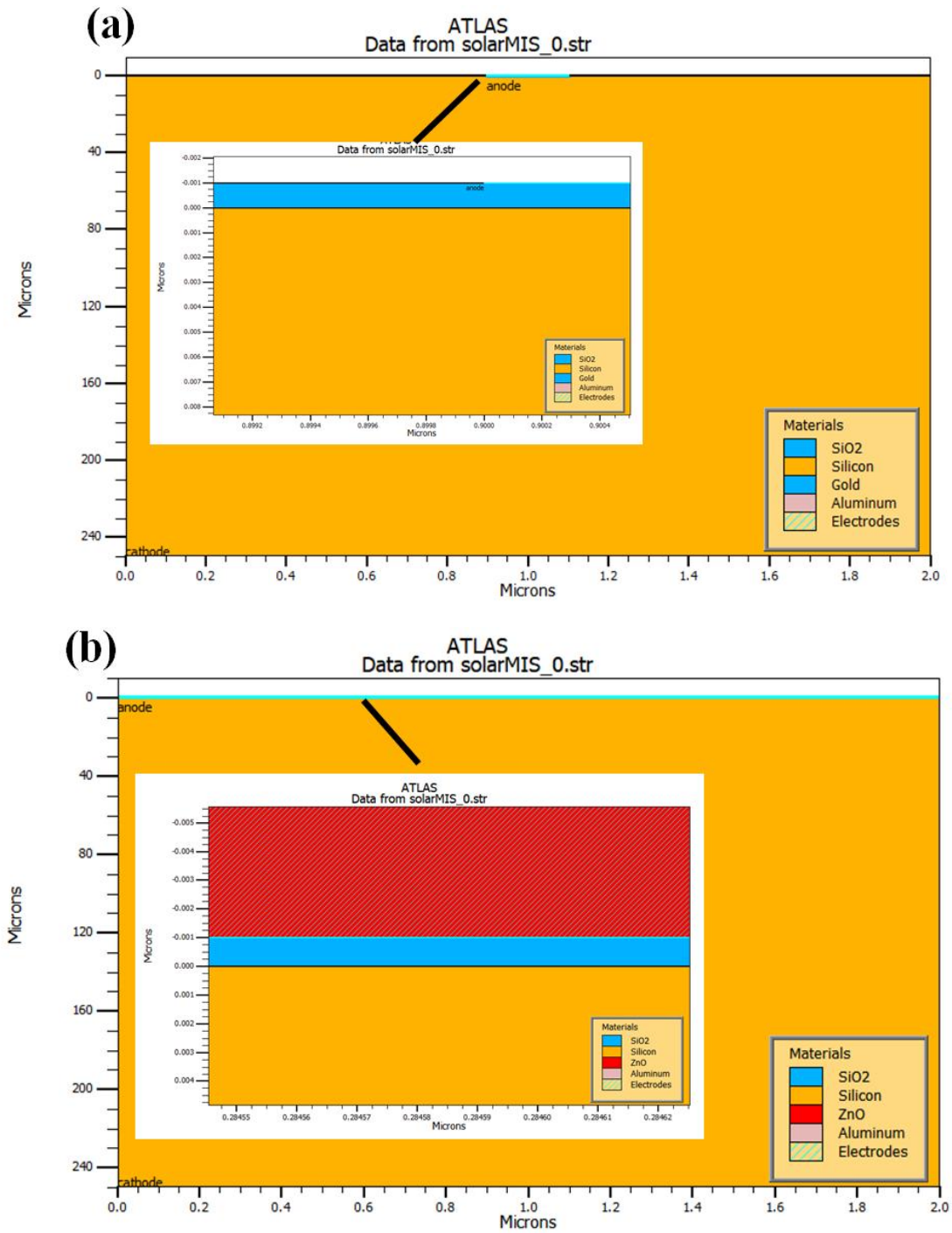


Figure III.1: Structure of the studied MIS silicon solar cell with: (a) Gold (Au) anode, (b) ZnO anode.

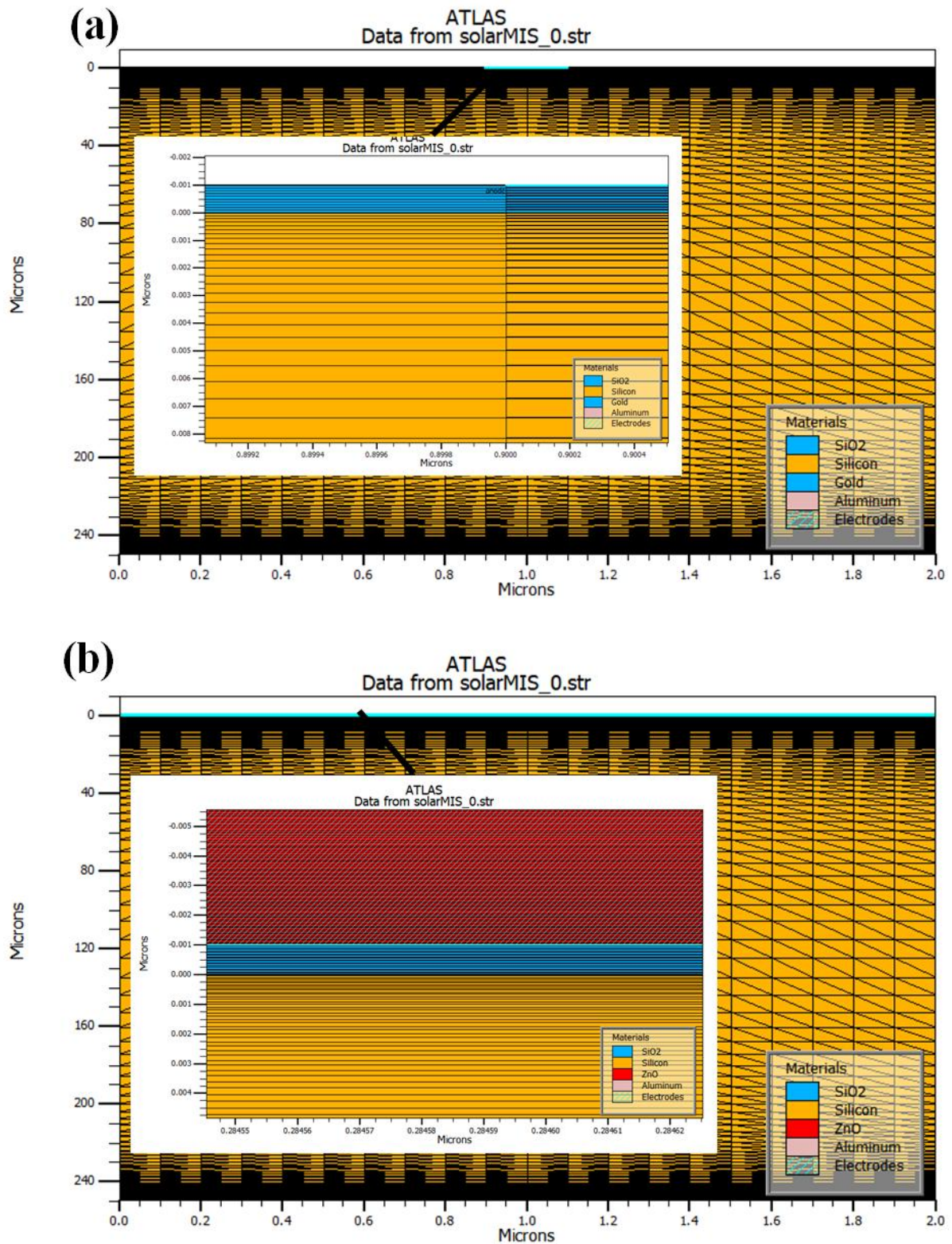


Figure III.2: Two dimensional (2D) mesh of the studied MIS silicon solar cell with: (a) Gold (Au) anode, (b) ZnO anode.

The optical constants, presented by the absorption coefficient (α) and the optical index of refraction (n), are measured data saved in Silvaco data base, and are presented in figure

III.3 for the different layers of the studied MIS silicon solar cell. Case (a) of figure III.3 corresponds to the structure with gold (Au) anode; case (b) of figure III.3 corresponds to the structure with ZnO anode.

Using Silvaco-Atlas, the Poisson equation, together with current density and continuity equations, are solved simultaneously to obtain the distribution of the electrical potential and carrier density along the solar cell structure; mainly along the silicon layer. The determination of these internal parameter distributions allows the calculation of current density of electrons and holes, and so the current density – voltage ($J - V$) electrical characteristic of the cell, either in dark condition or under illumination. In MIS solar cell, the photocurrent, J_{sc} , is dominated by minority carriers. If the insulator (oxide) layer between the anode and the n-type silicon layer is very thin, the photocurrent is dominated by the direct tunnelling mechanism through the potential barrier formed by the oxide layer. The ($J - V$) characteristic of MIS solar cell can be expressed as follows [54]:

$$J(V) = J_{sc} - J_s \left(\exp\left(\frac{q \cdot V}{k_B T}\right) - 1 \right) \quad (\text{III.1})$$

where J_s is the dark saturation current, and expressed in the following equation [54]:

$$J_s = A^* T^2 \exp\left(-\frac{q \phi_{B0}}{k_B T}\right) \exp\left(-\left(q \phi_{mi}\right)^{1/2} \cdot d\right) \quad (\text{III.2})$$

In Eq.(III.2), A^* is the effective Richardson constant, T is the absolute temperature in °K, q is the electronic charge and k_B is the Boltzmann constant. ϕ_{B0} is the metal–semiconductor barrier height, ϕ_{mi} is insulator–semiconductor barrier height, and d is insulating layer thickness.

Following the direct tunnelling mechanism, the current density, J_{tunnel} through the potential barrier formed by the insulating layer is given by :

$$J_{tunnel} = \frac{qkT}{2\pi^2 h^3} \sqrt{m_y m_z} \int T(E) \ln \left\{ \frac{1 + \exp\left(\frac{E_{Fr} - E}{kT}\right)}{1 + \exp\left(\frac{E_{Fl} - E}{kT}\right)} \right\} dE \quad (\text{III.3})$$

where $T(E)$ is the transmission probability of an electron or hole through the potential barrier formed by the oxide layer, E is the incident energy of the charge carrier perpendicular to the tunneling layer, E_{Fr} and E_{Fl} are the quasi Fermi levels on either side of

the tunneling layer. m_y and m_z are the effective masses of the semiconductor in the lateral direction [55, 56].

The physical models that we used to simulate the carrier transport through the device are stated via Silvaco-Atlas as follows:

```
models temperature=300 print conmobfldmobconsrhqtnlsc.hoqtnlsc.elqtnl.derivs
```

Table III.1 gives a brief description of each employed model [55].

Table III.1: Brief description of the employed models in simulation [55].

Physical model	Description
conmob	Specifies that a concentration dependent mobility model be used for silicon. This model is a doping versus mobility table valid for 300K only.
fldmob	The lateral electric field-dependent mobility model,
consrh	Specifies Shockley-Read-Hall recombination using concentration dependent lifetimes
qtnlsc.el	Enables the self-consistent direct quantum tunnelling model for electrons.
qtnlsc.ho	Enables the self-consistent direct quantum tunnelling model for holes.
qtnl.derivs	This will include extra terms in the Jacobian matrix ,which should improve convergence in the self-consistent direct quantum tunnelling models.

Table III.2 gives the input parameters of the MIS silicon solar cell simulated by Silvaco-Atlas [58, 57], where m_{mass} . Tunnel specifies the effective mass for band to band tunneling, m_e . tunnel and m_h . tunnelspecify the electron and hole effective masses for tunneling used in the universal Schottky tunneling model. To ensure a Schottky barrier at the (oxide/semiconductor) interface ($\text{SiO}_2/\text{n-type c-Si}$), the anode work function must be higher than the electron affinity of silicon, this is fulfilled for the two studied MIS silicon solar cells; the first one with gold (Au) anode and the second one with ZnO anode.

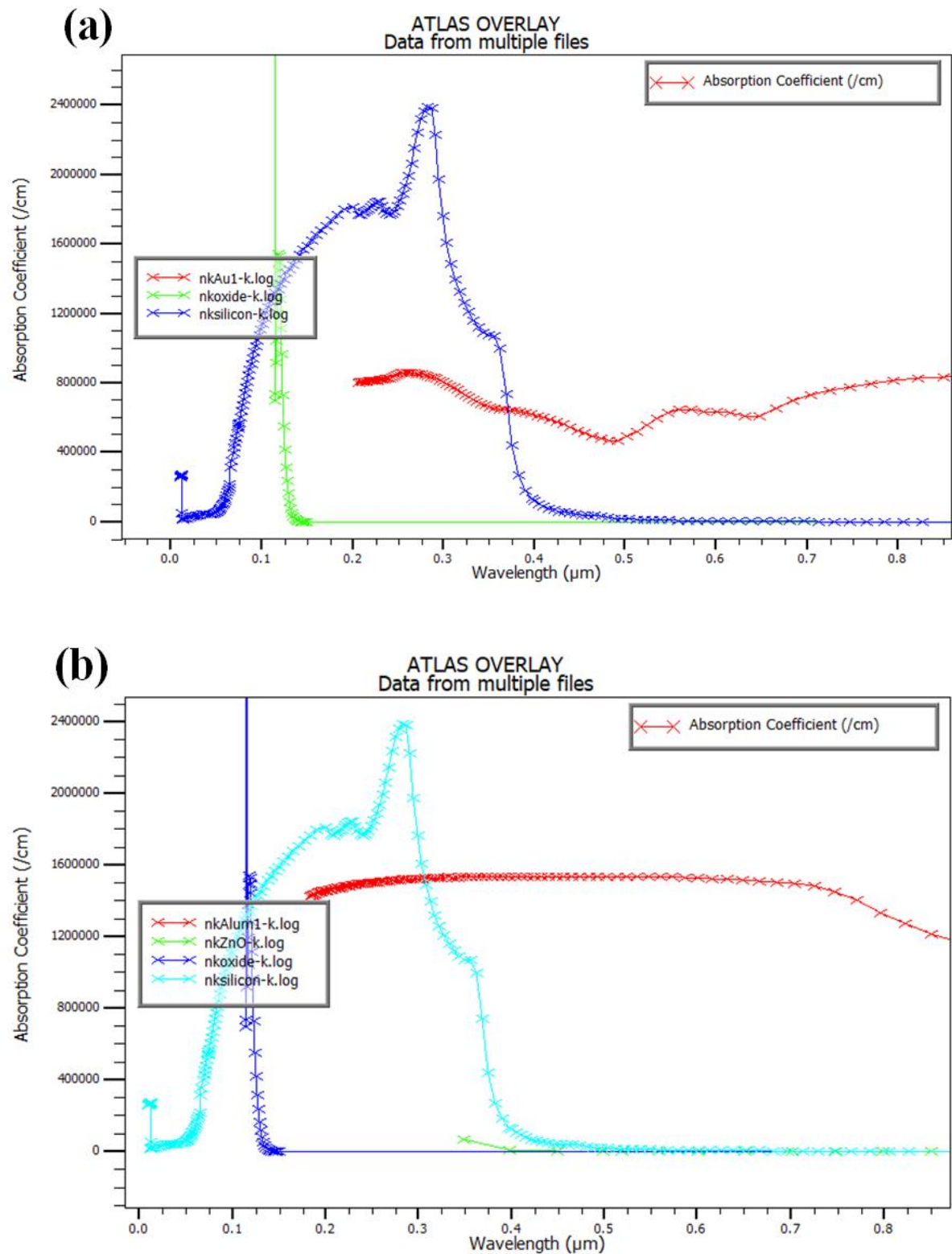


Figure III.3: Spectre of absorption coefficient (α) in the different layers of the studied MIS silicon solar cell: (a) structure with gold (Au) anode, (b) structure with ZnO anode.

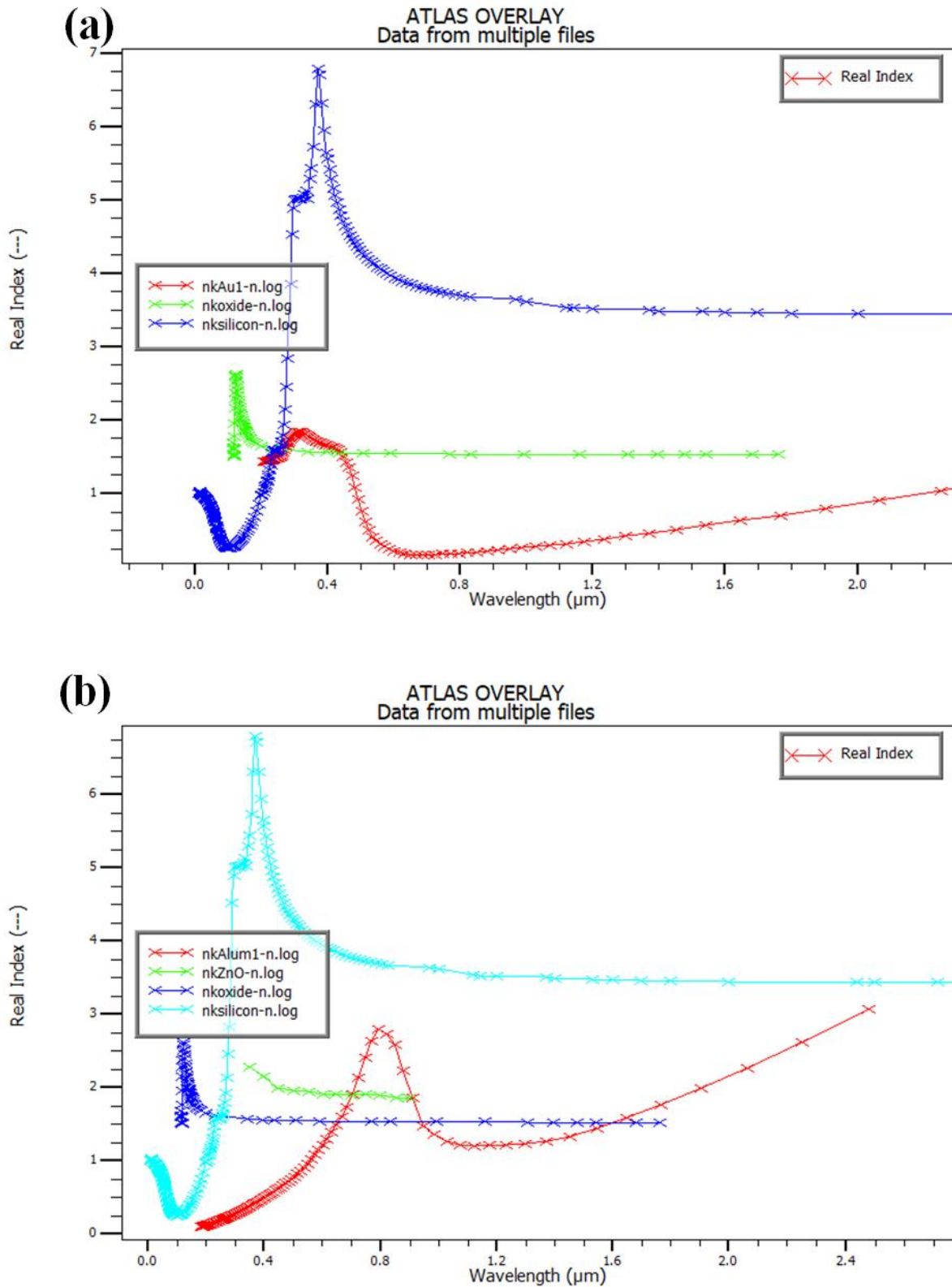


Figure III.4: Spectre of optical index of refraction (n) in the different layers of the studied MIS silicon solar cell: (a) structure with gold (Au) anode, (b) structure with ZnO anode.

Table III.2: Input parameters of the MIS silicon solar cell simulated by Silvaco-Atlas [55, 54].

Parameters		Value
Cell wide, x_{tot} (μm)		2
Thickness (μm)	ZnO region	0.05-20
	Oxide (SiO ₂) region	2-20 ($^{\circ}A$)
	Silicon region	10-500
Doping (n-type) (cm^{-3})	ZnO region	10^{20}
	Silicon region	$7 \times 10^{12} - 7 \times 10^{18}$
Energy gap, E_g (eV)	ZnO region	3.3
	Oxide (SiO ₂) region	9
	Silicon region	1.12
Permittivity, ϵ_r	ZnO region	9
	Oxide (SiO ₂) region	3.9
	Silicon region	11.8
Affinity, χ (eV)	ZnO region	4.35
	Oxide (SiO ₂) region	0.9
	Silicon region	4.3 vs 5.47 (Au) 3.2 vs 4.35 (ZnO) [57]
Electron mobility, μ_n ($cm^2V^{-1}s^{-1}$)		Conmob&fldmobmodels
Hole mobility, μ_p ($cm^2V^{-1}s^{-1}$)		Conmob&fldmobmodels
Effective density at E_C , N_C (cm^{-3})	ZnOregion	2.2×10^{18}
	Oxide (SiO ₂) region	10^{19}
	Siliconregion	2.8×10^{19}
Effective density at E_V , N_V (cm^{-3})	ZnOregion	1.8×10^{19}
	Oxide (SiO ₂) region	10^{19}
	Siliconregion	1.04×10^{19}
Band-to-band tunnelling Parameters	ZnOregion	mass.tunnel= 0.25
		me.tunnel = 0.197
		mh.tunnel=0.801
	Oxide (SiO ₂) region	mass.tunnel= 0.25
		me.tunnel = 0.42
		mh.tunnel=0.16
	Siliconregion	mass.tunnel= 0.25
		me.tunnel = 0.322
		mh.tunnel=0.16
Recombination Parameters	ZnOregion	$\tau_{n0} = 10^{-7} s, \tau_{p0} = 10^{-7} s$
	Oxide (SiO ₂) region	$\tau_{n0} = 1 s, \tau_{p0} = 1 s$
	Siliconregion	$\tau_{n0} = 10^{-6} s, \tau_{p0} = 10^{-6} s$
Anode (Au) work function(eV)		5.47

III.3. Results and discussion:

Figures III.5 and III.6 show, respectively, the band diagram of the MIS silicon solar cell with gold (Au) anode; and ZnO anode. Case (a) of the two figures corresponds to the thermal equilibrium; case (b) corresponds to the short – circuit condition under illumination. The thickness of the oxide (SiO_2) layer is 10°A , the silicon layer is $250\ \mu\text{m}$ thick with n-type doping concentration of $N_D = 7 \times 10^{15}\text{cm}^{-3}$. The ZnO anode layer is $0.5\ \mu\text{m}$ thick, n-type heavily doped with $N_D = 10^{20}\text{cm}^{-3}$. As the anode workfunction is higher than the electron affinity of silicon, at zero bias the bands of silicon at the SiO_2/Si interface bend upward. The role of the insulator layer (SiO_2) in this structure is to form a potential barrier for carriers. The photo-carrier transport from silicon to the anode layer through the barrier is considered to be dominated as we said above by quantum mechanical tunnelling process of the minority carrier. The potential barrier created by this insulator layer suppresses the dark saturation current of the device, which is contributed by the majority carrier, and the photo-voltage of the cells increases. This type of cell therefore shows higher output photo-voltage compared to the metal–semiconductor (Schottky) cell since the SiO_2 layer is used to increase the Schottky barrier. However, the insulating layer must be thin enough to enhance the tunnelling of photo-generated current J_{SC} as well as to reduce the dark current J_S .

The splitting of the quasi-Fermi levels, at short-circuit condition; show a significant increase in the minority carrier densities by photo-generation. This is clearly illustrated by Figure III.7 which shows, the carrier density distributions in the MIS silicon solar cell with gold (Au) anode (case (a)); and ZnO anode (case (b)), at thermal equilibrium and short-circuit condition.

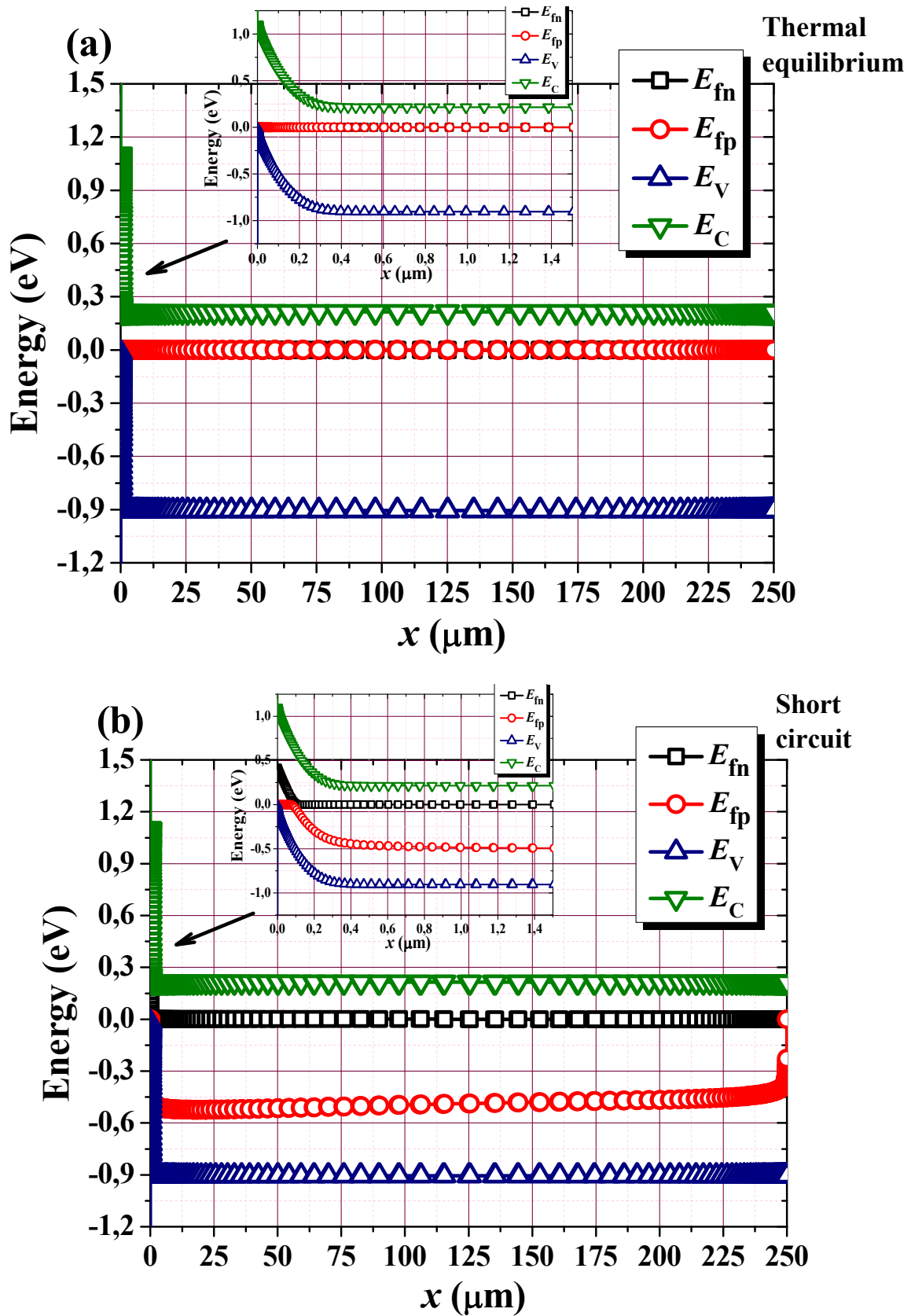


Figure III.5: Band diagram of the MIS silicon solar cell with gold (Au) anode: (a) at thermal equilibrium, (b) at short circuit condition.

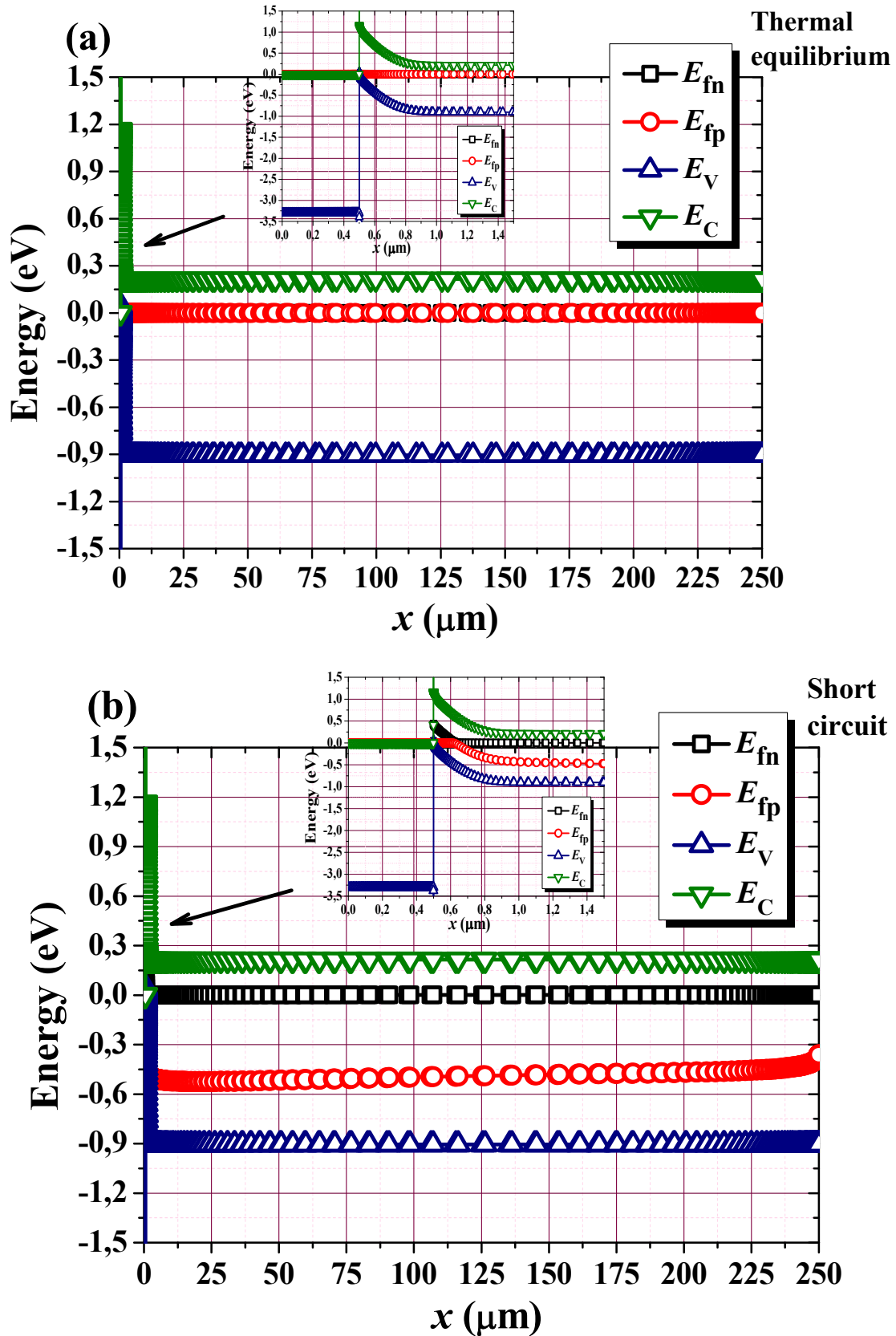


Figure III.6: Band diagram of the MIS silicon solar cell with ZnO anode: (a) at thermal equilibrium, (b) at short circuit condition.

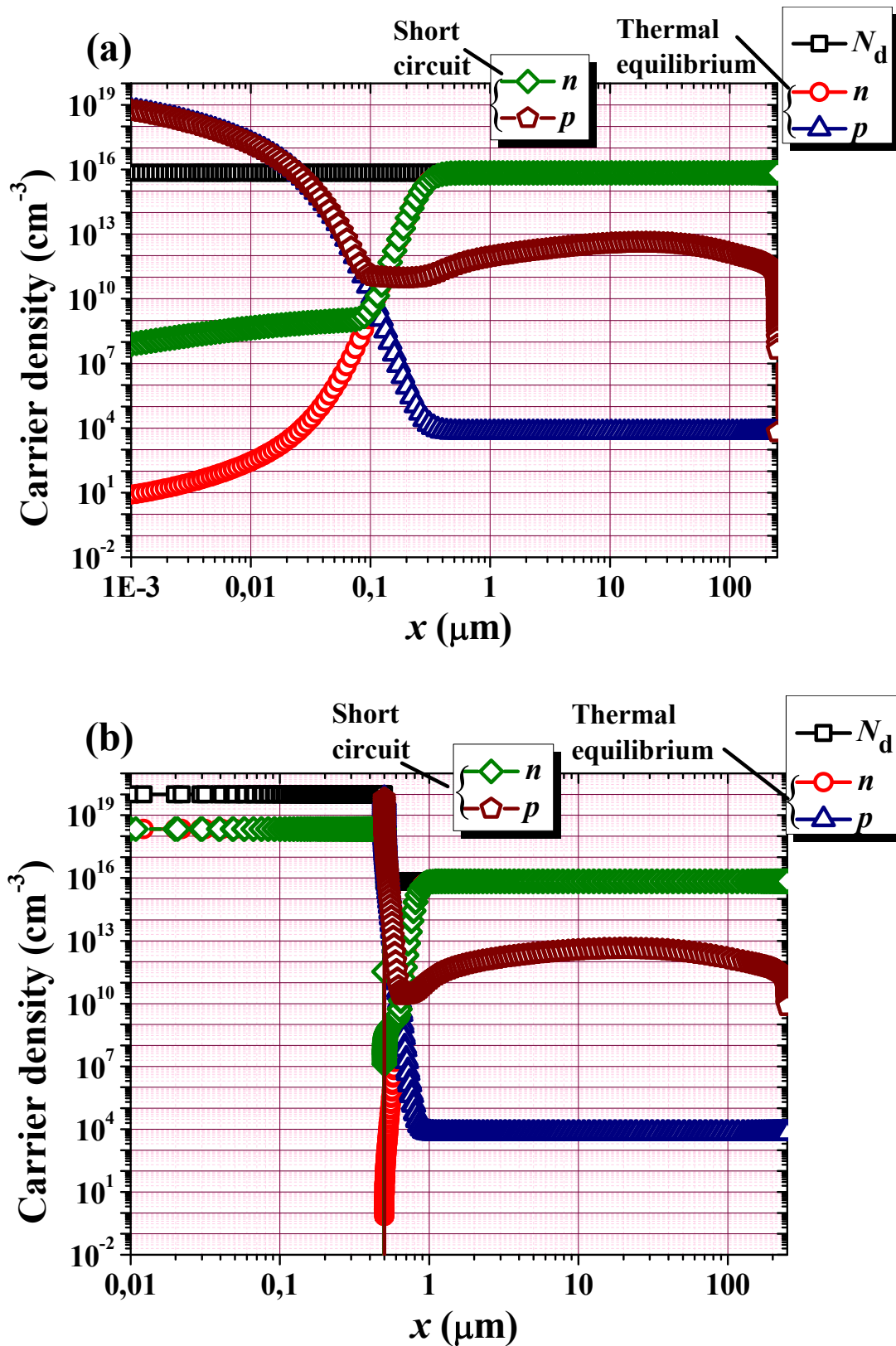


Figure III.7: Carrier density distributions in the MIS silicon solar cell at thermal equilibrium and short circuit condition: (a) with gold (Au) anode, (b) with ZnO anode.

Figure III.8 presents the simulated current density – voltage ($J - V$) and the provided power – voltage ($P - V$) characteristics of the MIS silicon solar cell with gold (Au) anode, under the AM1.5 standard spectrum and $T = 300^\circ\text{K}$. These results correspond to the oxide (SiO_2) layer thickness of 10°A , the silicon layer (base layer) of $250 \mu\text{m}$ thick with n-type doping concentration of $N_D = 7 \times 10^{15} \text{cm}^{-3}$. The output photovoltaic parameters of the cell are also shown on figure III.8.

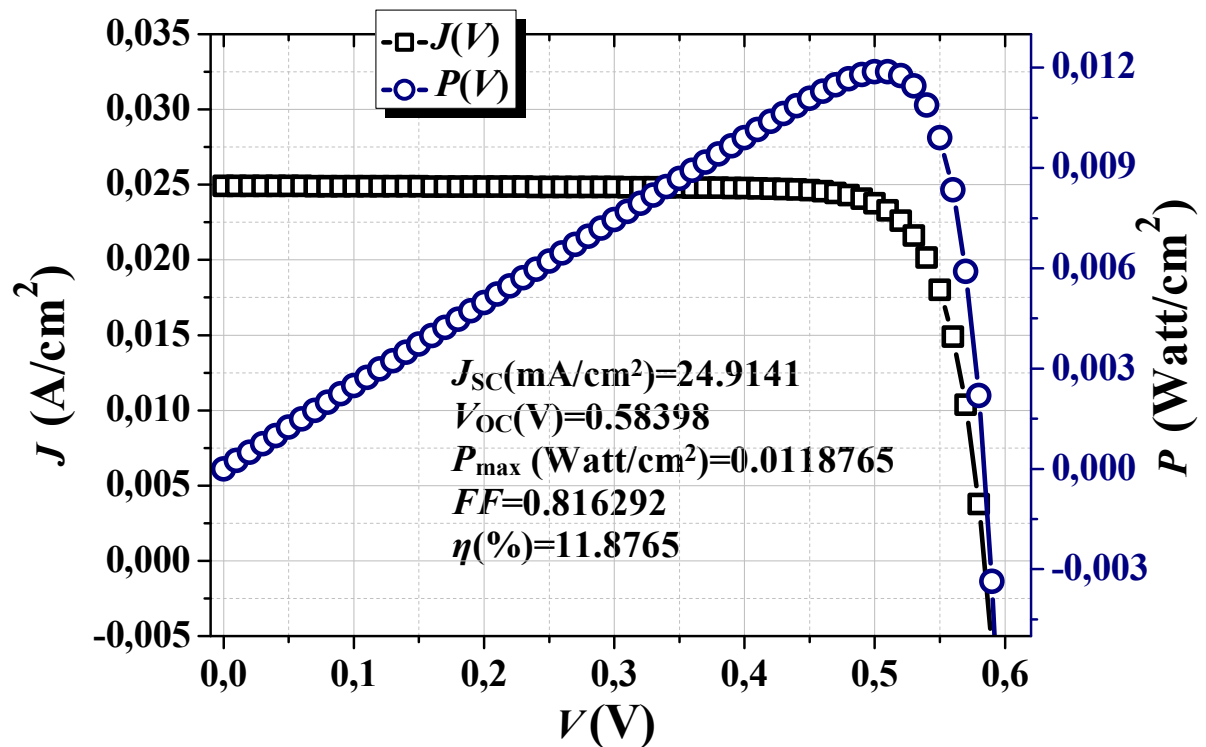


Figure III.8: Simulated $J - V$ and $P - V$ characteristics of the MIS silicon solar cell with gold (Au) anode, under the AM1.5 standard spectrum and $T = 300^\circ\text{K}$.

We tried to improve the output photovoltaic parameters of the cell by varying the silicon layer thickness in the range [10- 500 μm] with the oxide layer thickness fixed to 10°A as shown on figure III.9 and table III.3. The optimal thickness is around 175 μm which gives a conversion efficiency η of 11.8786%

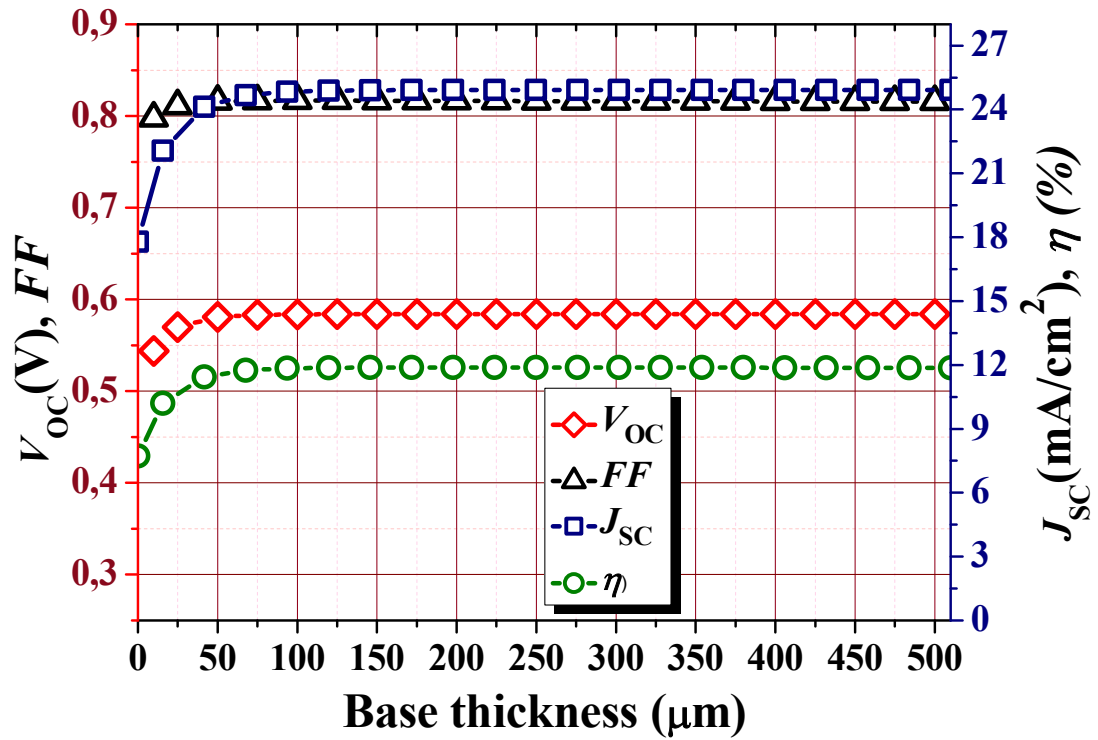


Figure III.9: Silicon layer thickness effect on the photovoltaic output parameters of the simulated MIS silicon solar cell with gold (Au) anode.

Table III.3: Silicon layer thickness effect on the photovoltaic output parameters of the simulated MIS silicon solar cell with gold (Au) anode.

Thickness (μm)	J_{sc} (mA/cm ²)	V_{oc} (V)	P_{max} (Watt/cm ²)	FF	η (%)
10	17.7927	0.543808	0.00771803	0.79766	7.71801
25	22.0619	0.569832	0.0101992	0.811295	10.1993
50	24.1178	0.580963	0.0114336	0.816013	11.4336
75	24.6739	0.583223	0.0117521	0.816663	11.7521
100	24.838	0.583784	0.0118422	0.816698	11.8421
125	24.8887	0.583923	0.0118693	0.816708	11.8693
150	24.9053	0.58396	0.0118769	0.816638	11.8769
175	24.911	0.583971	0.0118786	0.816551	11.8786
200	24.913	0.583975	0.0118784	0.816462	11.8784
225	24.9139	0.583978	0.0118775	0.816369	11.8775
250	24.9141	0.58398	0.0118765	0.816292	11.8765
275	24.9124	0.583982	0.0118757	0.816226	11.8757
300	24.9143	0.583983	0.0118748	0.816164	11.8748
325	24.9143	0.583985	0.0118739	0.816099	11.8739
350	24.9143	0.583986	0.011873	0.816036	11.873
375	24.9143	0.583988	0.0118721	0.815971	11.8721
400	24.9143	0.58399	0.0118712	0.815907	11.8712

425	24.9124	0.583991	0.0118703	0.815847	11.8703
450	24.9142	0.583993	0.0118694	0.815782	11.8694
475	24.9143	0.583994	0.0118685	0.815716	11.8685
500	24.9142	0.583996	0.0118676	0.815651	11.8676

In figure III.10 and table III.4, we present the thickness effect of the oxide (SiO_2) layer in the range $[2\text{-}20^\circ\text{A}]$ with the silicon layer thickness fixed to $250\ \mu\text{m}$.

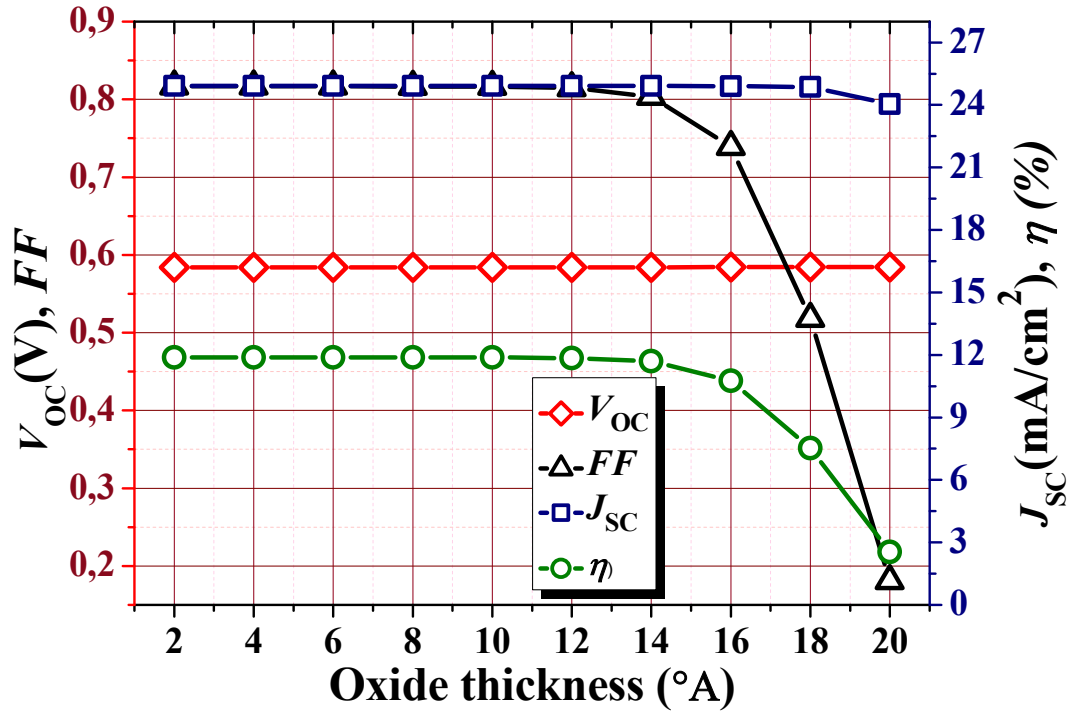


Figure III.10: Thickness effect of the oxide (SiO_2) layer on the photovoltaic output parameters of the simulated MIS silicon solar cell with gold (Au) anode.

Table III.4: Thickness effect of the oxide (SiO_2) layer on the photovoltaic output parameters of the simulated MIS silicon solar cell with gold (Au) anode.

Thickness ($^\circ\text{A}$)	J_{sc} (mA/cm^2)	V_{oc} (V)	P_{max} (Watt/cm^2)	FF	η (%)
2	24.9159	0.583972	0.0118835	0.816726	11.8835
4	24.9154	0.583972	0.0118831	0.816717	11.8832
6	24.915	0.583972	0.0118827	0.816699	11.8827
8	24.9146	0.583973	0.0118816	0.816637	11.8816
10	24.9141	0.58398	0.0118765	0.816292	11.8765
12	24.9135	0.584017	0.011854	0.81471	11.8539
14	24.9117	0.584174	0.0116948	0.80361	11.6948
16	24.9027	0.584393	0.0107593	0.739321	10.7593

18	24.8658	0.584442	0.00752789	0.518001	7.52791
20	24.0472	0.584437	0.0025452	0.181101	2.5452

From these results, we can see that the better output parameters, especially the FF and η , are obtained as the oxide layer becomes thinner; particularly thinner than 10°A . However, the J_{sc} and V_{oc} display insignificant sensitivity to the oxide layer thickness variation.

In figure III.11 and table III.5, we show the n-type doping concentration effect of the silicon layer (N_d) in the range $[7 \times 10^{12} - 7 \times 10^{18} \text{ cm}^{-3}]$, with the silicon layer thickness fixed to $250 \mu\text{m}$ and the oxide layer thickness of 10°A .

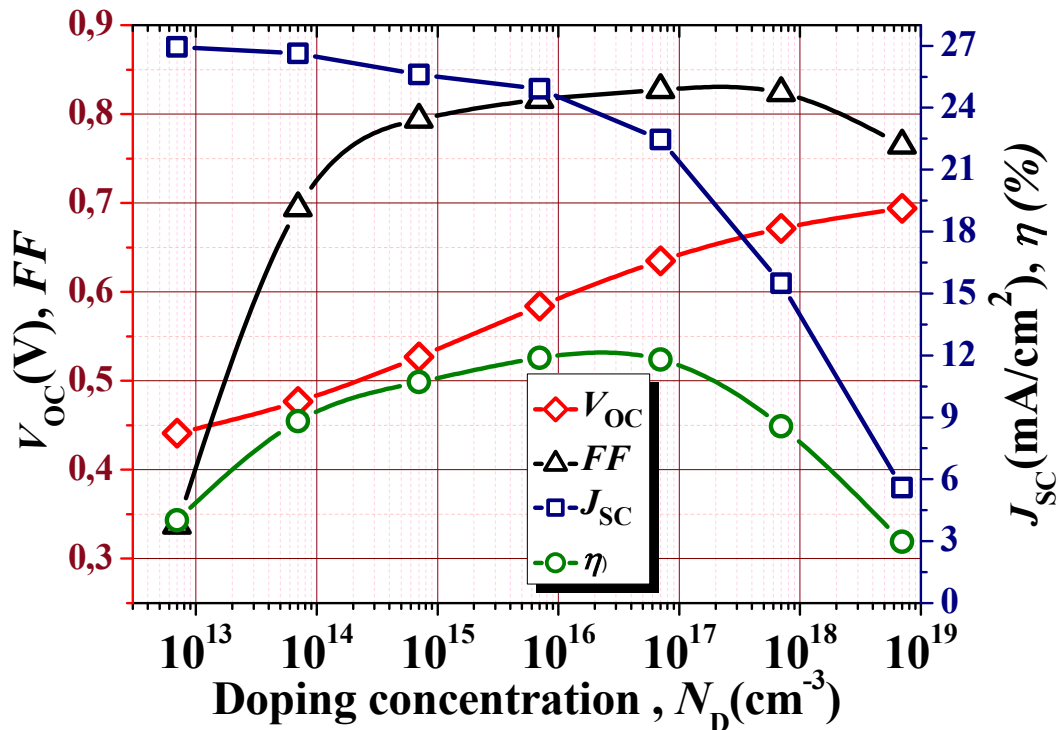


Figure III.11: Doping concentration effect of the silicon layer on the photovoltaic output parameters of the simulated MIS solar cell with gold (Au) anode.

Table III.5: Doping concentration effect of the silicon layer on the photovoltaic output parameters of the simulated MIS solar cell with gold (Au) anode .

Doping, N_d (cm^{-3})	J_{sc} (mA/cm^2)	V_{oc} (V)	P_{max} (Watt/cm^2)	FF	η (%)
7×10^{12}	26.9389	0.441242	0.00400985	0.337343	4.00985
7×10^{13}	26.6273	0.476642	0.00881066	0.694208	8.81068
7×10^{14}	25.6044	0.526918	0.0107128	0.794048	10.7128

7×10^{15}	24.9141	0.58398	0.0118765	0.816292	11.8765
7×10^{16}	22.4546	0.635058	0.0117954	0.827134	11.7954
7×10^{17}	15.4923	0.671274	0.00856842	0.823917	8.56839
7×10^{18}	5.59959	0.693824	0.00297187	0.764935	2.97187

The optimal value of doping is effectively $N_d = 7 \times 10^{15} \text{ cm}^{-3}$ which gives a conversion efficiency $\eta = 11.8765\%$. The V_{oc} is significantly enhanced from $\sim 0.44 \text{ V}$ to 0.69 V as the doping concentration increases from $7 \times 10^{12} \text{ cm}^{-3}$ to $7 \times 10^{18} \text{ cm}^{-3}$. Increase in doping levels results in larger open circuit voltage but smaller short circuit current. This can be explained simply by considering the MIS diode as an ideal p⁺-n junction diode in the voltage range of solar cell operation [56]. If the doping density increases the saturation current density J_s will decrease according to Eq. (III.4) and hence V_{oc} increases.

$$J_s = qn_i^2 \left(\frac{1}{N_A} \sqrt{\frac{D_n}{\tau_n}} + \frac{1}{N_D} \sqrt{\frac{D_p}{\tau_p}} \right) \quad (\text{III.4})$$

This means that the limiting open circuit voltages reached in MIS devices are those of ideal p-n junctions and their characteristics are determined solely by the substrate properties and do not depend critically on the barrier height at the semiconductor surface or the insulator properties. Hence V_{oc} is determined only by the saturation current J_s given by equation (III.4) where ϕ_{mi} does not enter into any of these expressions. Once the minority carrier MIS solar cell is obtained, the limiting open circuit voltage reached is that of ideal p-n junctions. Its characteristics are determined solely by the substrate properties and do not depend critically on the barrier height at the semiconductor surface or the insulator properties. In other words, the dominant current is governed by the transport properties in the semiconductor via diffusion of minority carriers once they have tunnel through the insulator. This essentially shows that minority carrier MIS diodes are identical to p-n junction diodes whose currents are limited only by diffusion [56].

Unfortunately the drawback for higher doping density is the decrease in short circuit current density J_{sc} due to the decrease in the minority carrier diffusion length L_D [56].

Figure III.12 presents the simulated current density – voltage ($J - V$) and the provided power – voltage ($P - V$) characteristics of the MIS silicon solar cell with ZnO anode, under the AM1.5 standard spectrum and $T = 300^\circ K$. These results correspond to the ZnO layer thickness of $0.5 \mu\text{m}$, the oxide (SiO_2) layer thickness of 10°A , the silicon layer of $250 \mu\text{m}$ thick with n-type doping concentration of $N_D = 7 \times 10^{15} \text{cm}^{-3}$. The output photovoltaic parameters of the cell are also shown on figure III.12.

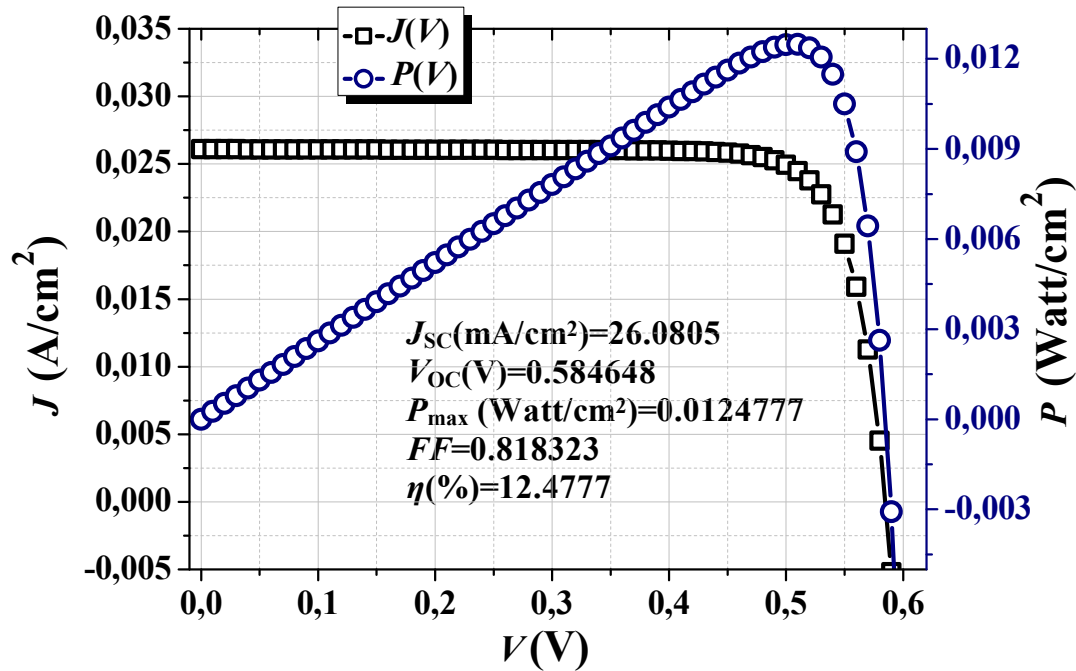


Figure III.12: Simulated $J - V$ and $P - V$ characteristics of the MIS silicon solar cell with ZnO anode, under the AM1.5 standard spectrum and $T = 300^\circ K$.

From figure III.12 and table III.6 we notify an enhancement in the output photovoltaic parameters of the cell as the anode metal (Au) is replaced by heavily doped ZnO (n^+ -type). Particularly, the J_{sc} is improved from $\sim 24.91 \text{ mA}/\text{cm}^2$ to $26.08 \text{ mA}/\text{cm}^2$, and so the conversion efficiency η enhanced from $\sim 11.87\%$ to 12.47% . Since ZnO is a wide bandgap semiconductor ($E_g = 3.3 \text{ eV}$) which absorb in the UV range, it will improve, as frontal layer, the optical absorption of the solar cell in UV range. Consequently, the J_{sc} is enhanced. The ZnO has also a good conductivity; particularly when it is heavily doped, so it can be used simultaneously as optical window and electrical frontal contact.

Table III.6: Comparison between the photovoltaic output parameters of the simulated MIS solar cell with gold (Au) anode and with ZnO anode.

Anode	J_{sc} (mA/cm^2)	V_{oc} (V)	P_{max} (Watt/cm^2)	FF	η (%)
Gold (Au)	24.9141	0.58398	0.0118765	0.816292	11.8765
ZnO (n^+ -type)	26.0805	0.584648	0.0124777	0.818323	12.4777

As shown on figure III.13 and table III.7, further amelioration in the output photovoltaic parameters of the cell is achieved by varying the silicon layer thickness in the range [10- 500 μm]. With the ZnO layer thickness of 0.5 μm , the oxide (SiO_2) layer thickness of 10 $^\circ\text{A}$, and the n-type doping concentration of the silicon layer $N_D = 7 \times 10^{15} \text{cm}^{-3}$, the optimal thickness is around 150 μm which gives a conversion efficiency η of $\sim 12.50\%$.

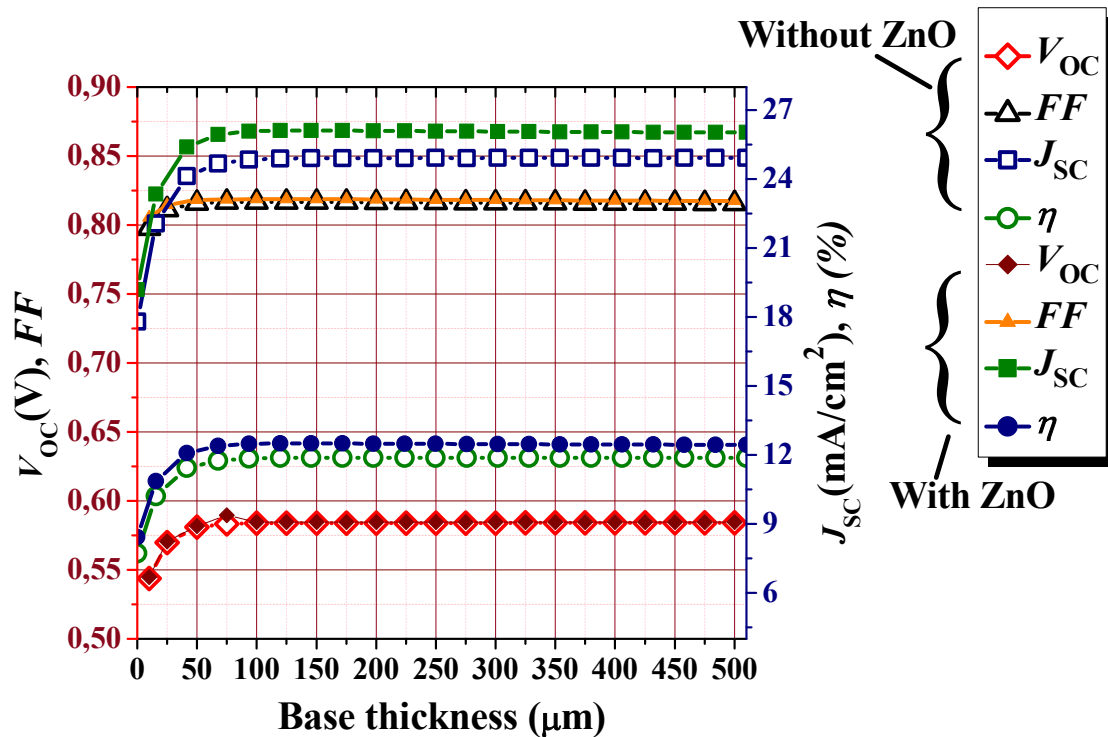


Figure III.13: Silicon layer thickness effect on the photovoltaic output parameters, and comparison between the two simulated MIS solar cells: with gold (Au) anode (without ZnO) and with ZnO anode.

Table III.7: Silicon layer thickness effect on the photovoltaic output parameters of the simulated MIS silicon solar cell with ZnO anode.

Thickness (μm)	J_{sc} (mA/cm^2)	V_{oc} (V)	P_{max} (Watt/cm^2)	FF	η (%)
10	19.1915	0.544701	0.00842168	0.805473	8.421669
25	23.3503	0.57059	0.0108546	0.814694	10.8545
50	25.3895	0.581665	0.012083	0.818178	12.083
75	25.932	0.58967	0.0123963	0.818593	12.3963
100	26.0791	0.584524	0.0124821	0.818828	12.4821
125	26.1133	0.584649	0.0125007	0.8188	12.5007
150	26.1151	0.584671	0.0125007	0.818716	12.5008
175	26.1078	0.584669	0.0124958	0.81862	12.4958
200	26.0984	0.584662	0.0124896	0.818524	12.4896
225	26.0891	0.584655	0.0124835	0.818424	12.4835
250	26.0805	0.584648	0.0124777	0.818323	12.4777
275	26.0725	0.584642	0.0124723	0.818227	12.4723
300	26.0653	0.584636	0.0124672	0.818127	12.4672
325	26.0587	0.584631	0.0124625	0.81803	12.4625
350	26.0526	0.584627	0.012458	0.817933	12.458
375	26.0471	0.584623	0.0124538	0.817833	12.4537
400	26.042	0.58462	0.0124498	0.817736	12.4498
425	26.0372	0.584616	0.0124459	0.817661	12.4459
450	26.0328	0.584614	0.0124423	0.817541	12.4423
475	26.0287	0.584611	0.0124388	0.817446	12.4388
500	26.0249	0.584609	0.0124354	0.817347	12.4354

In figure III.14 and table III.8, we present the thickness effect of the oxide (SiO_2) layer in the range $[2-20^\circ\text{A}]$ with the ZnO layer thickness of $0.5 \mu\text{m}$, the silicon layer thickness of $250 \mu\text{m}$ and the n-type doping concentration of the silicon layer $N_D = 7 \times 10^{15} \text{cm}^{-3}$.

From these results, we can see that the better output parameters, especially the FF and $\text{so}\eta$, are obtained as the oxide layer becomes thinner; particularly thinner than 12°A . However, the J_{sc} and V_{oc} display insignificant sensitivity to the oxide layer thickness variation. We can notify also that the use of ZnO as anode reduces significantly the degradation of FF and η as the oxide layer thickness increases. Indeed, the FF and η are reduced, respectively, to ~ 0.66 and 10.16% for the oxide layer thickness of 20°A , in comparison with 0.18 and 2.54% for the MIS solar cell with gold (Au) Anode.

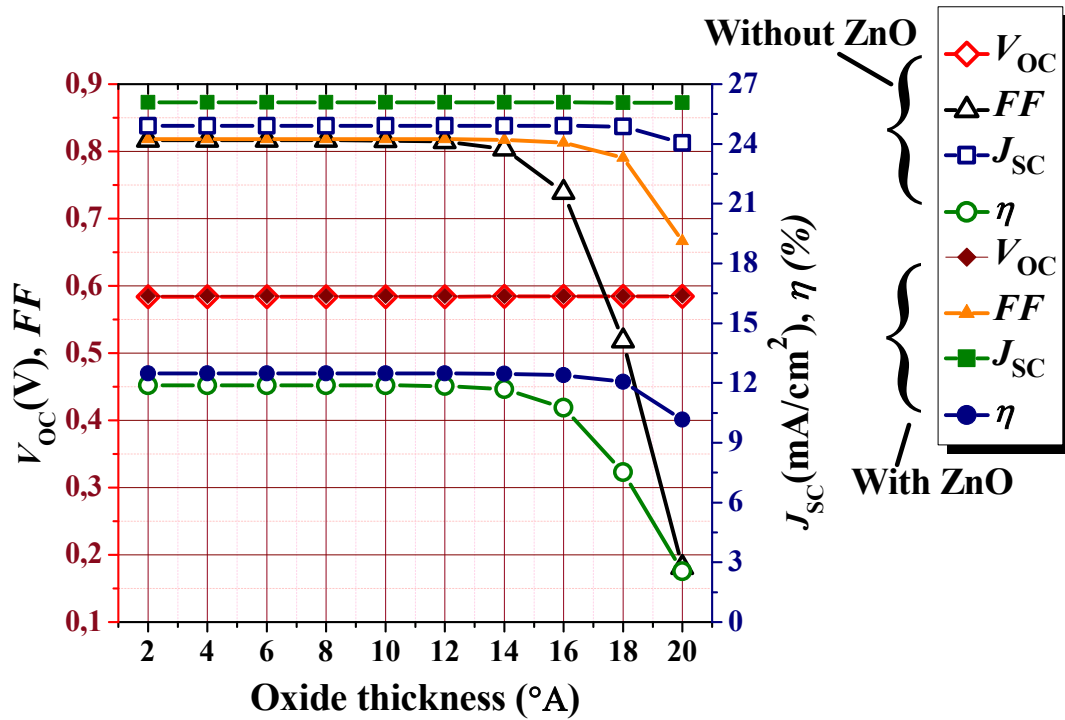


Figure III.14: Oxide thickness effect on the photovoltaic output parameters, and comparison between the two simulated MIS solar cells: with gold (Au) anode (without ZnO) and with ZnO anode.

Table III.8: Thickness effect of the oxide (SiO_2) layer on the photovoltaic output parameters of the simulated MIS silicon solar cell with ZnO anode.

Thickness ($^{\circ}\text{A}$)	J_{sc} (mA/cm^2)	V_{oc} (V)	P_{max} (Watt/cm^2)	FF	η (%)
2	26.0817	0.584648	0.0124789	0.818362	12.4789
4	26.0814	0.584648	0.0124787	0.818361	12.4787
6	26.0811	0.584648	0.0124786	0.818361	12.4786
8	26.0808	0.584647	0.0124783	0.818355	12.4783
10	26.0805	0.584648	0.0124777	0.818323	12.4777
12	26.0801	0.584651	0.012475	0.818154	12.475
14	26.0798	0.584668	0.0124601	0.817163	12.4601
16	26.079	0.584754	0.0124004	0.813148	12.4004
18	26.0765	0.585001	0.0120623	0.790712	12.0623
20	26.0629	0.585223	0.0101689	0.6667	10.1689

In figure III.15 and table III.9, we show the n-type doping concentration (N_d) effect of the silicon layer in the range $[7 \times 10^{12} - 7 \times 10^{18} \text{cm}^{-3}]$, with the ZnO layer thickness of $0.5 \mu\text{m}$, the silicon layer thickness fixed to $250 \mu\text{m}$ and the oxide layer thickness of 10°A .

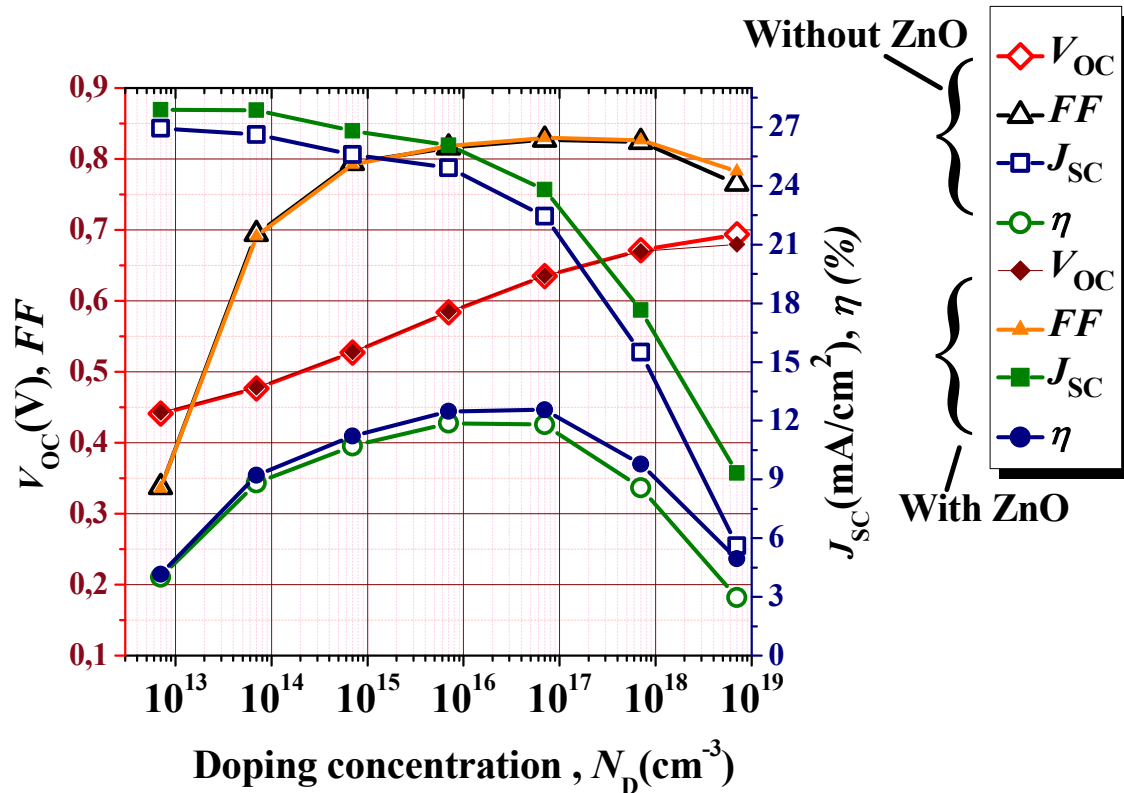


Figure III.15: Doping concentration effect on the photovoltaic output parameters, and comparison between the two simulated MIS solar cells: with gold (Au) anode (without ZnO) and with ZnO anode.

Table III.9: Doping concentration effect of the silicon layer on the photovoltaic output parameters of the simulated MIS solar cell with ZnO anode.

Doping, N_d (cm^{-3})	J_{sc} (mA/cm^2)	V_{oc} (V)	P_{max} (Watt/cm^2)	FF	η (%)
7×10^{12}	27.8888	0.442838	0.00414479	0.335605	4.1448
7×10^{13}	27.8655	0.478064	0.00920922	0.691306	9.20923
7×10^{14}	26.8037	0.527905	0.0112122	0.792389	11.2122
7×10^{15}	26.0805	0.584648	0.0124777	0.818323	12.4777
7×10^{16}	23.8171	0.635417	0.012558	0.829798	12.558
7×10^{17}	17.6594	0.669639	0.00977596	0.82669	9.77596
7×10^{18}	9.33129	0.679443	0.00495466	0.782635	4.95466

In this case (with ZnO anode), the optimal value of doping is $N_d = 7 \times 10^{16} \text{cm}^{-3}$ which gives a conversion efficiency $\eta = 12.558\%$. The V_{oc} is significantly enhanced from ~ 0.44 V to 0.679V as the doping concentration increases from $7 \times 10^{12} \text{cm}^{-3}$ to $7 \times 10^{18} \text{cm}^{-3}$.

The final improvement that we can achieve for the second solar cell (with ZnO anode) is by varying the ZnO layer thickness. This is shown on figure III.16 and table III.10; where the ZnO layer thickness is changed in the range [0.05-10 μm], while the oxide and silicon layer thicknesses are fixed respectively to 10 \AA and 250 μm , and the n-type doping concentration of the silicon layer $N_D = 7 \times 10^{15} \text{cm}^{-3}$. From these results we can notify a significant enhancement of the J_{sc} ; which increases from $\sim 25.08 \text{mA/cm}^2$ to 28.99mA/cm^2 , and so the amelioration of conversion efficiency η from $\sim 11.97\%$ to 13.94% .

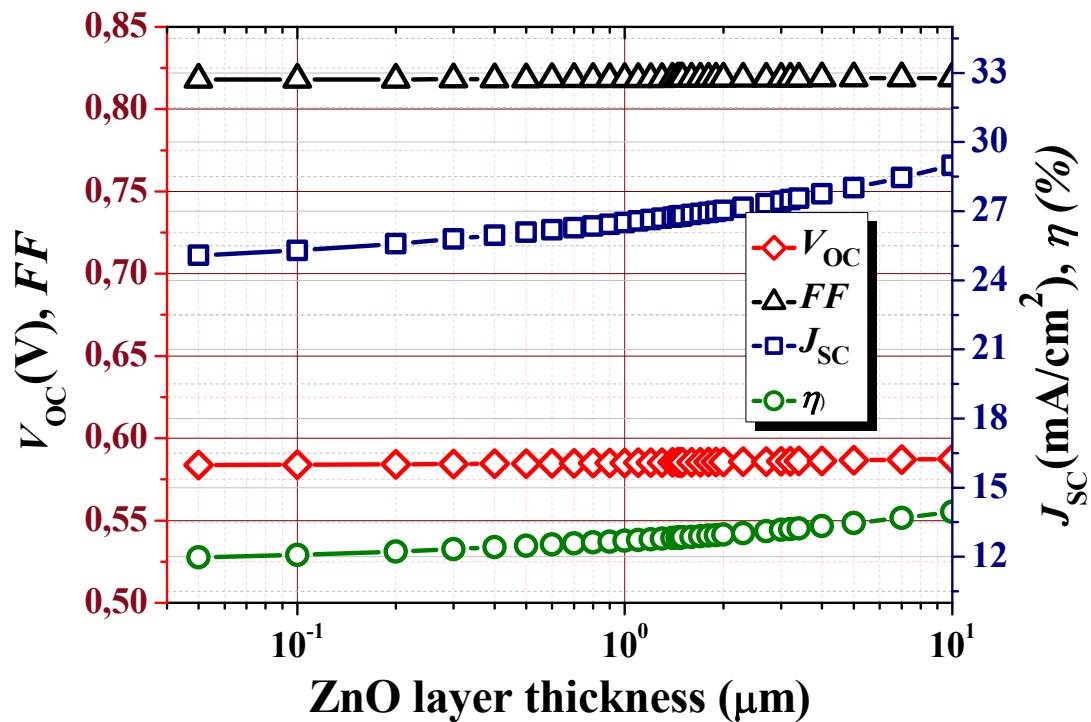


Figure III.16: Thickness effect of the ZnO anode layer on the photovoltaic output parameters of the simulated silicon solar cell with ZnO anode.

Table III.10: Thickness effect of the ZnO anode layer on the photovoltaic output parameters of the simulated silicon solar cell with ZnO anode.

Thickness (μm)	J_{sc} (mA/cm^2)	V_{oc} (V)	P_{max} (Watt/cm^2)	FF	η (%)
0.05	25.0854	0.58365	0.01198	0.81809	11.9778
0.1	25.2855	0.58385	0.01208	0.81806	12.0771
0.2	25.5846	0.58415	0.01223	0.81811	12.2269
0.3	25.7959	0.58436	0.01233	0.8182	12.3338
0.4	25.9545	0.58452	0.01241	0.81827	12.414
0.5	26.0805	0.58465	0.01248	0.81832	12.4777
0.6	26.1856	0.58475	0.01253	0.81836	12.5309

0.7	26.2767	0.58484	0.01258	0.8184	12.577
0.8	26.3581	0.58493	0.01262	0.81843	12.6181
0.9	26.4325	0.585	0.01266	0.81845	12.6557
1	26.5015	0.58507	0.01269	0.81847	12.6906
1.2	26.6274	0.58519	0.01275	0.81851	12.7542
1.4	26.7415	0.58531	0.01281	0.81855	12.8119
1.6	26.8468	0.58541	0.01287	0.81858	12.8652
1.8	26.9449	0.58551	0.01291	0.81861	12.9147
2	27.0371	0.5856	0.01296	0.81863	12.9613
2.3	27.166	0.58573	0.01303	0.81866	13.0265
2.7	27.3232	0.58589	0.01311	0.8187	13.106
3	27.432	0.58599	0.01316	0.81873	13.161
4	27.7506	0.58631	0.01332	0.81879	13.3221
5	28.0192	0.58658	0.01346	0.81884	13.458
7	28.4617	0.58702	0.01368	0.8189	13.6818
10	28.9907	0.58755	0.01395	0.81895	13.9496

III.4.Conclusion:

In this study, we have investigated two silicon-based solar cells. The first one consisting of Au / SiO₂ / n-type c-Si (MIS structure). In the second cell, the anode metal (Au) is replaced by heavily doped ZnO (n⁺-type) to give (n⁺-type ZnO / SiO₂ / n-type c-Si) structure. For the two considered solar cells, we have investigated the thickness variation effect of the silicon layer in the range [10- 500 μm], the thickness effect of the oxide (SiO₂) layer in the range [2-20°A], and the n-type doping concentration effect of the silicon layer (N_d) in the range [$7 \times 10^{12} - 7 \times 10^{18} \text{cm}^{-3}$]. For the second solar cell, further investigation was achieved under ZnO thickness effect in the range [0.05-10μm] to bring more improvement to the solar cell performance. The two studied solar cells are exposed to the AM1.5 standard spectrum at ambient temperature (300°K°). The investigation was carried out using the numerical simulation software SILVACO-ATLAS, which allows the calculation of all the internal parameters of the solar cell such as the distribution of the band diagram, the electron and holes concentrations...etc. The external parameters are also be calculated such as the current density-voltage ($J - V$) and the provided power – voltage ($P - V$) characteristics under illumination, which allow the extraction of the output photovoltaic parameters of the solar cell namely the short circuit current density J_{sc} , the open circuit voltage V_{oc} , the fill factor FF , the maximum power P_{max} provided by the cell and the photovoltaic conversion efficiency η of the cell.

For the first solar cell, we improved the output photovoltaic parameters of the cell by varying the silicon layer thickness in the range [10- 500 μm] with the oxide layer thickness fixed to 10 $^\circ\text{A}$ and the n-type doping concentration of the silicon layer $N_D = 7 \times 10^{15} \text{cm}^{-3}$. The optimal thickness is around 175 μm which gives a conversion efficiency η of $\sim 11.87\%$

The thickness variation effect of the oxide (SiO_2) layer in the range [2-20 $^\circ\text{A}$], with the silicon layer thickness of 250 μm and the n-type doping concentration of the silicon layer $N_D = 7 \times 10^{15} \text{cm}^{-3}$, shows that the better output parameters, especially the FF and so η , are obtained as the oxide layer becomes thinner; particularly thinner than 10 $^\circ\text{A}$. However, the J_{sc} and V_{oc} display insignificant sensitivity to the oxide layer thickness variation.

With the silicon layer thickness fixed to 250 μm and the oxide layer thickness of 10 $^\circ\text{A}$, the n-type doping concentration effect of the silicon layer (N_d) in the range [$7 \times 10^{12} - 7 \times 10^{18} \text{cm}^{-3}$] shows that the optimal value of doping is effectively $N_d = 7 \times 10^{15} \text{cm}^{-3}$; which gives a conversion efficiency $\eta = 11.8765\%$. The V_{oc} is significantly enhanced from $\sim 0.44 \text{ V}$ to 0.69 V as the doping concentration increases from $7 \times 10^{12} \text{cm}^{-3}$ to $7 \times 10^{18} \text{cm}^{-3}$.

In the second solar cell, we notified an enhancement in the output photovoltaic parameters of the cell as the anode metal (Au) is replaced by heavily doped ZnO (n $^+$ -type). Particularly, the J_{sc} is improved from $\sim 24.91 \text{ mA/cm}^2$ to 26.08 mA/cm^2 , and so the conversion efficiency η enhanced from $\sim 11.87\%$ to 12.47% .

Further amelioration in the output photovoltaic parameters of the cell is achieved by varying the silicon layer thickness in the range [10- 500 μm]. With the ZnO layer thickness of 0.5 μm , the oxide (SiO_2) layer thickness of 10 $^\circ\text{A}$, and the n-type doping concentration of the silicon layer $N_D = 7 \times 10^{15} \text{cm}^{-3}$, the optimal thickness is around 150 μm which gives a conversion efficiency η of $\sim 12.50\%$.

With the ZnO layer thickness of 0.5 μm , the silicon layer thickness of 250 μm and the n-type doping concentration of the silicon layer $N_D = 7 \times 10^{15} \text{cm}^{-3}$, the thickness effect of the oxide (SiO_2) layer in the range [2-20 $^\circ\text{A}$] shows that the better output parameters, especially the FF and so η , are obtained as the oxide layer becomes thinner; particularly thinner than 12 $^\circ\text{A}$. However, the J_{sc} and V_{oc} display insignificant sensitivity to the oxide layer thickness variation. We notified also that the use of ZnO as anode reduces significantly the degradation of FF and η as the oxide layer thickness increases. Indeed, the

FF and η are reduced, respectively, to ~ 0.66 and 10.16% for the oxide layer thickness of 20°A , in comparison with 0.18 and 2.54% for the MIS solar cell with gold (Au) Anode.

From the n-type doping concentration effect of the silicon layer (N_d) in the range [$7 \times 10^{12} - 7 \times 10^{18} \text{cm}^{-3}$], the optimal value of doping is $N_d = 7 \times 10^{16} \text{cm}^{-3}$ which gives a conversion efficiency $\eta = 12.558\%$ for the second solar cell. The V_{oc} is significantly enhanced from ~ 0.44 V to 0.679 V as the doping concentration increases from $7 \times 10^{12} \text{cm}^{-3}$ to $7 \times 10^{18} \text{cm}^{-3}$.

The final improvement that we have achieved for the second solar cell (with ZnO anode) is by varying the ZnO layer thickness in the range [0.05 - $10 \mu\text{m}$], while the oxide and silicon layer thicknesses are fixed respectively to 10°A and $250 \mu\text{m}$, and the n-type doping concentration of the silicon layer $N_D = 7 \times 10^{15} \text{cm}^{-3}$. From these results we notified a significant enhancement of the J_{sc} ; which increases from $\sim 25.08 \text{mA/cm}^2$ to 28.99mA/cm^2 , and so the amelioration of conversion efficiency η from $\sim 11.97\%$ to 13.94% .



General conclusion



General conclusion

One possibility for cost reduction in the solar cells lies in the method of junction fabrication and the idea of a simple deposited metal-semiconductor junction was very attractive. Metal deposition methods are consistent with high yield, fast throughput processing, and also involve low substrate temperatures, thus avoiding degradation of semiconductor minority carrier properties and suggesting a compatibility with thin film and non-single crystalline substrates. In practice, however, intimate contact metal-semiconductor solar cells exhibit a serious deficiency in the form of very poor photovoltage response. This stems from the fact that the usual thermionic emission dark current in Schottky barrier junctions leads to a considerably higher dark current than in many homojunction and heterojunction structures. It is possible to overcome this disadvantage, yet still preserve the attractive features of Schottky barrier technology, by allowing a very thin insulating layer to separate the metal and semiconductor. The deliberate introduction of such a layer yields a Metal-Insulator-Semiconductor (MIS) solar cell. In the MIS structure, the thermionic emission dark current can be reduced by either increasing the effective metal-semiconductor barrier height, decreasing the probability of majority carrier tunnelling, encouraging interface states with a large capture cross section for majority carriers, or reducing the number of majority carriers at the semiconductor surface.

In the last decades, the development of MIS type solar cells has considerably much progressed, such as the use of transparent conductive oxides (TCO) to replace metals that have low transparencies. TCO are basically semiconductors with wide band gap thus are mainly used as front contact allowing the incident light to penetrate into the substrate layer without losing much energy due to absorption. TCO usually used in MIS structures are indium tin oxide (ITO), SnO₂, TiO₂, fluorine tin oxide (FTO) and ZnO. Among these TCO, ZnO and ITO have the major advantage for their low-cost fabrication process and low-temperature needed for deposition.

In this study, we have investigated two silicon-based solar cells. The first one consisting of Au / SiO₂ / n-type c-Si (MIS structure). In the second cell, the anode metal (Au) is replaced by heavily doped ZnO (n⁺-type) to give (n⁺-type ZnO / SiO₂ / n-type c-Si) structure. For the two considered solar cells, we have investigated the thickness variation effect of the silicon layer in the range [10- 500 μm], the thickness effect of the oxide (SiO₂) layer in the range [2-20°Å], and the n-type doping concentration effect of the silicon layer (N_d) in the range [$7 \times 10^{12} - 7 \times 10^{18} \text{ cm}^{-3}$]. For the second solar cell,

General conclusion

further investigation was achieved under ZnO thickness effect in the range [0.05-10 μm] to bring more improvement to the solar cell performance. The two studied solar cells are exposed to the AM1.5 standard spectrum at ambient temperature (300 $^{\circ}\text{K}$). The investigation was carried out using the numerical simulation software SILVACO-ATLAS, which allows the calculation of all the internal parameters of the solar cell such as the distribution of the band diagram, the electron and hole concentrations...etc. The external parameters are also be calculated such as the current density-voltage ($J - V$) and the provided power - voltage ($P - V$) characteristics under illumination, which allow the extraction of the output photovoltaic parameters of the solar cell namely the short circuit current density J_{sc} , the open circuit voltage V_{oc} , the fill factor FF , the maximum power P_{max} provided by the cell and the photovoltaic conversion efficiency η of the cell.

For the first solar cell, we improved the output photovoltaic parameters of the cell by varying the silicon layer thickness in the range [10- 500 μm] with the oxide layer thickness fixed to 10 $^{\circ}\text{A}$ and the n-type doping concentration of the silicon layer $N_D = 7 \times 10^{15} \text{cm}^{-3}$. The optimal thickness is around 175 μm which gives a conversion efficiency η of ~11.87 %

The thickness variation effect of the oxide (SiO_2) layer in the range [2-20 $^{\circ}\text{A}$], with the silicon layer thickness of 250 μm and the n-type doping concentration of the silicon layer $N_D = 7 \times 10^{15} \text{cm}^{-3}$, shows that the better output parameters, especially the FF and so η , are obtained as the oxide layer becomes thinner; particularly thinner than 10 $^{\circ}\text{A}$. However, the J_{sc} and V_{oc} display insignificant sensitivity to the oxide layer thickness variation.

With the silicon layer thickness fixed to 250 μm and the oxide layer thickness of 10 $^{\circ}\text{A}$, the n-type doping concentration effect of the silicon layer (N_d) in the range [$7 \times 10^{12} - 7 \times 10^{18} \text{cm}^{-3}$] shows that the optimal value of doping is effectively $N_d = 7 \times 10^{15} \text{cm}^{-3}$; which gives a conversion efficiency $\eta = 11.8765\%$. The V_{oc} is significantly enhanced from ~ 0.44 V to 0.69 V as the doping concentration increases from $7 \times 10^{12} \text{cm}^{-3}$ to $7 \times 10^{18} \text{cm}^{-3}$.

In the second solar cell, we notified an enhancement in the output photovoltaic parameters of the cell as the anode metal (Au) is replaced by heavily doped ZnO (n $^+$ -type). Particularly, the J_{sc} is improved from ~24.91 mA/cm^2 to 26.08 mA/cm^2 , and so the conversion efficiency η enhanced from ~ 11.87 % to 12.47 %.

General conclusion

Further amelioration in the output photovoltaic parameters of the cell is achieved by varying the silicon layer thickness in the range [10- 500 μm]. With the ZnO layer thickness of 0.5 μm , the oxide (SiO_2) layer thickness of 10 $^\circ\text{A}$, and the n-type doping concentration of the silicon layer $N_D = 7 \times 10^{15} \text{cm}^{-3}$, the optimal thickness is around 150 μm which gives a conversion efficiency η of $\sim 12.50\%$.

With the ZnO layer thickness of 0.5 μm , the silicon layer thickness of 250 μm and the n-type doping concentration of the silicon layer $N_D = 7 \times 10^{15} \text{cm}^{-3}$, the thickness effect of the oxide (SiO_2) layer in the range [2-20 $^\circ\text{A}$] shows that the better output parameters, especially the FF and so η , are obtained as the oxide layer becomes thinner; particularly thinner than 12 $^\circ\text{A}$. However, the J_{sc} and V_{oc} display insignificant sensitivity to the oxide layer thickness variation. We notified also that the use of ZnO as anode reduces significantly the degradation of FF and η as the oxide layer thickness increases. Indeed, the FF and η are reduced, respectively, to ~ 0.66 and 10.16 % for the oxide layer thickness of 20 $^\circ\text{A}$, in comparison with 0.18 and 2.54% for the MIS solar cell with gold (Au) Anode.

From the n-type doping concentration effect of the silicon layer (N_d) in the range [$7 \times 10^{12} - 7 \times 10^{18} \text{cm}^{-3}$], the optimal value of doping is $N_d = 7 \times 10^{16} \text{cm}^{-3}$ which gives a conversion efficiency $\eta = 12.558\%$ for the second solar cell. The V_{oc} is significantly enhanced from ~ 0.44 V to 0.679V as the doping concentration increases from $7 \times 10^{12} \text{cm}^{-3}$ to $7 \times 10^{18} \text{cm}^{-3}$.

The final improvement that we have achieved for the second solar cell (with ZnO anode) is by varying the ZnO layer thickness in the range [0.05-10 μm], while the oxide and silicon layer thicknesses are fixed respectively to 10 $^\circ\text{A}$ and 250 μm , and the n-type doping concentration of the silicon layer $N_D = 7 \times 10^{15} \text{cm}^{-3}$. From these results we notified a significant enhancement of the J_{sc} ; which increases from $\sim 25.08 \text{mA/cm}^2$ to 28.99mA/cm^2 , and so the amelioration of conversion efficiency η from $\sim 11.97\%$ to 13.94%.



References



References

- [1]H. J: Hovel, "Solar Cells, Vol. 11, Semiconductors and Semimetals", Academic Pres(1975).
- [2]M. A. Green, R. B. Godfrey and L. W. Davies, "The Development of Metal-Insulator-Semiconductor Solar Cells", The Australian Physicist, November (1976).
- [3]W. A. Anderson and A. E. Delahoy, "Schottky Barrier Diodes for Solar Energy Conversion", Proc. IEEE 60, 1457 (1972).
- [4]W. A. Anderson, A. E. Delahoy and R. A. Milano, "An 8% Efficient Layer Schottky-Barrier Solar Cell", J. Appl. Phys. 45, 3913 (1974).
- [5]W. A. Anderson and R. A. Milano, "I-V Characteristics for Silicon Schottky Solar Cells", Proc. IEEE, 206 (1975).
- [6]S. M. Vernon and W. A. Anderson, "Temperature Effects in SchottkyBarrier Silicon Solar Cells", Appl. Phys. Lett. 26, 707 (1975).
- [7]D. L. Pulfrey and R. F. McQuat, "Schottky Barrier Solar Cell Calculations", Appl. Phys. Lett. 24, 167 (1974).
- [8]M. A. Green and R. B. Godfrey, "MIS Solar Cell - General Theory and New Experimental Results for Silicon", Appl. Phys. Lett. 29, 610 (1976).
- [9]Md. MehediHasan, SanzidaAkther and Md. IqbalBaharChowdhury, Investigation of Graphene/Silicon-di Oxide/Gallium Arsenide Based MIS Solar Cell Using Silvaco TCAD, Proceedings of 14th Global Engineering and Technology Conference 29-30 December 2017, BIAM Foundation, 63 Eskaton, Dhaka, Bangladesh, ISBN: 978-1-925488-60-9.
- [10] Muhammad Johirul Islam, Md. MahmudulHasan, Rifat Sami and Md.IqbalBaharChowdhury, Modeling of Graphene/SiO₂/Si(n) Based Metal-Insulator-Semiconductor Solar Cells, IEEE (2016), 4th International Conference on The Development in the Renewable Energy Technology (ICDRET), DOI: 10.1109/ICDRET.2016.7421491, Bangladesh.

References

- [11] Fandi Oktasendra, Rahmat Hidayat and Rizky Indra Utama, Effects of Interface State Density On The carrier Transport and Performance of Metal-Insulator-Semiconductor (MIS) Type Thin Film Solar Cells, IOP Conf. Series: Journal of Physics: Conf. Series 1481 (2020) 012005, Doi:10.1088/1742-6596/1481/1/012005.
- [12] Chanchai Vithsupalert B.E., Theory Of Metal-Insulator-Semiconductor (MIS) Solar Cells, Thesis (1977), University of New South Wales.
- [13] Sadia Maifi, Kahina Lagha, Fazia Boumedine, and Mohammed Said Belkaid, M-I-S-S Structure Based Silicon and TCO, 978-1-4244-4321-5/09/\$25.00 ©2009 IEEE.
- [14] T. Minami, "Transparent conducting oxide semiconductors for transparent electrodes", *Semicond. Sci. Technol.*, Vol. 20, pp. S 35- S 44, 2005.
- [15] R. G. Gordon, "Criteria for choosing transparent conductors", *MRS Bulletin*, pp. 52-57, August 2000.
- [16] G. P. Srivastava and P. K. Bhatnagar, Theory Of Metal-Oxide-Semiconductor Solar Cells, *Solid-State Electronics* (1979) Vol. 22. pp. 581-587.
- [17] Kwok K. NG and Howard C. Card, A Comparison of Majority- and Minority-Carrier Silicon MISSolar Cells, *IEEE Transactions On Electron Devices*, Vol. Ed-27, No. 4, April 1980.
- [18] David L. Pulfrey, MIS Solar Cells: A Review, *IEEE Transactions On Electron Devices*, Vol. Ed-25, No. 11, November 1978.
- [19] O.M. Nielsen, Current mechanism of tunnel m.i.s, solar cells, *IEEPROC*, Vol. 127, Pt. I, No. 6, December 1980
- [20] Stirn, R.L., and Yeh, Y.C.M.: 'A 15% efficient antireflection coated metal-oxide-semiconductor solar cell', *ibid.*, 1975, 27, pp. 95-98
- [21] Lillington, D.R., and Townsend, W.G.: 'Effects of interfacial oxide layers on the performance of silicon Schottky-barrier solar cells', *Appl. Phys. Lett.*, 1976, 28, pp. 97-98

References

- [22] R. Van Overstraeten, R. Mertens, Optimisation Of New Types Of MIS Silicon Solar Cells, EC Solar Energy R&D Program Project C - Photovoltaic Conversion, 1982, Leuven - Heverlee (Belgium).
- [23] J. Lindmayer and J. Allison, *OmsatTechn. Rev.* 3,1 (1973).
- [24] YousafHameedKhattak, Modeling of High Power Conversion Efficiency Thin Film Solar Cells, PhD Thesis (2019), Universitat Politècnica de València.
- [25] T.N.S. news Page, National Aeronautics and Space Administration, <Http://Science.Nasa.Gov/Science-News/Science-at-Nasa/2002/Solarcells/>. (n.d.).
- [26] M.Z. Klaus Jager, Olindo Isabella, Arno H. M. Smets, Rene A. C. M. M. van Swaaij, *Solar Energy Fundamentals, Technology and Systems*, 2014. doi:10.1007/SpringerReference_29746.
- [27] P. Würfel, *Physics of Solar Cells from Principles to nNew Concepts*, 2009. doi:10.1002/9783527618545.
- [28] S.S. Li, *Semiconductor Physical Electronics*, Springer US, Boston, MA, 1993. doi:10.1007/978-1-4613-0489-0.
- [29] A. Ortiz-Conde, F. García-Sánchez, J. Muci, A. Sucre-González, A review of diode and solar cell equivalent circuit model lumped parameter extraction procedures, *Facta Univ. - Ser. Electron. Energ.* 27 (2014) 57–102. doi:10.2298/FUEE14010570.
- [30] F.A. Lindholm, J.G. Fossum, E.L. Burgess, Application of the superposition principle to solar-cell analysis, *IEEE Trans. Electron Devices.* 26 (1979) 165–171. doi:10.1109/T-ED.1979.19400.
- [31] S.M. Sze, K.K. Ng, *Physics of Semiconductor Devices*, John Wiley & Sons, Inc., Hoboken, NJ, USA, 2006. doi:10.1002/0470068329.
- [32] H. Ullah, B. Marí, H.N. Cui, Investigation on the Effect of Gallium on the Efficiency of CIGS Solar Cells through Dedicated Software, *Appl. Mech. Mater.* 448–453 (2013) 1497–1501. doi:10.4028/www.scientific.net/AMM.448-453.1497.

References

- [33] Y.H. Khattak, F. Baig, S. Ullah, B. Mari, S. Beg, H. Ullah, Numerical modeling baseline for high efficiency (Cu₂FeSnS₄) CFTS based thin film kesterite solar cell, *Optik (Stuttg)*. 164 (2018) 547–555. doi:10.1016/j.ijleo.2018.03.055.
- [34] B. Qi, J. Wang, Fill factor in organic solar cells, *Phys. Chem. Chem. Phys.* 15 (2013) 8972. doi:10.1039/c3cp51383a.
- [35] H. C. Card, Photovoltaic Properties Of MIS-Schottky Barriers, *Solid-State Electronics*, 1977. Vol. 20, pp. 971-976.
- [36] Md. Mehedi Hasan, Sanzida Akther and Md. Iqbal Bahar Chowdhury, Investigation of Graphene/Silicon-dioxide/Gallium Arsenide Based MIS Solar Cell Using Silvaco TCAD, Proceedings of 14th Global Engineering and Technology Conference 29-30 December 2017, BIAM Foundation, 63 Eskaton, Dhaka, Bangladesh, ISBN: 978-1-925488-60-9.
- [37] Fandi Oktasendra, Rahmat Hidayat and Rizky Indra Utama, Effects of Interface State Density On The carrier Transport and Performance of Metal-Insulator-Semiconductor (MIS) Type Thin Film Solar Cells, *IOP Conf. Series: Journal of Physics: Conf. Series* 1481 (2020) 012005, Doi:10.1088/1742-6596/1481/1/012005.
- [38] A. S. Grove, *Physics and Technology of Semiconductor Devices*, p. 184, Wiley, New York (1967).
- [39] H. C. Card and E. H. Rhoderick, *J. Phys. D: Appl. Phys.* 4, 1589 (1971).
- [40] Wenas WW, Riyadi S. 2006 *Sol Energ Mat Sol C*. **22** 3261–3267.
- [41] Pür FZ, Tataroğlu A. 2012 *Phys Scripta*. **86** 035802.
- [42] Gao J, Kempa K, Giersig M, et al. 2016 *Adv Phys*. **65** 553–617.
- [43] Cheknane A. 2009 *J Phys D Appl Phys*. **42** 115302.
- [44] Hu YH, Xu HJ, Gao H, et al. 2011 *Mater Sci Forum*. **663** 1077–1080.
- [45] Hocine D, Belkaïd MS, Lagha K. 2008 *Rev Energ Renew*. **11** 379–384.
- [46] Thomas KRJ, Baheti A. 2013 *Mater Technol*. **28** 71–87.
- [47] Kim C, Jo HJ, Kim DH, et al. 2012 *Mol Cryst Liq Cryst*. **565(1)** 52–58.

References

- [48] Qin H, Liu HF, Yuan YZ. 2013 *Energ Mater.* **29** 70–76.
- [49] Mishra A, Kumar A, Hodges D, et al. 2017 *Mater Technol.* **32** 829–837.
- [50] Vadivel B, Sudha S, Gowrisankar P, et al. 2018 *Mater Technol.* **33(6)** 414–420.
- [51] Zahirullah S, Prince J, Inbaraj FH. 2017 *Mater Technol.* **32** 755–763.
- [52] Green, Shawn E., Interdigitated back-surface-contact solar cell modeling using Silvaco Atlas, thesis (2015), Monterey, California: Naval Postgraduate School *Atlas User's Manual*, Silvaco International, Santa Clara, CA, 2005.
- [53] *about SILVACO*. Available from:
<http://www.silvaco.com/company/profile/profile.html>.
- [54] Wilson W. Wenas, Syarif Riyadi, Carrier transport in high-efficiency ZnO/SiO₂/Si solar cells, *Solar Energy Materials & Solar Cells* 90 (2006) 3261–3267.
- [55] A. U. s. M. D. S. S. (2013), "Atlas User's Manual DEVICE SIMULATION SOFTWARE.(2013)," ed.
- [56] Chanchaivithsupalertb.e., Theory of metal-insulator-semiconductor (mis) solar cells, Thesis, University of New South Wales (1977).

Abstract

We have investigated two MISsilicon-based solar cells. The first one consists of Au / SiO₂ / n-type c-Si, and in the second one, the anode metal (Au) is replaced by heavily doped ZnO (n⁺-type) to give (n⁺-type ZnO / SiO₂ / n-type c-Si) structure. The investigation of the thickness variation effect, of the silicon layer in the range [10- 500 μm], shows an optimal thickness of 175 μm for the first cell with a conversion efficiency η of ~11.87 %. For the second one, the optimal thickness is 150 μm with a conversion efficiency η of ~12.50%. An enhancement is notified, particularly in J_{sc} and the conversion efficiency η , as the anode metal (Au) is replaced by heavily doped ZnO (n⁺-type). The thickness variation effect of the oxide (SiO₂) layer in the range [2-20 Å], shows better output parameters for FF and η , as the oxide layer becomes thinner. The J_{sc} and V_{oc} , however, display insignificant sensitivity to the oxide layer thickness variation. The optimal value of doping is $N_d = 7 \times 10^{15} \text{ cm}^{-3}$ for the first cell with a conversion efficiency η of ~11.87%, and is $N_d = 7 \times 10^{16} \text{ cm}^{-3}$ for the second solar cell with a conversion efficiency η of ~12.558%. The V_{oc} is significantly enhanced as the doping concentration increases for both solar cells. Varying the ZnO layer thickness in the range [0.05-10 μm] brings further improvement to the second cell; a significant enhancement of the J_{sc} is notified leading to a conversion efficiency improvement from ~ 11.97% to 13.94%.

ملخص

قمنا بدراسة خليتين شمسيتين من السيلكون ببنية MIS ، الأولى مكونة من Au / SiO₂ / n-type c-Si و في الثانية تم استبدال الأنود من معدن الذهب بأنود من ZnO مطعم بشدة نوع n⁺ للحصول على البنية (n⁺-type ZnO / SiO₂ / n-type c-Si). دراسة تأثير تغيير سمك طبقة القاعدة من السيلكون في المجال [10- 500 μm] بين أن أحسن سمك للخلية الأولى هو 175 μm الذي يعطي مردود تحول فوتوفولطائي % 11.87 ، و أحسن سمك للخلية الثانية هو 150 μm مع مردود % 12.50. على العموم هناك تحسن ملحوظ في كل من J_{sc} و المردود η عند استبدال الأنود من معدن الذهب بأنود من ZnO مطعم بشدة نوع n⁺. تأثير تغيير سمك طبقة الأكسيد في المجال [2-20 Å] يظهر أحسن وسائط خروج فوتوفولطائية من أجل FF و η عندما يتناقص سمك طبقة الأكسيد أكثر فأكثر. في حين V_{oc} و I_{sc} لا تتأثر بشكل ملحوظ مع تغيير سمك طبقة الأكسيد. أحسن قيمة لتركيز التطعيم هي $N_d = 7 \times 10^{15} \text{ cm}^{-3}$ من أجل الخلية الأولى و التي تعطي مردود % 11.87 ، أحسن قيمة لتركيز التطعيم هي $N_d = 7 \times 10^{16} \text{ cm}^{-3}$ من أجل الخلية الثانية مع مردود % 12.558. V_{oc} يزداد بشكل ملحوظ مع زيادة تركيز التطعيم في طبقة السيلكون لكلا الخليتين. تغيير سمك طبقة ZnO في المجال [0.05-10 μm] يقدم تحسين إضافي للخلية الثانية. J_{sc} يتحسن بشكل ملحوظ مؤديا إلى تحسن في مردود الخلية من % 11.97 ~ إلى % 13.94.